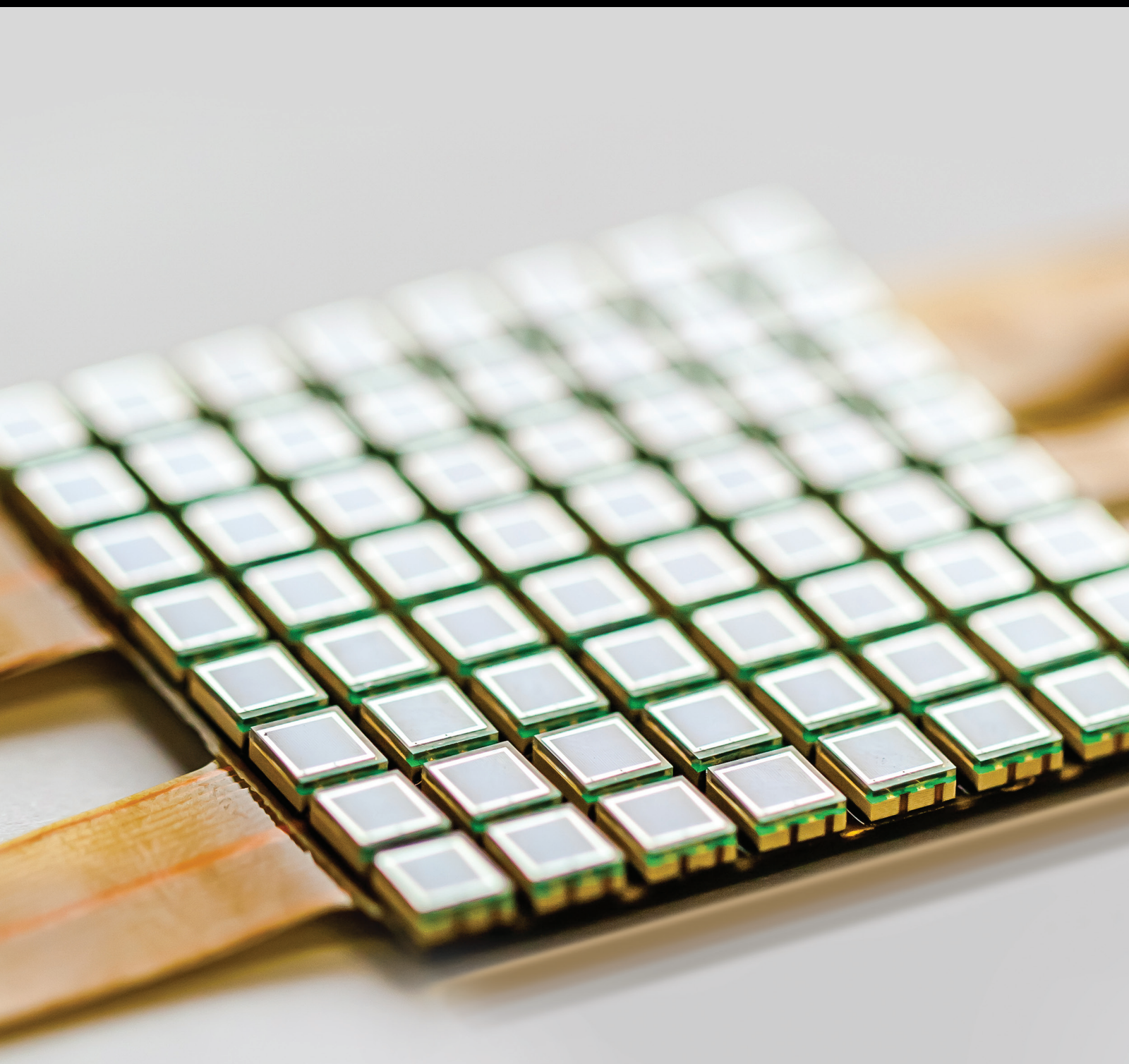


Healthcare Sensors for Daily Life

Guest Editors: Toshiyo Tamura, Wenxi Chen, Kwang-Suk Park, and Rita Paradiso





Healthcare Sensors for Daily Life

Journal of Sensors

Healthcare Sensors for Daily Life

Guest Editors: Toshiyo Tamura, Wenxi Chen, Kwang-Suk Park,
and Rita Paradiso



Copyright © 2016 Hindawi Publishing Corporation. All rights reserved.

This is a special issue published in "Journal of Sensors." All articles are open access articles distributed under the Creative Commons Attribution License, which permits unrestricted use, distribution, and reproduction in any medium, provided the original work is properly cited.

Editorial Board

Harith Ahmad, Malaysia
Francisco J. Arregui, Spain
Francesco Baldini, Italy
Fernando Benito-Lopez, Ireland
Romeo Bernini, Italy
Shekhar Bhansali, USA
Wojtek J. Bock, Canada
Hubert Brändle, Switzerland
Davide Brunelli, Italy
Belén Calvo, Spain
Stefania Campopiano, Italy
Jian-Nong Cao, Hong Kong
Sara Casciati, Italy
Chi Chiu Chan, Singapore
Nick Chaniotakis, Greece
Nicola Cioffi, Italy
Elisabetta Comini, Italy
Marco Consales, Italy
Jesus Corres, Spain
Andrea Cusano, Italy
Dzung V. Dao, Japan
Catherine Dehollain, Switzerland
Manel del Valle, Spain
Ignacio Del Villar, Spain
Utkan Demirci, USA
Junhang Dong, USA
Abdelhamid Errachid, France
Stephane Evoy, Canada
Vittorio Ferrari, Italy
Luca Francioso, Italy
Laurent Francis, Belgium
Mohammad Reza Ganjali, Iran

Wei Gao, Japan
Michele Giordano, Italy
Banshi D. Gupta, India
M. del Carmen Horrillo, Spain
Wieslaw Jakubik, Poland
Hai-Feng Ji, USA
K. Kalantar-Zadeh, Australia
Sher Bahadar Khan, KSA
Sang Sub Kim, Republic of Korea
Challa Kumar, USA
Hiroki Kuwano, Japan
Laura M. Lechuga, Spain
Chengkuo Lee, Singapore
Chenzhong Li, USA
Eduard Llobet, Spain
Yu-Lung Lo, Taiwan
Oleg Lupan, Moldova
Eugenio Martinelli, Italy
J. R. Martinez-de Dios, Spain
Yasuko Y. Maruo, Japan
Ignacio R. Matias, Spain
Mike McShane, USA
Igor L. Medintz, USA
Fanli Meng, China
Aldo Minardo, Italy
Joan Ramon Morante, Spain
Lucia Mosiello, Italy
Masayuki Nakamura, Japan
Vincenzo Paciello, Italy
Marimuthu Palaniswami, Australia
Alberto J. Palma, Spain
Gyuhae Park, Republic of Korea

Alain Pauly, France
Giorgio Pennazza, Italy
Michele Penza, Italy
Andrea Ponzoni, Italy
Biswajeet Pradhan, Malaysia
Ioannis Raptis, Greece
Christos Riziotis, Greece
Maria L. Rodríguez-Méndez, Spain
Albert Romano-Rodriguez, Spain
Josep Samitier, Spain
Giorgio Sberveglieri, Italy
Luca Schenato, Italy
Michael J. Schöning, Germany
Andreas Schütze, Germany
Woosuck Shin, Japan
Pietro Siciliano, Italy
Vincenzo Spagnolo, Italy
Weilian Su, USA
Tong Sun, UK
Hidekuni Takao, Japan
Isao Takayanagi, Japan
Pierre Temple-Boyer, France
Guiyun Tian, UK
Suna Timur, Turkey
Hana Vaisocherova, Czech Republic
Qihao Weng, USA
Matthew J. Whelan, USA
Stanley E. Woodard, USA
Hai Xiao, USA
Hyeonseok Yoon, Republic of Korea

Contents

Healthcare Sensors for Daily Life

Toshiyo Tamura, Wenxi Chen, Kwang-Suk Park, and Rita Paradiso
Volume 2016, Article ID 7280831, 2 pages

Structural Optimization of a Wearable Deep Body Thermometer: From Theoretical Simulation to Experimental Verification

Ming Huang, Toshiyo Tamura, Zunyi Tang, Wenxi Chen, and Shigehiko Kanaya
Volume 2016, Article ID 4828093, 7 pages

Long-Term Measurement of Maternal Pulse Rate Dynamics Using a Home-Based Sleep Monitoring System

Ying Chen, Wenxi Chen, Kei-ichiro Kitamura, and Tetsu Nemoto
Volume 2016, Article ID 5730142, 11 pages

Challenges and Issues in Multisensor Fusion Approach for Fall Detection: Review Paper

Gregory Koshmak, Amy Loutfi, and Maria Linden
Volume 2016, Article ID 6931789, 12 pages

Interrupt-Based Step-Counting to Extend Battery Life in an Activity Monitor

Seung Young Kim and Gu-In Kwon
Volume 2016, Article ID 5824523, 6 pages

Miniaturized Human Insertable Cardiac Monitoring System with Wireless Power Transmission Technique

Jong-Ha Lee
Volume 2016, Article ID 5374574, 7 pages

Editorial

Healthcare Sensors for Daily Life

Toshiyo Tamura,¹ Wenxi Chen,² Kwang-Suk Park,³ and Rita Paradiso⁴

¹*Faculty of Biomedical Engineering, Osaka Electro-Communication University, Neyagawa, Osaka 572-8530, Japan*

²*Biomedical Information Technology Laboratory, The University of Aizu, Aizu-Wakamatsu, Fukushima 965-8580, Japan*

³*Department of Biomedical Engineering, College of Medicine, Seoul National University, Seoul 110-799, Republic of Korea*

⁴*Smartex srl, Navacchio, 56023 Pisa, Italy*

Correspondence should be addressed to Toshiyo Tamura; tamurat@isc.osakac.ac.jp

Received 11 October 2015; Accepted 11 October 2015

Copyright © 2016 Toshiyo Tamura et al. This is an open access article distributed under the Creative Commons Attribution License, which permits unrestricted use, distribution, and reproduction in any medium, provided the original work is properly cited.

With the advent of information and communication technology (ICT) and its pervasive application in medical and healthcare domains, life expectancy worldwide has extended over 80s in both females and males. Decline in health condition due to aging would deteriorate personal quality of life and pose extreme burden in global financial expenditure. Healthy aging is therefore of paramount importance.

To support “aging in place” and “daily health promotion,” accurate detection and early warning of health condition change are indispensable and imminent. Numerous technical innovations are provoked. Seamless monitoring of physiological information in various living scenarios without disturbing daily activities over a long-term period can significantly enhance caregivers’ ability to deliver evidence-based care and becomes one of the effective approaches.

In pursuing seamless monitoring of multifaceted physiological information in daily life environment, many academic goals have been challenged and variety of technological conundrums has been experienced over the past decades. Endeavors in research and development have gone through different approaches which enhance several aspects such as miniaturization, comfortableness, and concealment to achieve better user affinity in different application scenarios of daily life. Miniaturization aims at implementation of portable monitors for ambulatory application. Wearable monitors target for pervasive application in daily activities without much discomfort. Invisible methods are usually realized by concealing sensors or transducers into furniture and appliances for indoor application. Some of these outcomes have matured and have been commercialized in daily setting;

yet some of them remain unanswered and require further elaboration.

This special issue focuses on device development, data analysis, and system integration aiming at health monitoring in daily life which has considerable potential for preventing and predicting diseases, without significant discomfort or inconvenience to the home users. Thus, this issue contains (1) review of the devices used for falling risk assessment; (2) discussion of long-term data collection and analysis using Big Data techniques; (3) new devices for further application of new technologies.

The problem in elderly community is the fall risk assessment in daily life environment. There are several inertial sensors used to provide the fall risk assessment and prevention. Image processing technology also has been applied in the home. In this issue, the image processing with multi-sensor fusion technologies to assess and detect the falling is reviewed.

Secondly, long-term records collected from daily living need to be evaluated and help for further prevention and prediction of diseases. In the issue, cardiac recovery process in the pregnancy and after delivery was analyzed from the long-term pulse records.

Thirdly, three papers present new ideas for monitoring at daily living. The wearable deep body thermometer may be a promising technology for preventing heat stroke and monitoring mental stress and circadian rhythms.

Other papers also show technologies to improve current healthcare sensors. For improving quality of life, the elderly used to wear pedometer. The unique algorithm is applied to

reduce power consumption of pedometer. One more paper presents the cardiovascular monitor for real time detection of atrial fibrillation.

Acknowledgments

Finally, we would like to thank all the authors for their valuable contributions and also the reviewers for their critical help necessary to achieve a high level of papers' quality and make the completion of this special issue possible. Also, we would like to thank all members of the editorial board for approving this special issue.

*Toshiyo Tamura
Wenxi Chen
Kwang-Suk Park
Rita Paradiso*

Research Article

Structural Optimization of a Wearable Deep Body Thermometer: From Theoretical Simulation to Experimental Verification

Ming Huang,¹ Toshiyo Tamura,² Zunyi Tang,² Wenxi Chen,³ and Shigehiko Kanaya¹

¹Graduate School of Information Science, Nara Institute of Science and Technology, Ikoma 6300192, Japan

²Department of Biological Engineering, Osaka Electro-Communication University, Shijonawate, Japan

³Biomedical Information Technology Laboratory, The University of Aizu, Tsuruga, Aizuwakamatsu, Japan

Correspondence should be addressed to Ming Huang; alex-mhuang@is.naist.jp

Received 15 May 2015; Revised 24 September 2015; Accepted 29 September 2015

Academic Editor: Junhang Dong

Copyright © 2016 Ming Huang et al. This is an open access article distributed under the Creative Commons Attribution License, which permits unrestricted use, distribution, and reproduction in any medium, provided the original work is properly cited.

Deep body temperature (DBT) has yet to be measured continuously in everyday life, even though it is useful in physiological monitoring and chronobiology studies. We tried to address this issue by developing a transcutaneous thermometer based on the dual-heat-flux method (DHFM) invoking the principle of heat transfer, for which measurement error was mitigated by elaborate design. First, a structural modification based on the original design of the DHFM was implemented by the finite element method. Based on the results of the simulations, prototypes were then implemented and tested with an experimental system that mimicked the thermometer being applied to skin. The simulation phase proposed the adoption of an aluminum cover to boost measurement accuracy and suggested that thermometers of different height be chosen according to specified requirements. The results of the mock-up experiments support the modification put forward in the simulation phase: the standard type (15 mm in height) achieved the accuracy with error below 0.3°C while the thin type (9 mm in height) attained accuracy with error less than 0.5°C under normal ambient temperature ranging from 20 to 30°C. Even though the design should also be examined *in vivo*, it is believed that this study is an important step in developing a practical noninvasive deep body thermometer.

1. Introduction

Deep body temperature (DBT) is one of the vital signs for human beings and is typically referred to as the temperature of the natural cavities, for example, the abdomen and the thorax. Strictly speaking, DBT can only be measured by invasive methods such as catheter insertion into rectum [1].

However, noninvasive methods are more acceptable and are therefore more widely used. They can provide approximation to the DBT, which is the temperature at a certain depth under the skin reflecting the real DBT. One good alternative to the invasive methods is the zero-heat-flux method [2], which was improved by Togawa's group [3] and implemented in the CoreTemp medical device (Terumo, Tokyo, Japan). It showed good agreement with distal esophageal temperature [4] and pulmonary blood temperature [5]. Developed with an inlaid heater, this device is considered to be stable (robust

to changes in the ambient environment) and sensitive [5]. On the other hand, the heater consumes considerable power, which makes this kind of device only applicable indoors, mainly in hospitals during therapy.

However, continuous DBT measurement is necessary in situations such as heat strain monitoring [6] and female menstrual cycle management [7] and in the treatment of sleep disorders [8] for the estimation of biorhythms. These needs could be met by wearable devices. We suggest that the display and data accumulating functions could be allocated to a smartphone/watch, with the data further analyzed and modeled on a server. In the initial stage of signal extraction, a noninvasive thermometer with low power consumption is indispensable.

More often, it is the temperature fluctuations rather than absolute temperature readings that interest us in the health-care domain. However, the changes in readings by the devices

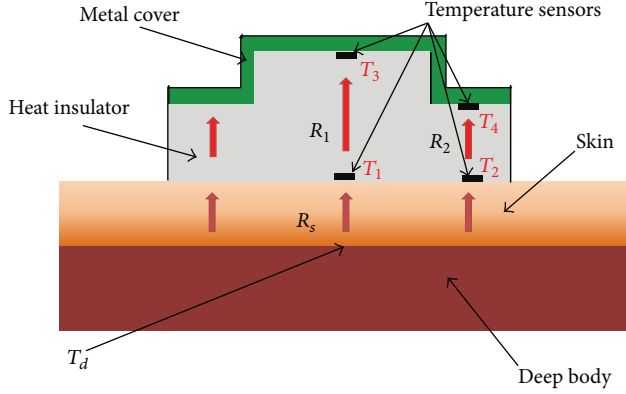


FIGURE 1: Illustration of dual-heat-flux method. The heat flows from deep body into the thermometer longitudinally and thus the DBT can be calculated with the four inlaid sensors (T_1 - T_4) theoretically.

should be caused by actual changes in the physiological state and not by some external influence. From this viewpoint, an ear-inserted thermometer is not a good choice because its measurements are evidently influenced by the ambient environment. The infrared tympanic thermometer is able to reflect internal change but is sensitive to its positioning.

The mechanism of the thermometer should also be universal; it should be applicable to different people. More specifically, even in the same person, the thermal conductivity of the skin might differ temporally and spatially. A thermometer based on the exact value of the personal physiological condition [9] should be further generalized.

The above concerns can be addressed properly by the dual-heat-flux method (DHFM) [10], the mechanism of which is depicted in Figure 1. The DHFM uses at least four temperature sensors to calculate the DBT, based on the idealized situation that heat flows from the human body into the thermometer longitudinally. This assumption would bring about error in the temperature calculation; however, it requires little information from the user. Moreover, the idealized situation can be approximated by dimensional or thermophysical modification [11].

The criterion of accuracy for clinical use is 0.1°C conventionally, which is not readily met by noninvasive methods [9, 11]. Hence, we considered 0.5°C as the margin for acceptable accuracy in this study. However, for the original design, this level of accuracy is achieved at the cost of a device that is too large to wear or an ultrathin design that is difficult to implement [11]. On the basis of the above understanding, this study aimed to improve the structural design to achieve this level of accuracy without compromising its small size. To reach this target, we first designed and examined the structural modification based on the finite element method (FEM). Then, the validated new structures were fabricated and their capabilities were examined by mock-up experiments.

2. Materials and Method

2.1. About DHFM. At least four inlaid temperature sensors are necessary for a thermometer based on DHFM. They

are T_1 - T_4 in Figure 1. On account of temperature gradient, heat flow arises and flow through the skin layer into the thermometer as shown by red arrows. T_d is the general DBT beneath the skin and subcutaneous layer. Assuming that the heat flow from the deep body into the thermometer remains the same, Fourier's law applies, giving

$$\frac{(T_d - T_1)}{R_s} = \frac{(T_1 - T_3)}{R_1}, \quad (1)$$

$$\frac{(T_d - T_2)}{R_s} = \frac{(T_2 - T_4)}{R_2}.$$

T_1 and T_2 are skin temperatures measured by two cutaneous temperature sensors inside the thermometer. T_3 and T_4 are the temperatures measured by the other two sensors. R_s is the heat resistance of the skin, with R_1 and R_2 being the heat resistance of the two heat paths inside the thermometer. According to (1), T_d then can be expressed as [10]

$$T_d = T_1 + \frac{(T_1 - T_2)(T_1 - T_3)}{k(T_2 - T_4) - (T_1 - T_2)}. \quad (2)$$

Hence, $k = R_1/R_2$, and it can be represented as the ratio of the heights of the two concentric cylinders used in the thermometer fabrication.

Generally speaking, DBT is strictly regulated by hypothalamus and it changes tardily in accordance to biorhythm. These characteristics make the measurement with DHFM applicable. For such a passive method with heat insulator as the substrate material, it takes time for initial response.

2.2. Simulation Based on FEM. Bioheat transfer involves blood perfusion and metabolic processes. It can be well described by the Pennes equation [12]:

$$\rho c_p \frac{\partial T(\mathbf{X}, t)}{\partial t} = \nabla \cdot [k(\mathbf{X}) \nabla T(\mathbf{X}, t)] + \omega_b \rho_b c_b (T_b - T(\mathbf{X}, t)) + q_m(\mathbf{X}, t) \quad (3)$$

$$\mathbf{X} \in \Omega_T.$$

The parameters T , ρ , c_p , and k are the local temperature, the density (kg/m^3), the specific heat ($\text{J}/\text{kg}\cdot^\circ\text{C}$), and the thermal conductivity ($\text{W}/\text{m}\cdot^\circ\text{C}$) of the local tissue, respectively. T_b , ω_b , ρ_b , and c_b are the blood temperature, blood perfusion rate ($\text{m}^3/\text{m}^3\cdot\text{s}$), blood density (kg/m^3), and the specific heat of blood ($\text{J}/\text{kg}\cdot^\circ\text{C}$), respectively.

The second and third terms on the right denote the heating effect of blood perfusion and metabolism. However, these two terms were not considered in this model because this kind of evenly distributed heat source would alter the actual value of the measurement somewhat but would not invalidate the qualitative relations from the simulation. Further, because the DBT should vary in a quasistatic manner, the temporal change was not considered.

Because we assumed that the thermometer and skin were covered by suitable clothing, heat convection was neglected. However, radiation was inevitable; therefore, the boundary

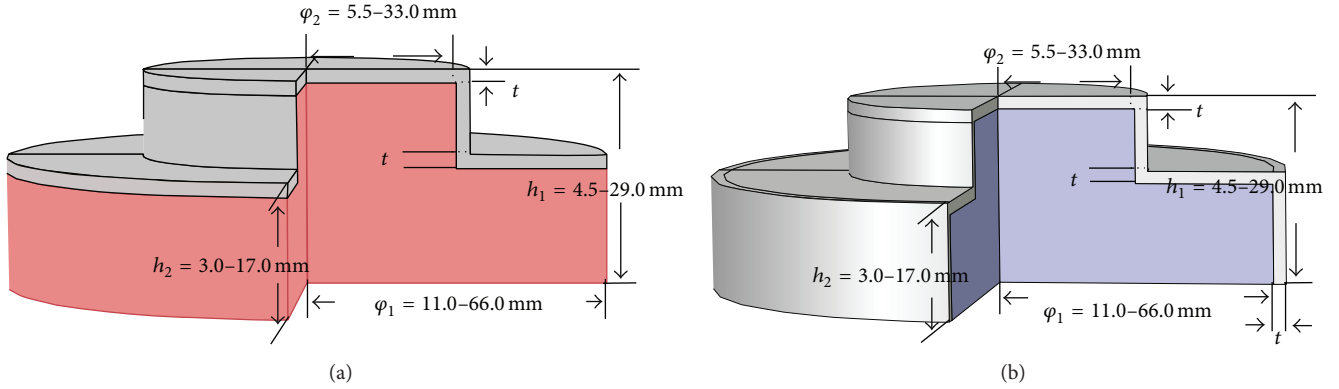


FIGURE 2: Sectional view of two models. The original structure is without PAR (a), while the modified structure with PAR is shown by (b).

conditions of the thermometer and its surrounding skin could be described by the Stefan-Boltzmann law [13]:

$$-\mathbf{n} \cdot [-k(\mathbf{X}) \nabla T(\mathbf{X}, t)] = \varepsilon \sigma (T_{\text{amb}}^4 - T_{\text{boun}}^4(\mathbf{X}, t)), \quad (4)$$

$$X \in \Gamma,$$

where T_{amb} is the ambient temperature, T_{boun} the local temperature value at the boundary, σ the Stefan-Boltzmann constant, and ε the emissivity of the boundary.

In the simulation phase, we sought to improve the thermometer's accuracy by structural modification, while reserving the wearability of the thermometer. Therefore, an additional component, a peripheral aluminum ring (PAR), was introduced in view of the high emissivity of the insulator component. There were two kinds of thermometers in this simulation, with and without the PAR, as shown in Figures 2(a) and 2(b).

As shown in Figure 2, we considered four combinations of heights, namely, (29.0, 17.0), (15.0, 9.0), (8.0, 5.0), and (4.5, 3.0), for (h_1, h_2) . Similarly, we considered six combinations of radii, namely, (66.0, 33.0), (55.0, 27.5), (44.0, 22.0), (33.0, 16.5), (22.0, 11.0), and (11.0, 5.5), for (φ_1, φ_2) , respectively. (We also labeled these configurations in terms of their h_1 and φ_1 values.) In fact, because a radius larger than 50.0 mm is not suited for wearable application, we introduced 66.0 mm and 55.0 mm sizes just for the whole picture of the relation between radius and accuracy. In total, there were 24 dimensional combinations, all of which were simulated by our models. In Figure 2(b), the PAR made of aluminum was represented in silver with $t = 1.0$ mm, a size that will not bring about distinct change in volume and weight. The ambient temperature of the simulation was $T_{\text{amb}} = 25.0^\circ\text{C}$ and $T_d = 37.0^\circ\text{C}$. The thickness of the skin and subcutaneous layer was 10.0 mm.

In this model, the rubber was used as insulator and the aluminum was used as the metal. Necessary physical parameters are tabulated in Table 1. The models were built, simulated, and analyzed with LiveLink for MATLAB based on COMSOL Multiphysics 4.3a (COMSOL Inc., Stockholm, Sweden). Unconstructed mesh was generated by COMSOL adapting to the current physics and geometries. The numbers of elements were different across the models (e.g., 57544

TABLE 1: Thermal properties of various materials*.

Component	Conductivity (W/m \cdot °C)	Density (kg/m 3)	Specific heat (J/kg \cdot °C)	Emissivity
Skin	0.17	1100	3500	0.98
Rubber	0.06	180	2010	0.95
Aluminum	400	8700	385	0.05

*The properties used here were cited from the materials library of COMSOL Multiphysics.

for standard type model); however, the minimum element quality (q) was kept bigger than 0.1. q has a considerable impact on accuracy of the solution, and, for 3D model, the mesh quality should not affect the solution's quality if $q > 0.1$.

In practical implementation, the values of the parameters or even the specified materials may be different. The lower the conductivity of the insulator, the higher the accuracy at the cost of a longer initial response in general. The simulation here serves as an examination of the new design.

2.3. Fabrication of Prototypes. Based on the results of the simulation, we fabricated two prototypes of different heights, $h_1 = 9.0$ mm (thin type) and $h_1 = 15.0$ mm (standard type), as shown in Figure 3. Both prototypes were of the same radius, $\varphi_1 = 22.0$ mm. The prototypes consisted of two parts: the probe to be applied to the skin for measurement and the processing circuit. As designed in the simulation phase, the probe consists of a heat resistor made of chloroprene rubber and metal components made of aluminum 2017 alloy. Miniature digital temperature sensors LM73 (11–14 bits; Texas Instruments, Dallas, TX) were used as the four inlaid sensors and communicated with the central board with I 2 C.

The probe of the thermometer connects to the main processing board by USB cable (Mini to Standard plug). The main processing board consists mainly of the controlling unit (ATmega164A, Atmel RISC Microcontroller; Atmel, San Jose, CA), a memory unit with 8 Mb serial flash memory to store the infradian data, and a battery unit to supply three days of energy for the whole local system. Data stored locally can be retrieved with a specialized program run on the PC as a CSV file.

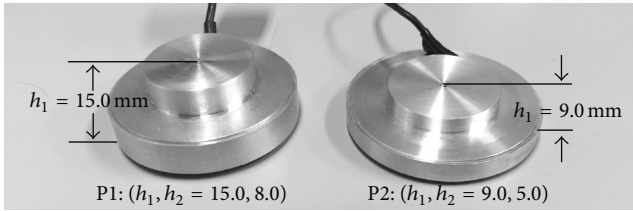


FIGURE 3: Prototypes of thermometers based on DHFM. Line-up of the standard type and thin type is shown.

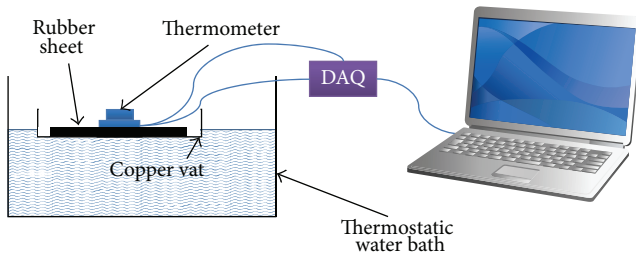


FIGURE 4: Illustration of the mock-up experiment system. The temperature of the water was used to mimic the DBT, while the natural rubber was used to mimic the skin layer.

2.4. Mock-Up Experiment. The structures suggested by the simulation phase should be validated by mock-up experiments before being applied in practical measurement. A standard experimental system [10, 14] was used to examine the thermometer's capability. An illustration of the system is shown in Figure 4. The thermometer was placed on a natural rubber sheet (sheets of 2.0, 4.0, 6.0, 8.0, and 10.0 mm in thickness), which was laid inside a copper vat. The vat floated on temperature-controlled water. In view of the excellent heat conductivity of copper, the boundary between the rubber sheet and copper vat was considered isothermal. Silicon grease was applied to the boundary between the probe and the rubber sheet to minimize thermal resistance. The temperature of the water inside a thermostatic water bath (FR-004, $\pm 0.1^\circ\text{C}$; TKG, Tokyo, Japan) was used to mimic T_d , while the natural rubber sheet was used to mimic human skin, based on the physical similarities of these two materials.

The prototypes were tested in three conditions: without PAR (N), with PAR (A), and without PAR but with sponge cover (S). Through this phase, we hoped to find out whether the new component (i.e., the PAR) would influence the measurements as predicted by the simulation. Condition S was adopted to confirm the effect of the sponge in measuring accuracy; although it is obstructive in practical measurement, it is reportedly indispensable [10].

The range of normal T_d falls in between 36.0°C and 38.0°C , while normal indoor T_{amb} is $20.0\text{--}30.0^\circ\text{C}$, which may influence the measurements. Thus, we further tested the prototypes in the following three combinations:

Combination 1: $T_{\text{amb}} = 20.0^\circ\text{C}$, $T_d = 36.0^\circ\text{C}$.

Combination 2: $T_{\text{amb}} = 25.0^\circ\text{C}$, $T_d = 37.0^\circ\text{C}$.

Combination 3: $T_{\text{amb}} = 30.0^\circ\text{C}$, $T_d = 38.0^\circ\text{C}$.

For each combination, experiments were conducted three times and for each condition of the thermometer (N, A, and S) 30 minutes was given for the establishment of heat equilibrium inside the probes. The two probes (thin and standard types) were tested in rotation to remove the heat stored in the previous trial.

3. Results

3.1. Results of Simulation. In this phase, while the ambient temperature T_{amb} and the DBT T_d did not change, the specific combination of these two parameters is sufficient to reveal the relations between the physical structure and the accuracy [11].

For thermometers both with and without PAR, all 24 thermometers defined by the combinations of 4 different heights and 6 different radii were considered and modeled. The measurements from each thermometer are summarized in Figure 5(a) (without PAR) and Figure 5(b) (with PAR). Markers in one interpolating curve indicate the measuring values with thermometers of the same height.

From the results, we can see that the effects of the dimensions were different. For the thermometer without PAR, generally, the accuracy was proportional to the radius, but inversely proportional to the height. A change of dimensions influences the measuring accuracy greatly when the radius is less than 40 mm. Furthermore, the radius is more effective than the height. A twofold increase in radius benefits the accuracy much more significantly than does a half-size decrease in height.

For the thermometers with PAR, the accuracy was proportional to height and radius. It is easier for them to attain much greater accuracy with a radius greater than 20 mm. Moreover, the height is definitive in these thermometers, as no distinct improvement can be seen by changing the radius of thermometers of the same height, with a radius larger than 30 mm.

3.2. Results of the Mock-Up Experiment. According to the simulation results, with both standard and thin types, we can attain the acceptable margin of error ($<0.5^\circ\text{C}$) that is hard to attain in the designs without PAR.

In this phase, the combinations of experimental conditions (Combination 1, Combination 2, and Combination 3) were all tested and Combination 2 was the same as in the simulation phase. For both thermometers, all three conditions (A, N, and S) were tested three times each.

The results for these tests are shown in Figure 6, where the results were concluded based on the type of thermometer. In both A and N conditions, the quantitative relations conform to the results of the simulation. That is, thermometers with PAR attain better accuracy than their condition N counterparts. In condition A, a thicker design gives good accuracy at the expense of a larger volume. In condition S, the measurements showed the best accuracy for both prototypes.

In condition N, the spans of the error were about 0.5 and 0.3°C for standard and thin type, respectively. By contrast, the spans were about 0.2°C for both types in condition A. This suggests that the PAR takes effect in resisting the influence of the ambient environment.

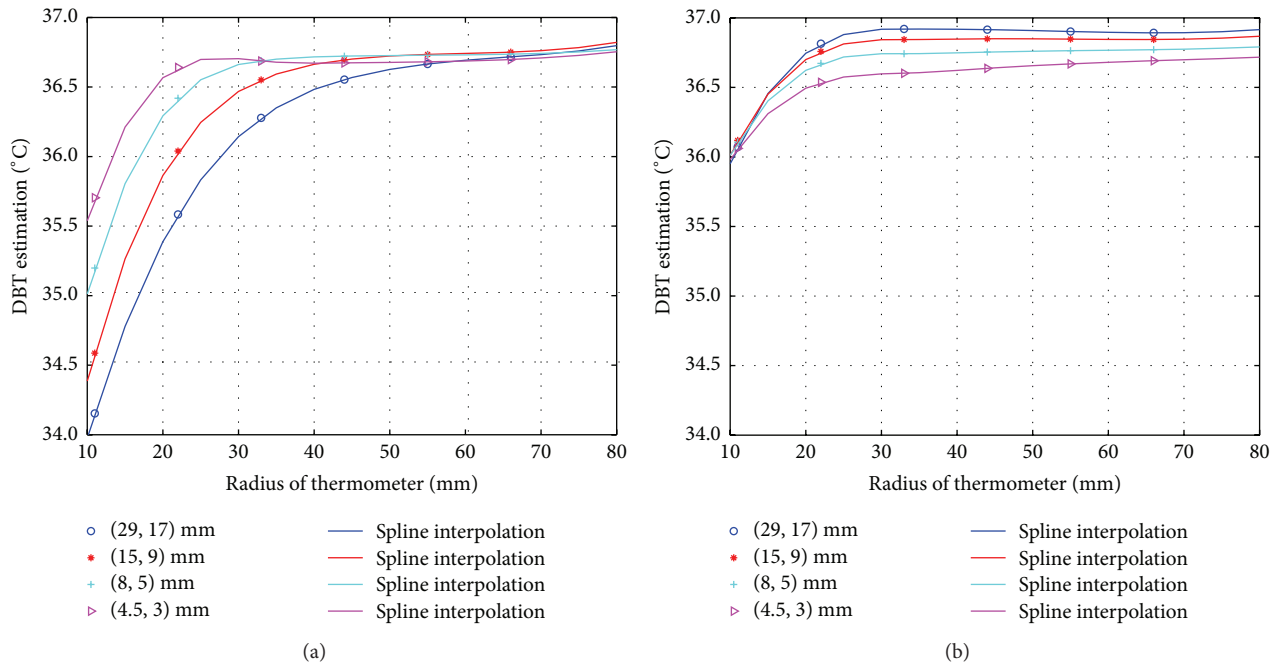


FIGURE 5: Results of simulation based on FEM. (a) and (b) show the measurements of thermometers in condition N and condition A, respectively.

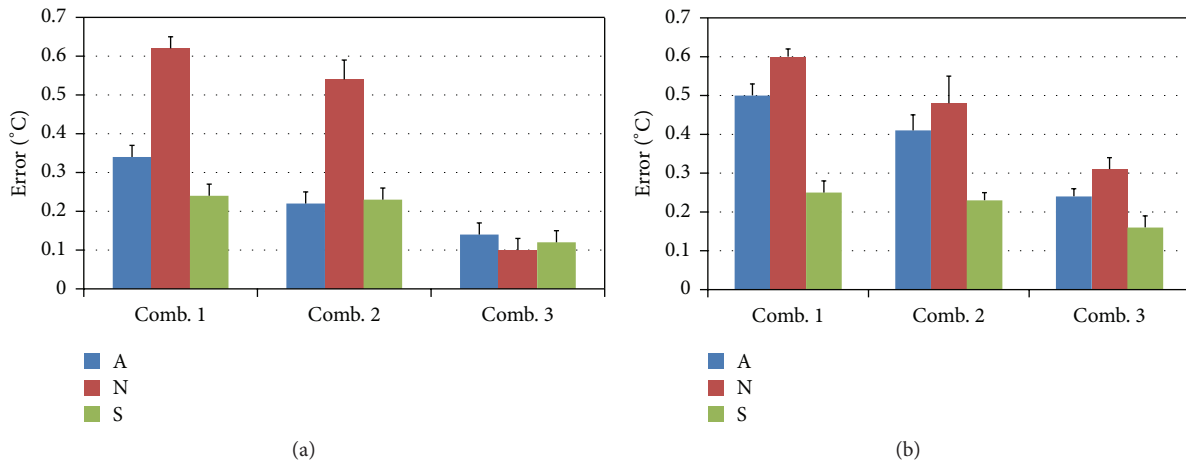


FIGURE 6: Results of mock-up experiments for both thermometers. Results of standard type were summarized in (a) and thin type in (b).

4. Discussion

4.1. The Practical Use. As we have introduced, the method is applicable in measuring the DBT that change at a slow manner. For extreme situation such as anesthesia or heatstroke, time delay happens. In a simulation whose results were not shown here, the standard type was used to monitor the abrupt change of DBT at a rate of $0.2^{\circ}\text{C}/\text{minute}$ lasting for 10 minutes. The thermometer could indicate the change in about 4 minutes and became stable in 20 minutes after the change. For such situation, the thin type, whose reading will become stable in about 10 minutes, might be suited to trace the change.

If the thermometer is applied to the upper torso, for example, the thorax, the thermometer may come into contact

with clothes from time to time. The physically thin layer and low conductivity of clothes would hardly change the resistance of the thermometer. However, the relatively high emissivity (0.75–0.90) [13] may be influential. Assuming that the thermometer comes into contact with the clothes made of cotton of 0.5 mm thickness for an hour, the transient study of simulation was carried out. Its result showed that the measurement of the sensor changed (decreased) after about half an hour by 0.1°C , and then the measurement became stable gradually. In a practice, contact between the thermometer and the clothes is often erratic. In consideration of the slow and subtle change of the measurement, we considered the influence of clothes to be minor in common situation.

4.2. The Simulation. The adoption of a PAR was based on the physical characteristics of metals, which usually have a much lower emissivity than heat insulators (e.g., rubber), and, at the same time, the radioactive energy exchange is the main reason for the horizontal heat flow distorting the practical situation from the theoretical assumption of DHFM. With a PAR, the influence of the ambient environment may be mitigated remarkably because this thermometer is designed to be worn on the torso with suitable clothing, which will shield the thermometer from the influence of airflow from concerted movement. It is also the reason why the convection was neglected in the boundary condition of the simulation.

In the simulation phase, only one pair of T_{amb} and T_d was used, and the quantitative conclusions were extended to other conditions. This extension is plausible because these two factors affect the readings of the individual thermometer; however, the qualitative relations remain valid.

By comparing the results with and without PAR, distinctly different patterns of the dimensional effects (height and radius) could be seen. Further, improvements in accuracy were attained for thermometers of the same size.

In the previous study on DHFM-based thermometers [11], the radius was decisive because a larger radius means a larger area covering the skin; therefore, the heat dissipated on boundaries could be greatly compensated for by the heat from the surrounding skin. In other words, the situation will approximate the theoretical assumption of DHFM. However, with PAR, the influence of radius becomes minor, which means that less heat is demanded from the skin, resulting from less radioactive heat dissipation.

In the simulation phase, multiple sizes (height and radius) were tested, but only the 22.0 mm radius and the 15.0 and 9.0 mm heights were adopted in the fabrication stage; this limitation was imposed to retain only compact wearable sizes. An increase in radius to more than 30 mm gives minor improvement but will bring about difficulties in installation and an obstructive feeling.

4.3. The Mock-Up Experiment. Only 3 combinations of the ambient temperature and the DBT were investigated here. For ambient temperature, lower value results in lower accuracy due to radiation, while the relatively higher DBT would contribute to a more accurate result [11]. Therefore, Combination 1 and Combination 3 can be used to confirm the span of error under moderate environment.

In the experimental phase, condition S was adopted to confirm the influence of the sponge in measuring accuracy. Its positive influence on measuring accuracy may be because of the heat-insulating effect shielding the thermometer and the surrounding surface of skin from the ambient environment. However, it is actually obstructive in practical measurement and may not be suitable for wearable use.

As previously mentioned, at the mock-up experiment stage, rubber sheets of different thicknesses were tested. As we expected, the thicker the sheet, the larger the measuring error. The two prototypes were able to measure the DBT (water temperature) accurately until the thickness was increased to 8.0 mm. The error became larger than 0.5°C for both thermometers when the sheet was increased to 10.0 mm in

thickness. The main reason may lie in the abrupt decrease of the reading of sensor T_1 . It may suggest that the experimental system is unable to deliver enough heat to the surface of the rubber sheet because of the lower heat conductivity of the rubber sheet [12] compared with skin. From this point of view, it is still possible for a DHFM-based thermometer to monitor the temperature about 10 mm under the skin. Further, to measure sites such as the forehead or the pit of the stomach with thin skin layer and bone immediately beneath [15], the measuring depth may be extended. Simulation or experiments on the measuring depth for these positions will be interesting.

For this kind of thermometer, which depends on a heat source from the human body, the resistance to the influence of ambient change is crucial. Judging from the results of these experiments, the error spans that came with the change of T_{amb} were shortened considerably with this PAR.

The theory of this method suggests that k here can be represented by the lengths of both heat paths. In practice, k can be optimized experimentally.

With the measurements in this study, we also tried to adjust k , denoted by k_A hereafter. k_A for both prototypes was different and k_A was set as 1.3 for the standard type and 1.1 for the thin type. For all the measurements, the accuracies were improved in varying degrees. What is more, the standard type in condition S achieves the accuracy level within $\pm 0.1^{\circ}\text{C}$. In the coming *in vivo* experiment to verify the thermometers' accuracies, adjustment of k seems beneficial in attaining the best accuracies.

5. Conclusions

This was a preliminary study on the capability of a new kind of noninvasive DBT thermometer based on DHFM. The simulation study based on FEM brought this theory to a practical stage by proposing a new component, the PAR, to improve the accuracy and stability.

The designs were then implemented and validated through mock-up experiments. The measurement errors were mitigated to a level of less than 0.5°C for both designs. The standard type of 15 mm in height had better accuracy than the thin type, as the simulation predicted. Even though further *in vivo* experiments are necessary for this kind of thermometer, we believe that it can serve as an alternative to the heat-generating noninvasive DBT thermometer and is suited for wearable modality.

Conflict of Interests

The authors declare that there is no conflict of interests regarding the publication of this paper.

Acknowledgments

This study was supported by the Keihanna Science City Healthcare Project of the Ministry of Education, Culture, Sports, Science and Technology, Japan, and by Tateisi Science and Technology Foundation, Japan. The authors wish

to thank Professor Yoshida Masaki for his kind support throughout the experiment stage.

References

- [1] P. Kyriacou, *Biomedical Sensors*, Momentum Press, London, UK, 2010.
- [2] R. H. Fox and A. J. Solman, "A new technique for monitoring the deep body temperature in man from the intact skin surface," *Journal of Physiology*, vol. 212, no. 2, pp. 8–10, 1971.
- [3] T. Tamura, T. Nemoto, and T. Togawa, "A zero-heat-flow transducer for monitoring perfusion blood temperature," *IEEE Transactions on Biomedical Engineering*, vol. 11, pp. 644–646, 1979.
- [4] L. P. J. Teunissen, J. Klewer, A. De Haan, J. J. De Koning, and H. A. M. Daanen, "Non-invasive continuous core temperature measurement by zero heat flux," *Physiological Measurement*, vol. 32, no. 5, pp. 559–570, 2011.
- [5] M. Yamakage and A. Namiki, "Deep temperature monitoring using a zero-heat-flow method," *Journal of Anesthesia*, vol. 17, no. 2, pp. 108–115, 2003.
- [6] D. S. Moran, A. Shitzer, and K. B. Pandolf, "A physiological strain index to evaluate heat stress," *The American Journal of Physiology—Regulatory Integrative and Comparative Physiology*, vol. 275, no. 1, pp. R129–R134, 1998.
- [7] M. D. Coyne, C. M. Kesick, T. J. Doherty, M. A. Kolka, and L. A. Stephenson, "Circadian rhythm changes in core temperature over the menstrual cycle: method for noninvasive monitoring," *American Journal of Physiology—Regulatory Integrative and Comparative Physiology*, vol. 279, no. 4, pp. R1316–R1320, 2000.
- [8] B. Bjorvatn and S. Pallesen, "A practical approach to circadian rhythm sleep disorders," *Sleep Medicine Reviews*, vol. 13, no. 1, pp. 47–60, 2009.
- [9] H.-C. Gunga, M. Sandsund, R. E. Reinertsen, F. Sattler, and J. Koch, "A non-invasive device to continuously determine heat strain in humans," *Journal of Thermal Biology*, vol. 33, no. 5, pp. 297–307, 2008.
- [10] K.-I. Kitamura, X. Zhu, W. Chen, and T. Nemoto, "Development of a new method for the noninvasive measurement of deep body temperature without a heater," *Medical Engineering & Physics*, vol. 32, no. 1, pp. 1–6, 2010.
- [11] M. Huang, T. Tamura, W. Chen, and S. Kanaya, "Evaluation of structural and thermophysical effects on the measurement accuracy of deep body thermometers based on dual-heat-flux method," *Journal of Thermal Biology*, vol. 47, pp. 26–31, 2015.
- [12] H. H. Pennes, "Analysis of tissue and arterial blood temperatures in the resting human forearm," *Journal of Applied Physiology*, vol. 1, no. 2, pp. 93–122, 1948.
- [13] F. P. Incropera, D. P. DeWitt, T. L. Bergman, and A. S. Lavine, *Fundamentals of Heat and Mass Transfer*, John Wiley & Sons, 6th edition, 2006.
- [14] T. Nemoto and T. Togawa, "Improved probe for a deep body thermometer," *Medical and Biological Engineering and Computing*, vol. 26, no. 4, pp. 456–459, 1988.
- [15] R. Y. Ha, K. Nojima, W. P. Adams Jr., and S. A. Brown, "Analysis of facial skin thickness: defining the relative thickness index," *Plastic and Reconstructive Surgery*, vol. 115, no. 6, pp. 1769–1773, 2005.

Research Article

Long-Term Measurement of Maternal Pulse Rate Dynamics Using a Home-Based Sleep Monitoring System

Ying Chen,¹ Wenxi Chen,¹ Kei-ichiro Kitamura,² and Tetsu Nemoto²

¹Biomedical Information Technology Laboratory, The University of Aizu, Ikki-machi, Aizuwakamatsu, Fukushima 965-8580, Japan

²Department of Laboratory Science, Institute of Medical, Pharmaceutical and Health Sciences, Kanazawa University, Kanazawa, Ishikawa 920-1192, Japan

Correspondence should be addressed to Wenxi Chen; wenxi@u-aizu.ac.jp

Received 13 May 2015; Accepted 24 August 2015

Academic Editor: Guiyun Tian

Copyright © 2016 Ying Chen et al. This is an open access article distributed under the Creative Commons Attribution License, which permits unrestricted use, distribution, and reproduction in any medium, provided the original work is properly cited.

Major adaptations occur in the maternal cardiovascular system during pregnancy and after delivery; knowledge of these changes is essential to the health management of pregnant women. This paper presents a longitudinal study and proposes a methodology to monitor daily pulse rates (PRs) and characterize the weekly changes in maternal PRs before and after delivery. PRs were recorded during nightly sleep using an automatic monitoring system. PRs of the nonpregnant woman were taken as a reference. Weekly PR properties were characterized by histogram and a two-Gaussian mixture model. A coupling use of sample entropy and pulse rate was applied to cluster the stages during recovery period after delivery. Results depicted a profile of individual's cardiac recovery process in late pregnancy and after delivery. The results reveal that maternal PRs show different patterns in various stages of recovery. Later stages of recovery seemed to require a much longer period. The present study introduced a convenient approach in long-term maternal cardiac condition monitoring.

1. Introduction

The maternal cardiovascular system undergoes remarkable changes during pregnancy before and after delivery to meet the increased metabolic demands of pregnancy [1–5]. Recent laboratory studies have reported some specific turning points during restoration when significant changes of cardiac dynamics can be observed [1–3, 6–9]. However, so far, the extent and the timing of cardiac recovery have been a subject of debate. Heart rate (HR) was reported to return slowly to baseline levels by 2–6 weeks postpartum in some studies [1, 2, 6, 9–11]. In other studies, a continued decrease in cardiac output was observed to last over the next 24 weeks [9]. However, there has also been concern that the changes in cardiac function associated with pregnancy might not ultimately return to prepregnancy levels [8, 9, 11]. The controversy was probably caused by different cohort and protocols used in data collection. Apart from cardiac adaptation, postpartum recovery can be influenced by many other factors, such as physical and age differences, mode of delivery, sufficient rest, appropriate exercise, and ample

supplies of nutrients. Besides, if sympathetic-predominant autonomic balance is not smoothly recovered, postpartum women might become vulnerable to external stressors and may develop mental disorders which can inversely postpone the cardiac recovery [12–14].

Previous studies on maternal HR were mostly based on short durations [8, 15–17]. Few longitudinal analyses were performed to assess continuous HR changes individually during pregnancy. Even less information is available on how these changes in the HR develop during the postpartum period. The knowledge of these changes is essential to the management of women with cardiovascular disease and also helpful in health monitoring during and after normal pregnancy [7, 8, 18, 19].

Conventional noninvasive techniques of electrocardiogram (ECG), echocardiography, and echo Doppler methods can be used for the measurement of maternal cardiac activity without risk or discomfort to the subject. However, they are not suitable for daily application over a long-term period because of high cost and complexity. In the current study, we conducted a long-term observation of maternal pulse rate

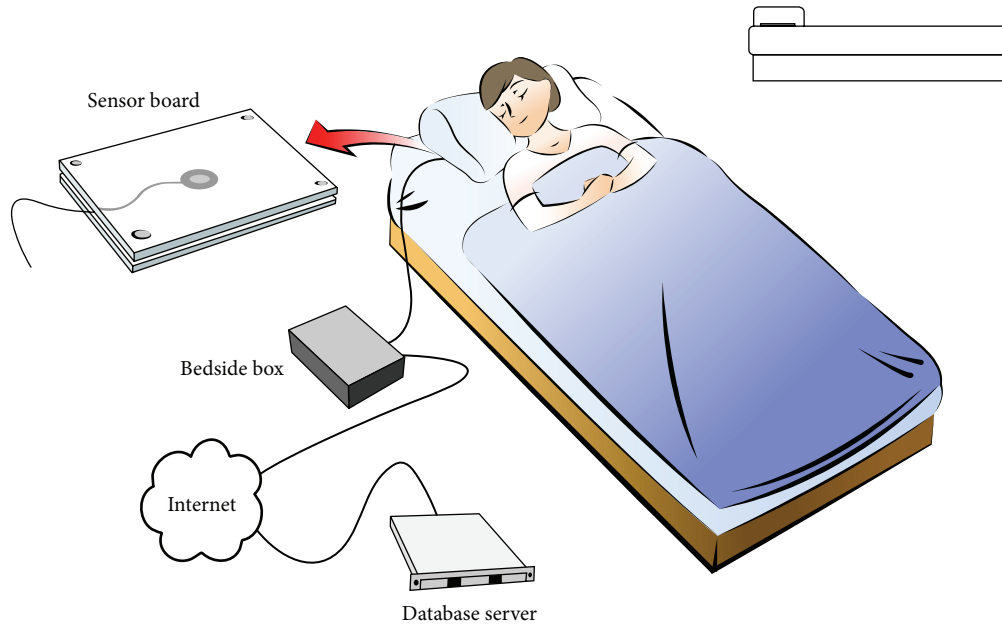


FIGURE 1: Experiment setting for long-term automatic data collection during sleep.

(PR) using a simple and low-cost sleep monitoring system during late pregnancy and up to 1 year after delivery. Pulse signal has been found as effective as ECG in measuring the parameters of heart rate variability (HRV) [20], widely applied for clinical physiological measurements [21–23], but its application for maternal cardiology during pregnancy is still rarely reported up to date. In this paper, the combined use of histogram and a two-Gaussian mixture model was applied to characterize weekly PR property. A coupling of nonlinear dynamical analysis by sample entropy (SampEn) and PR was used to classify stages after delivery. Some novel information about maternal cardiac recovery can be revealed by the introduced model and the combination of the features. This study serves to introduce a convenient protocol in daily PR monitoring and explore the potential applications of daily PR in revealing the progression of cardiac functions during pregnancy and its restoration after parturition.

2. Materials and Methods

2.1. Subjects. A 30-year-old healthy nulliparous woman (BMI before pregnancy: 21.2) with a singleton pregnancy was enrolled in this study. One year of PR data from a healthy nonpregnant female volunteer (BMI: 20.0) in her thirties was studied for reference. She did not have a history of pregnancy. Both subjects were free of any cardiac pathology or smoking or drinking habits or suffered from anxiety. The pregnant woman was in the absence of pregnancy induced hypertension and did not take any medicine during the recording period. She had a vaginal delivery and chose a mixed feeding (breast and bottle) after delivery. From 35th week postpartum, the baby had not lived with the mother. Informed consents were obtained from both subjects.

2.2. Experiment Setting and Data Collection. Both PR recordings were performed at each volunteer's home during their

nightly sleep. Pulse signal was acquired by our own designed sleep monitoring system as shown in Figure 1, and the details of the system had been described in previous publications [24, 25]. In order to facilitate usability in daily data collection, the system was developed based on Internet for daily measurement which causes neither restriction nor discomfort and brings no intervention to users' daily life. It can send the data automatically to a database server through Internet without any operations by the user so that a high rate in daily data collection can be achieved over long term. This system consisted of a sensor board, a bedside box, and a network database server. The sensor board was installed under the subject's pillow to measure the occipital pressure signals caused by heartbeats and respiratory movements. The bedside box amplified the analog pressure signal, digitized the signal at a sampling rate of 100 Hz, and transmitted the data stream continuously to a database server via an Internet connection. This monitoring system was always in standby state. It was switched on 30 s after the subject lay down in the bed and was terminated and went back into standby mode 5 min after the subject rose in the morning.

Digital signal processing for pulse wave peak detection was implemented using a wavelet-based algorithm [26]. Figure 2 shows a sample of a raw pressure signal and the corresponding reconstructed pulse waveform. The pulse interval (PI) series was obtained as the sequence of the times occurring between each pair of consecutive pulse wave peaks. The corresponding PR (with unit of "beat per minute") can be computed by $PR = 1 \text{ (minute)} \times 60 \text{ (s)} \times 1000 \text{ (ms)}/PI \text{ (in ms)} = 60000/PI \text{ (beat per minute)}$. Performance of PR detection from the pressure signal was evaluated on the beat-by-beat basis using manual method by visually comparing with detections from finger photoplethysmogram measured simultaneously. The sensitivity and positive predictivity of PR detection were 98.91% and 98.47%, respectively [26].

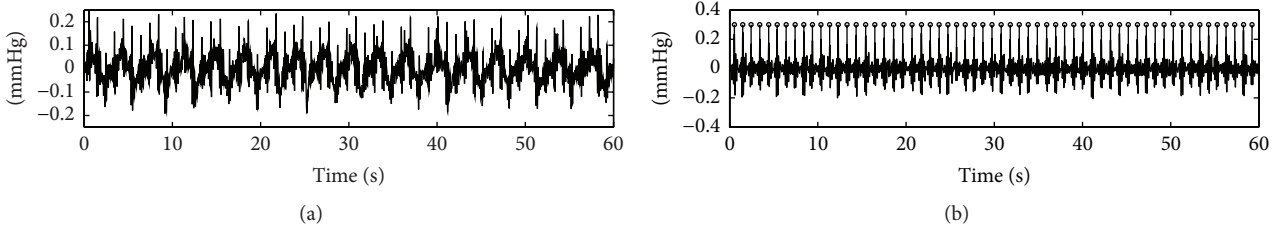


FIGURE 2: An example of fully detected beat-by-beat pulse rate in one minute from the pregnant woman. (a) The raw pressure signal, (b) the reconstructed pulse-related waveform. Open circles “o” indicate the detected characteristic points for pulse rate determination.

Data recording from the pregnant woman started from the late trimester (in the 30th week after conception, July 1, 2010) and ended on the 63rd week postpartum (November 30, 2011). Delivery occurred in the 40th week plus 2 days of gestation (September 14, 2010). A total of 373 nights of data were available for analysis. The woman stayed in the hospital for the first week after delivery; so the data was not recorded during that period. From the 2nd week to the 6th week, she returned home but did not sleep regularly in her original bed for taking care of the baby in another bed. Only sporadic data were collected during that period. A second lost period was from the 26th week to the 34th week postpartum because the subject was absent. Other sporadic data losses were because the subject was away from home. In the nonpregnant control individual, PR data were taken from April 1, 2004, to April 1, 2005; data were available for a total of 332 nights. Only PR data segments measured from 01:00 am to 07:00 am were used in this analysis.

2.3. Weekly Pulse Rate Modeling. We applied histograms graphically to represent the distribution of weekly PR data. A two-Gaussian mixture model was used to fit each weekly histogram to detect its two modes. Since weekly PR distributions may present different patterns throughout the recording period, they might be unimodal (single peak), flat (no peak), or bimodal (two distinct peaks). Different patterns might indicate different stages of PR development during pregnancy and recovery. Thus, a mixture model can better describe each distribution and help in understanding PR development and locating the transitions points of PR changes. The Gaussian model can be described by the following formula:

$$f(x) = \sum_{i=1}^2 a_i e^{-(x-b_i)^2/c_i^2}, \quad i = 1, 2, \quad (1)$$

where a_i was the peak value of the i th model, indicating the percentage of the PR mean value in the i th Gaussian component, b_i was the peak position of the i th model referring to the mean value of PR in the i th Gaussian component, and c_i was related to the standard deviation (SD) of the PR data series fitted by the i th model. All the signal processing and data analysis were implemented using MATLAB and its “Curve Fitting Toolbox.”

2.4. Sample Entropy. Sample entropy (SampEn), a refinement of the approximate entropy (ApEn) of statistics introduced by

Pincus [27], is one of the nonlinear analysis methods which has been widely used in both cardiovascular research and clinical applications. Here, we applied SampEn coupled with PR to prove whether the stages that we defined based on characteristics observed from the weekly PR models can be well clustered or not. SampEn was defined as the negative natural logarithm of the conditional probability that, within a data set of length N , two sequences similar to m points (within a given tolerance r) will remain similar when the next point is included, without counting self-matches. It reduced the bias of ApEn and has closer agreement with theory for datasets with known probabilistic content. Lower value of SampEn indicates more self-similarity and regular time series (less complexity), whereas higher value indicates more irregularity (high complexity) and therefore is difficult to predict. SampEn can be calculated as follows.

For a given time series $X = x_1, x_2, \dots, x_N$, N is the total number of the data points. To form m -length subseries X_{im} within X : $X_{im} = [x_i, x_{i+1}, \dots, x_{i+m-1}]$, where $i = 1, 2, \dots, N - m + 1$ and m is the embedding dimension. Comparisons were then made against each X_{im} :

$$B_i = \frac{n_i(m, r)}{N - m + 1}, \quad (2)$$

where B_i is the probability that any vectors will be similar to X_{im} and $n_i(m, r)$ is the number of vectors in X_{jm} that are similar to X_{im} if and only if

$$d(X_{im}, X_{jm}) \leq r, \quad i \neq j, \quad (3)$$

where $d(X_{im}, X_{jm})$ is defined as the maximal absolute difference between X_{im} and X_{jm} and r specifies the threshold for similarity (tolerance).

The total average probability can be calculated as

$$B_m(r) = \frac{1}{N - m + 1} \sum_{i=1}^{N-m+1} B_i(m, r). \quad (4)$$

$B_{m+1}(r)$ can be calculated in a similar process for an embedded dimension $m + 1$.

Finally, SampEn, given m and r , can be calculated by

$$\text{SampEn}(m, r) = \log \left[\frac{B_m(r)}{B_{m+1}(r)} \right]. \quad (5)$$

To calculate SampEn, m and r are critical and may differ in different types of datasets. So far, no guidelines exist for

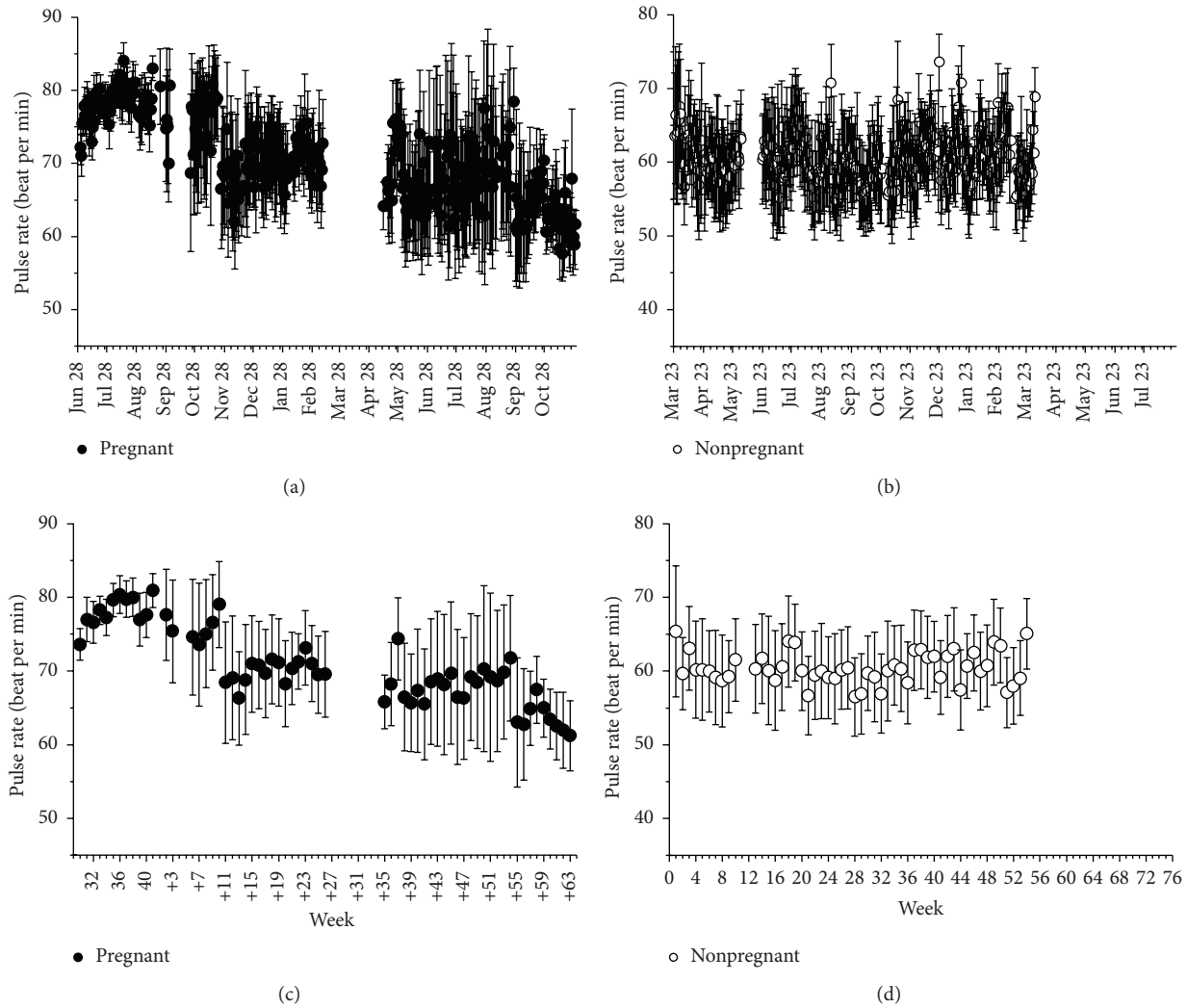


FIGURE 3: Daily and weekly fluctuations of PR in both the pregnant subject ((a) and (c)) and the nonpregnant control individual ((b) and (d)). (a) and (b) show the daily variations, while (c) and (d) present weekly changes of PR throughout the entire recording period.

optimizing their values; recommended values are the use of r between 0.1 and 0.25 and m of 1 or 2 for data length N ranging from 100 to 5,000 [27, 28].

3. Results

3.1. Daily and Weekly Pulse Rate Fluctuations. Daily mean PR and its SD were obtained from PR data series measured during one-night sleep. Weekly mean PR and its SD were calculated based on all data measured in the week. Figure 3 depicts the daily and weekly profiles of PR fluctuations of both subjects throughout the recording period. In the pregnant woman, daily PR changed in both its mean level and its SD throughout the whole period. The weekly mean PR (74 ± 2 bpm) increased from the 30th week of gestation and reached a peak (80 ± 3 bpm) on the 36th week. It then declined slightly during the 39th week (77 ± 4 bpm) at 2 weeks before childbirth. A sudden increase in PR mean level (81 ± 2 bpm) was observed on the day of delivery. It dropped within 6 weeks after delivery accompanied by

a remarkable increase in the SD of the mean compared with that on the date of parturition. The PR raised in the following 4 weeks to 79 ± 6 bpm by the 10th week. A sudden drop occurred in the 11th week postpartum to around 68 bpm. Thereafter, this declination slowed and the PR kept stable with only small variations over the following 44 weeks. There was a significant increase (by 9%) in PR mean level on the 37th week postpartum. Another notable decrease in the PR happened on the 55th week postpartum (by 12% compared with the previous week, to around 63 bpm), accompanied by a reduction in the SD. Conversely, both daily and weekly PR dynamics of the nonpregnant control subject remained stable throughout the recording period, with only small variations. On average, she had a mean PR of 60 ± 6 bpm with occasional higher PRs during sleep.

3.2. Weekly Pulse Rate Properties. To characterize the PR properties, weekly histograms and their skewness values for both subjects are plotted in Figures 4 and 5. In the healthy nonpregnant woman, the PR histogram presented

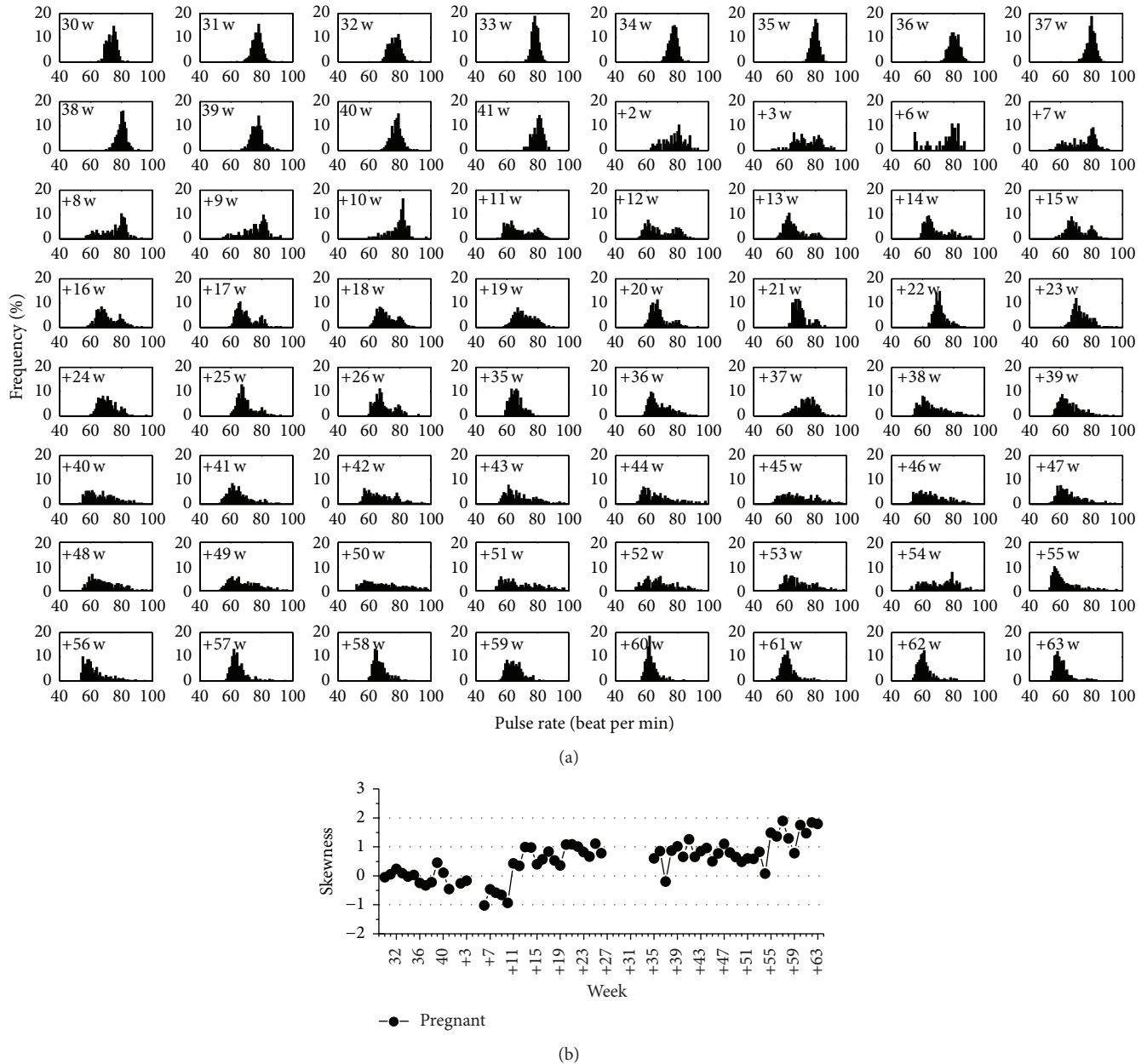


FIGURE 4: Characteristics of weekly PR distributions in the pregnant subject. (a) Weekly PR histograms, (b) weekly variations of the skewness index.

an approximately asymmetrical or a slightly positive skewed unimodal pattern as shown in Figure 5. In contrast, the pregnant woman demonstrated obvious weekly changes in the PR distribution with the progress of pregnancy (Figure 4).

In Figure 4, the data presented an approximately asymmetric but rather leptokurtic distribution from the 30th week indicating that most PRs were within a limited high level. The PR values quickly changed to wide and platykurtic distributions from the 2nd week after delivery indicating a severe increase in pulse rate variability. From the 2nd to 10th weeks postpartum, the PR presented a negatively skewed distribution (Figure 4(b)). In the 11th week postpartum, the PR distribution suddenly skewed to the right. A bimodal and

positively skewed distribution was first detected within this period, indicating a transition point of the PR's development. This positive reversion of skewness suggested that the acceleration of PR was decreasing. The positively skewed distribution as well as the mean level of weekly PR waved around 70 ± 2 bpm from the 11th week for the following 15 weeks. The weekly PR histograms in the 20th week changed from a wide platykurtic pattern back to a high and narrow distribution. This was during the transition time in which a previous study reported a restoration of the cardiovascular activities postpartum [9, 30]. Indeed, the pattern of PR distribution after the 20th week was similar to that of the nonpregnant woman, as shown in Figure 4(b). However, the average PR

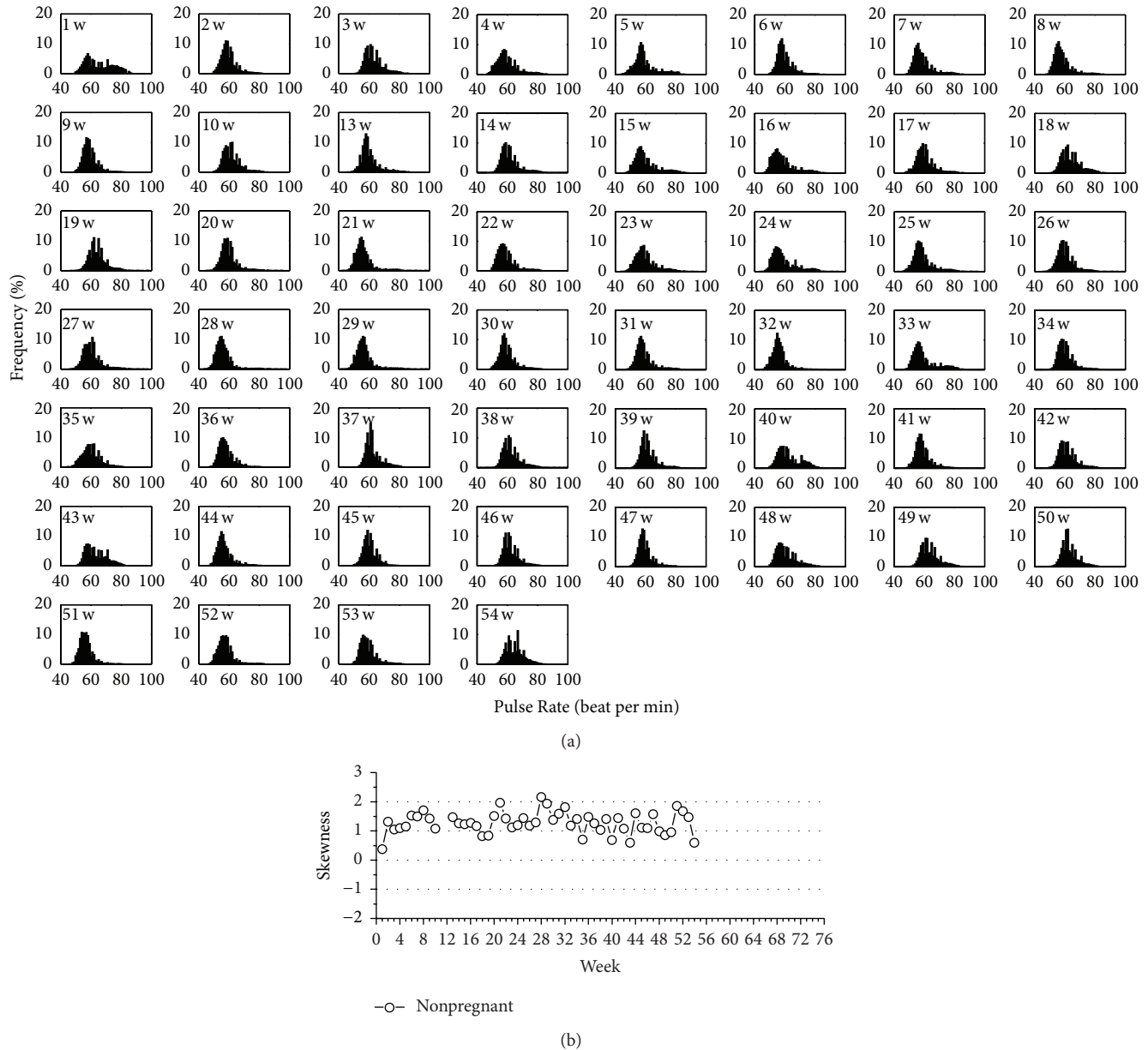


FIGURE 5: Characteristics of weekly PR distributions in the nonpregnant subject. (a) Weekly PR histograms, (b) weekly variations of the skewness index.

level was still high around 68 bpm and the PR pattern was observed to remain unstable (Figure 4(a)). In other words, the recovery of cardiac function was still underway at the 20th week postpartum. This was confirmed by the 37th week, when the PR distribution gradually became wide and platykurtic again. This period lasted a long time until the 55th week postpartum, when there was a second significant reduction (from 72 to 63 bpm) in PR mean level. Meanwhile, the shape of the histogram changed from a wide-base, platykurtic pattern back to a leptokurtic pattern as shown in Figure 4(a). Most of the PR data declined to around 64 bpm with only a few higher PRs creating skewness to the right. This transformation indicated a deceleration of the increased PR and both the pattern and PR level entered a stable state.

By this time, both the skewness and histogram pattern of PR distribution appear similar to that of the healthy nonpregnant woman, which may be inferred that the subject's PR dynamics had readjusted and recovered to a normal physical condition.

3.3. Weekly Indexes of the Gaussian Model. The weekly indexes of the fitted Gaussian model are shown in Figure 6. In the pregnant woman (a, c), the mean PRs of the two components were rather close to each other in the late trimester after the 30th week of gestation. A departure between the two peaks was detected after delivery. After the 6th week postpartum, the mean PR of the main component stayed high while the adjoining mean PR of the subcomponent headed

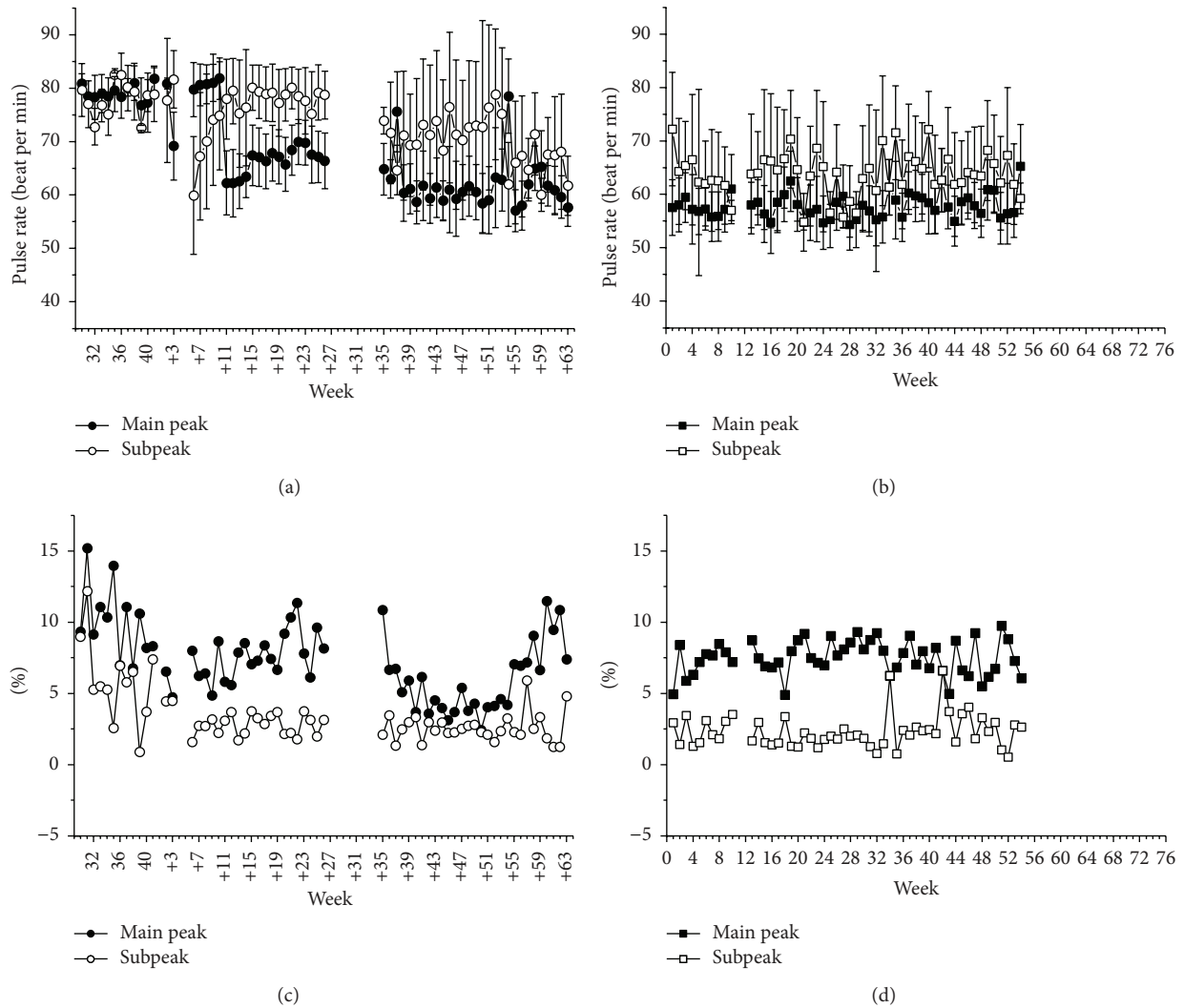


FIGURE 6: Changes in the two components of the weekly PR in both the pregnant ((a) and (c)) and nonpregnant ((b) and (d)) subjects. (a) and (b) show fluctuations of the mean PR values of the two components. (c) and (d) present variations in the respective percentage of each mean PR.

down to a significantly low level accompanied by an increase in the SD. A reversal of the two peaks took place on the subsequent 11th week, when the main mean PR dropped and left the mean PR of the subcomponent at a high level. The percentage of the main peak also increased. On the 37th week postpartum, the main mean PRs increased remarkably (by 12 bpm) accompanied by a decrease in the mean PR of the subcomponent (by 7 bpm) and a sharp reduction in the main peak percentage as shown in Figure 6(a). The percentages of both peaks approached each other at the 55th week after delivery and the main peak percentage rose back. Compared with that in the pregnant woman, the two components in the weekly PR data of the control subject appeared to be in a steady state throughout the whole period (Figures 6(b) and 6(d)). The mean PR of both components maintained a stable distance with each other and undulated at their own level (58 ± 5 bpm versus 64 ± 9 bpm). The percentages of the two peaks also remained stable with no apparent changes ($8 \pm 1\%$ versus $2 \pm 1\%$).

3.4. Clustering the Stages. Based on above observations, we found some specific turning points during PR dynamic recovery, such as 6th, 11th, 20th, 37th, and 55th weeks. Some of them have been reported in previous publications to indicate specific point of time when significant physiological changes take place, while others have not yet been revealed. We segmented the whole period recorded after delivery into six stages divided by the specific weeks as mentioned above (Table 1). A coupling of weekly SampEn and PR was used to approve our hypothesis of whether the six stages can be well clustered. Figures 7 and 8 show the weekly SampEn versus weekly PR extracted from pulse signal of the pregnant woman. It can be observed that the distributions of weekly SampEn and PR representing different stages are presented in much more compact and well-defined clusters when using the main (Figure 8(a)) or subpeaks (Figure 8(b)) of weekly PRs than using only the mean PRs (Figure 7). Centers of each cluster are listed in Table 2. It further proves that the recovery of cardiac functions underwent different stages, and the use

TABLE 1: Segmentation of recorded data and main features of each stage.

Stage	Period (week)	PR (bpm) (mean \pm SD)	Histogram	Two peaks of Gaussian model	SampEn (mean \pm SD)
AP ^a	30th~41th	78 \pm 2	Asymmetric, leptokurtic	Similar High	3.15 \pm 0.17
PP ^b 1	+1th~+5th	77 \pm 2	Negatively skewed, platykurtic	Similar High	3.35 \pm 0.22
PP 2	+6th~+10th	76 \pm 2	Negatively skewed, platykurtic	Main peak stays high; subpeak drops down	3.96 \pm 0.03
PP 3	+11th~+19th	70 \pm 2	Positively skewed, platykurtic, and bimodal	Main peak drops down; subpeak reverses high	3.63 \pm 0.07
PP 4	+20th~+36th	70 \pm 2	Positively skewed, leptokurtic	Main peak stays low; subpeak stays high	3.43 \pm 0.09
PP 5	+37th~+54th	69 \pm 2	Positively skewed, platykurtic	Both decrease	3.62 \pm 0.08
PP 6	+55th~+63rd	64 \pm 2	Positively skewed, leptokurtic	Both come close together	3.30 \pm 0.08
Nonpregnant woman	Whole period	60 \pm 2	Positively skewed, leptokurtic	Both stay close together	2.40 \pm 0.20

“+” indicates weeks after delivery.

^aAntepartum.

^bPostpartum.

TABLE 2: The center of each cluster.

Stage	SampEn versus weekly mean PR	SampEn versus main peak of weekly PR model	SampEn versus subpeak of weekly PR model
AP ^a	(3.15, and 74)	(3.15, and 79)	(3.15, and 78)
PP ^b 1	(3.35, and 77)	(3.35, and 75)	(3.35, and 80)
PP 2	(3.96, and 76)	(3.96, and 81)	(3.96, and 75)
PP 3	(3.63, and 70)	(3.63, and 65)	(3.63, and 78)
PP 4	(3.43, and 70)	(3.43, and 67)	(3.43, and 77)
PP 5	(3.62, and 69)	(3.62, and 62)	(3.62, and 72)
PP 6	(3.30, and 64)	(3.30, and 61)	(3.30, and 66)

^aAntepartum.

^bPostpartum.

of Gaussian model can better reveal the characteristics of the under dynamics of PR development.

4. Discussion

Late pregnancy is associated with dramatic cardiovascular adaptations. Increased cardiac output, hormonal changes, increased circulation burden, and aortocaval compression as a result of the gravid uterus are responsible for an increased PR when supine and right lateral decubitus positions are assumed during sleep [29]. The rise in cardiac output in late pregnancy is mostly caused by a rise in the HR for maintaining an elevated cardiac output as term approaches [6, 7, 30–32]. We observed that the mean PR increased after the 31st week during pregnancy compared with the 30th week. This significant rise might have been because of the fetus's weight gain after the 31st week. This could increase aortocaval compression as well as the circulation burden. Another

possible reason could be the rise in plasma volume through increased aldosterone levels. The PR rose apparently during the late phase of the last trimester but began to decrease 2 weeks before term. This declination was in accordance with previous reports that the HR decreases slightly in the final weeks of pregnancy [2]. Greater aortocaval compression was expected to interfere with autonomic nervous activity with induced higher sympathetic activation and greater vagal suppression. Therefore, the relief from aortocaval compression after delivery might have contributed to an increase in HRV.

The PR declined shortly after delivery and reached a relatively low level. This was in accordance with a report that most of the decrease, including cardiac output and HR, occurs within 2 weeks after delivery [2, 6, 7, 9]. However, the PR of our subject did not return to normal within 6 weeks, as asserted in previous studies [1, 2, 6, 9–11]. Conversely, it increased from the 7th week to the 11th week postpartum. SampEn also increased significantly during this

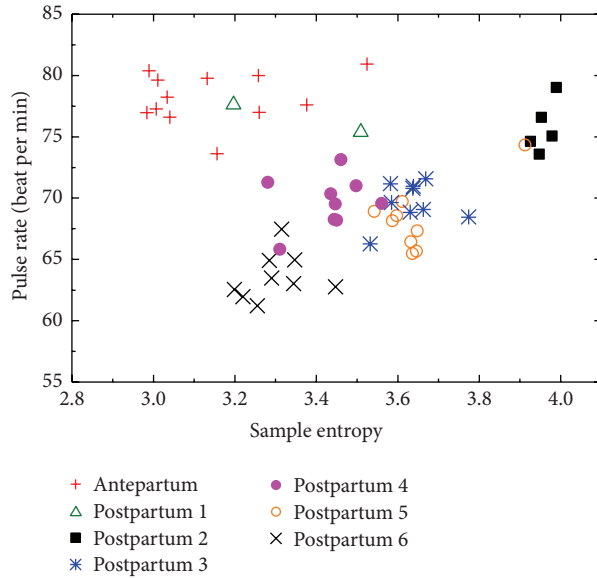


FIGURE 7: Plot of weekly PRs versus weekly SampEn features of different stages before and after delivery.

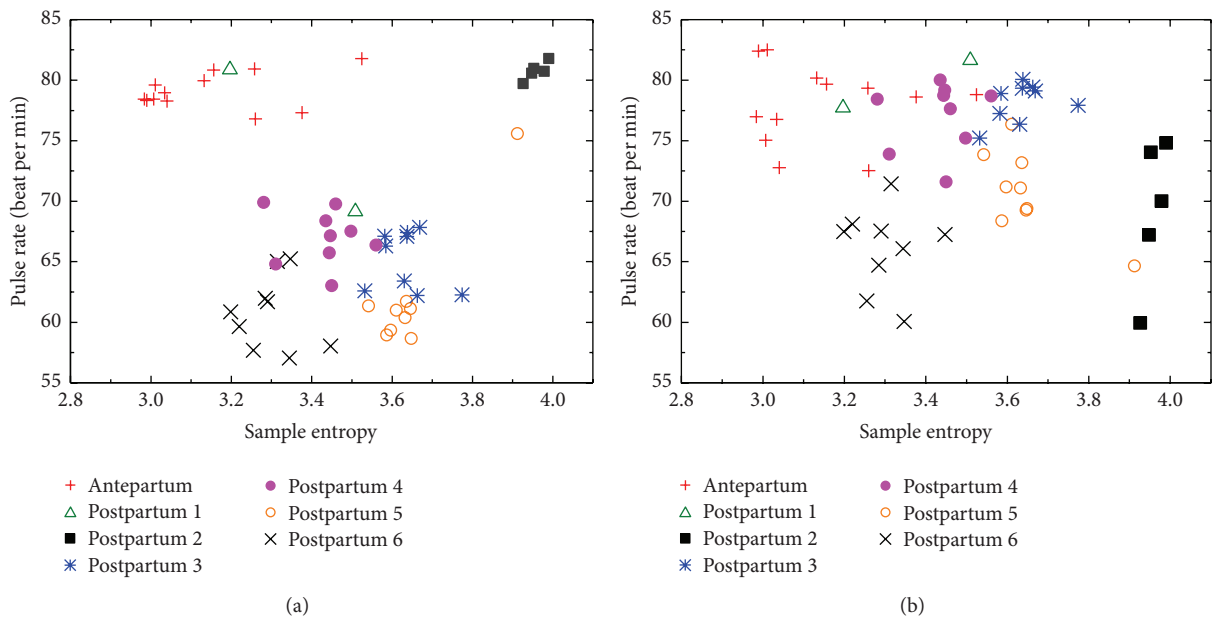


FIGURE 8: Plots of main peaks of weekly PRs versus weekly SampEn features (a) as well as subpeaks of weekly PRs versus weekly SampEn features (b) of different stages during before and after delivery.

stage (Figures 7 and 8) indicating an increase in HR non-linearity. Possible reasons for this rebound might be that although the circulation burden was released postpartum, the subject's body still needed time to readjust to a new physiological state and to recover from postpartum exhaustion, uterine contraction, "after-pains," perineal pain, and general edema. In one report, the recovery period was around 20 weeks [7, 9]. However, other studies indicated that cardiac activities might not return to original levels even after 1 year [8, 11].

Previous studies reported different times or even an indefinite time for recovery by recording heart rate changes. Possible reasons might be due to different data collection and

analysis methods. Most of previous conclusions were based on data collected from regular physical examinations at intermittently rather than on a daily continuous base. Therefore, it is difficult to obtain a complete profile. In our study, the sleep monitoring system enabled a longitudinal study over a long period. Compared with conventional measurements, it seemed to be more effective in monitoring PR dynamics over time. In addition, signals were recorded during the restful state of nighttime sleep periods while the subject was unconscious, which could avoid interference from the outside environment and the subject's daily activities. Therefore, it can better reflect the underlying biorhythms. This similar

protocol had been proved to success in detection of health changes in a patient with cardiac disorder in our previous research [24].

HR and HRV are two of the most important parameters in evaluating cardiac function. Previous studies usually calculated HR or HRV within limited recording period. Even the averaged HR have dropped to a reference baseline, the cardiac system may be still not fully recovered. A combined use of histogram and a two-Gaussian mixture model can visually reveal the dynamic transition of PR by decomposing weekly PR into two components. In Figure 7, stages 3 and 4 during postpartum period cannot be classified well when using only the weekly mean PR. But after decomposing them into two components, stages can be clustered and distinguished better with each other as shown in Figure 8. Thus, the introduced model enables a better capture of the characteristics in adaptations and the restorations process of the cardiac function during normal pregnancy. We have summarized the main features of different stages in Table 1.

Although only one pregnant woman was included in the current study, it is worth noting that our observations are in quite accordance with some previous reports regarding the time point for significant PR changes during pregnancy and after delivery [2, 6, 7]. Particularly, one study [8] depicted a cardiovascular data profile before, during, and 52 weeks after normal pregnancy based on intermittent collected data from 30 women. The profile was quite similar with our results obtained from daily measurement of a single subject. However, whether the PR dynamics return to a preconception level cannot be concluded. We still need the prepregnant or early pregnant data for reference. Possible time and stages required for recovery have been also suggested by our study; even though conclusive results cannot be given before more subjects can be included, at least it can be derived from our findings that recovery from pregnancy may take longer time than previously reported 6 or 20 weeks.

5. Conclusions

We have introduced a feasible approach to characterize daily PR dynamics during pregnancy and after delivery. In this study, the PR did not decline steadily after delivery but differed in stages. Relief of circulation burden and aortocaval compression as a result of delivery might be the main cause of a significant return to normal PR values during an early stage after delivery. Postpartum changes in hormones—including readjustments of aldosterone, estrogen, and progesterone levels—might also contribute to the return to normal cardiac activity after delivery. However, the later stages of recovery seemed to require a much longer period. In our study, the pregnant woman underwent five stages in recovery and it took about one year for the PR dynamics to readjust to a normal physical condition. We hope the findings can provide helpful applications in maternal cardiac monitoring and studying the maternal cardiac progression during pregnancy and after delivery.

Conflict of Interests

The authors declare that there is no conflict of interests regarding the publication of this paper.

Acknowledgments

The authors would like to thank the volunteers for their endurance in daily data collection and colleagues in the research project. The support provided in part by the University of Aizu Competitive Research Funding P-21 is gratefully acknowledged.

References

- [1] S. Hunter and S. C. Robson, "Adaptation of the maternal heart in pregnancy," *British Heart Journal*, vol. 68, no. 12, pp. 540–543, 1992.
- [2] J. J. Duvekot and L. L. H. Peeters, "Maternal cardiovascular hemodynamic adaptation to pregnancy," *Obstetrical & Gynecological Survey*, vol. 49, no. 12, pp. S1–S14, 1994.
- [3] T. L. Weissgerber and L. A. Wolfe, "Physiological adaptation in early human pregnancy: adaptation to balance maternal-fetal demands," *Applied Physiology, Nutrition and Metabolism*, vol. 31, no. 1, pp. 1–11, 2006.
- [4] O. Savu, R. Jurcuț, S. Giușcă et al., "Morphological and functional adaptation of the maternal heart during pregnancy," *Circulation: Cardiovascular Imaging*, vol. 5, no. 3, pp. 289–297, 2012.
- [5] K. Melchiorre, R. Sharma, and B. Thilaganathan, "Cardiac structure and function in normal pregnancy," *Current Opinion in Obstetrics and Gynecology*, vol. 24, no. 6, pp. 413–421, 2012.
- [6] A. C. C. van Oppen, R. H. Stigter, and H. W. Bruinse, "Cardiac output in normal pregnancy: a critical review," *Obstetrics & Gynecology*, vol. 87, no. 2 I, pp. 310–318, 1996.
- [7] S. Fujitani and M. R. Baldisseri, "Hemodynamic assessment in a pregnant and peripartum patient," *Critical Care Medicine*, vol. 33, no. 10, pp. S354–S361, 2005.
- [8] J. F. Clapp III and E. Capeless, "Cardiovascular function before, during, and after the first and subsequent pregnancies," *The American Journal of Cardiology*, vol. 80, no. 11, pp. 1469–1473, 1997.
- [9] S. C. Robson, W. Dunlop, M. Moore, and S. Hunter, "Haemodynamic changes during the puerperium: a Doppler and M-mode echocardiographic study," *British Journal of Obstetrics and Gynaecology*, vol. 94, no. 11, pp. 1028–1039, 1987.
- [10] W. C. Mabie, T. G. DiSessa, L. G. Crocker, B. M. Sibai, and K. L. Arheart, "A longitudinal study of cardiac output in normal human pregnancy," *American Journal of Obstetrics & Gynecology*, vol. 170, no. 3, pp. 849–856, 1994.
- [11] E. L. Capeless and J. F. Clapp, "When do cardiovascular parameters return to their preconception values?" *American Journal of Obstetrics & Gynecology*, vol. 165, no. 4, pp. 883–886, 1991.
- [12] N. Kudo, H. Shinohara, and H. Kodama, "Heart rate variability biofeedback intervention for reduction of psychological stress during the early postpartum period," *Applied Psychophysiology Biofeedback*, vol. 39, no. 3-4, pp. 203–211, 2014.
- [13] A. Shimizu, H. Nishiumi, Y. Okumura, and K. Watanabe, "Depressive symptoms and changes in physiological and social

- factors 1 week to 4 months postpartum in Japan,” *Journal of Affective Disorders*, vol. 179, pp. 175–182, 2015.
- [14] F. T. Burgut, A. Bener, S. Ghuloum, and J. Sheikh, “A study of postpartum depression and maternal risk factors in Qatar,” *Journal of Psychosomatic Obstetrics and Gynecology*, vol. 34, no. 2, pp. 90–97, 2013.
- [15] N. Sohnchen, K. Melzer, B. M. Tejada et al., “Maternal heart rate changes during labour,” *European Journal of Obstetrics & Gynecology and Reproductive Biology*, vol. 158, pp. 173–178, 2011.
- [16] D. J. Sherman, E. Frenkel, Y. Kurzweil, A. Padua, S. Arieli, and M. Bahar, “Characteristics of maternal heart rate patterns during labor and delivery,” *Obstetrics & Gynecology*, vol. 99, no. 4, pp. 542–547, 2002.
- [17] S. C. Robson, R. J. Boys, S. Hunter, and W. Dunlop, “Maternal hemodynamics after normal delivery and delivery complicated by postpartum hemorrhage,” *Obstetrics and Gynecology*, vol. 74, no. 2, pp. 234–239, 1989.
- [18] P. Ray, G. J. Murphy, and L. E. Shutt, “Recognition and management of maternal cardiac disease in pregnancy,” *British Journal of Anaesthesia*, vol. 93, no. 3, pp. 428–439, 2004.
- [19] A. Wacker-Gußmann, M. Thriemer, M. Yigitbasi, F. Berger, and N. Nagdyman, “Women with congenital heart disease: long-term outcomes after pregnancy,” *Clinical Research in Cardiology*, vol. 102, no. 3, pp. 215–222, 2013.
- [20] C. V. Russoniello, V. Pougatchev, E. Zhirnov, and M. T. Mahar, “A measurement of electrocardiography and photoplethysmography in obese children,” *Applied Psychophysiology Biofeedback*, vol. 35, no. 3, pp. 257–259, 2010.
- [21] F. Javed, P. M. Middleton, P. Malouf et al., “Frequency spectrum analysis of finger photoplethysmographic waveform variability during haemodialysis,” *Physiological Measurement*, vol. 31, no. 9, pp. 1203–1216, 2010.
- [22] G. S. H. Chan, A. Fazalbhoy, I. Birznieks, V. G. Macefield, P. M. Middleton, and N. H. Lovell, “Spontaneous fluctuations in the peripheral photoplethysmographic waveform: roles of arterial pressure and muscle sympathetic nerve activity,” *The American Journal of Physiology—Heart and Circulatory Physiology*, vol. 302, no. 3, pp. H826–H836, 2012.
- [23] J. Allen and A. Murray, “Age-related changes in the characteristics of the photoplethysmographic pulse shape at various body sites,” *Physiological Measurement*, vol. 24, no. 2, pp. 297–307, 2003.
- [24] Y. Chen and W. Chen, “Long-term tracking of a patient’s health condition based on pulse rate dynamics during sleep,” *Annals of Biomedical Engineering*, vol. 39, no. 12, pp. 2922–2934, 2011.
- [25] W. Chen, X. Zhu, and T. Nemoto, “A new sensory device and optimal position for monitoring HR/RR during sleep,” in *World Congress on Medical Physics and Biomedical Engineering, September 7–12, 2009, Munich, Germany*, vol. 25/7 of *IFMBE Proceedings*, pp. 126–129, Springer, Berlin, Germany, 2009.
- [26] X. Zhu, W. Chen, T. Nemoto et al., “Real-time monitoring of respiration rhythm and pulse rate during sleep,” *IEEE Transactions on Biomedical Engineering*, vol. 53, no. 12, pp. 2553–2563, 2006.
- [27] S. M. Pincus, “Approximate entropy as a measure of system complexity,” *Proceedings of the National Academy of Sciences of the United States of America*, vol. 88, no. 6, pp. 2297–2301, 1991.
- [28] J. S. Richman and J. R. Moorman, “Physiological time-series analysis using approximate and sample entropy,” *The American Journal of Physiology—Heart and Circulatory Physiology*, vol. 278, no. 6, pp. H2039–H2049, 2000.
- [29] G.-Y. Chen, C.-D. Kuo, M.-J. Yang, H.-M. Lo, and Y.-S. Tsai, “Return of autonomic nervous activity after delivery: role of aorticaval compression,” *British Journal of Anaesthesia*, vol. 82, no. 6, pp. 932–934, 1999.
- [30] S. C. Robson, W. Dunlop, R. J. Boys, and S. Hunter, “Cardiac output during labour,” *British Medical Journal*, vol. 295, no. 6607, pp. 1169–1172, 1987.
- [31] F. Westling, I. Milsom, H. Zetterstrom, and B. Ekstrom-Jodal, “Effects of nitrous oxide/oxygen inhalation on the maternal circulation during vaginal delivery,” *Acta Anaesthesiologica Scandinavica*, vol. 36, no. 2, pp. 175–181, 1992.
- [32] J. G. Ouzounian and U. Elkayam, “Physiologic changes during normal pregnancy and delivery,” *Cardiology Clinics*, vol. 30, no. 3, pp. 317–329, 2012.

Review Article

Challenges and Issues in Multisensor Fusion Approach for Fall Detection: Review Paper

Gregory Koshmak,¹ Amy Loutfi,² and Maria Linden¹

¹*School of Innovation, Design and Engineering, Mälardalen University, Högscoleplan 1, 721 23 Västerås, Sweden*

²*Center for Applied Autonomous Sensor Systems (AASS), Örebro University, Fakultetsgatan 1, 701 82 Örebro, Sweden*

Correspondence should be addressed to Gregory Koshmak; gregory.koshmak@mdh.se

Received 14 May 2015; Revised 23 July 2015; Accepted 5 August 2015

Academic Editor: Toshiyo Tamura

Copyright © 2016 Gregory Koshmak et al. This is an open access article distributed under the Creative Commons Attribution License, which permits unrestricted use, distribution, and reproduction in any medium, provided the original work is properly cited.

Emergency situations associated with falls are a serious concern for an aging society. Yet following the recent development within ICT, a significant number of solutions have been proposed to track body movement and detect falls using various sensor technologies, thereby facilitating fall detection and in some cases prevention. A number of recent reviews on fall detection methods using ICT technologies have emerged in the literature and an increasingly popular approach considers combining information from several sensor sources to assess falls. The aim of this paper is to review in detail the subfield of fall detection techniques that explicitly considers the use of multisensor fusion based methods to assess and determine falls. The paper highlights key differences between the single sensor-based approach and a multifusion one. The paper also describes and categorizes the various systems used, provides information on the challenges of a multifusion approach, and finally discusses trends for future work.

1. Introduction

According to the latest United Nation statistic reports, the mean age of the population is expected to grow rapidly in developed countries within the next several decades [1]. This will subsequently increase the cost of the healthcare and result in significant loss for the national budgets. At the same time fall injury is considered to be one of the most common risks among an elderly population. The estimated fall incidence for both hospitalized and independently living people over the age of 75 is at least 30% every year. Close to half of nursing home residents experience falls each year, with 40% falling more than once [2]. These accidents can often have both physical [3] (often head and hip injury) and psychological [4] (fear of falling) consequences. Other serious issues associated with falls include unconsciousness after falling, recovery time due to fall related injury, and death, and many of these issues can be overcome by improving medical response level and rescue time.

The recent development in information and communication technology has triggered an intensive research effort towards detection and prevention of emergency situation

associated with falls. This area is commonly considered as a part of Ambient Assisted Living (AAL) community which is a multidisciplinary field exploiting ICT in personal healthcare for countering the effects of aging population [5]. Modern AAL systems can also help to promote independent lifestyle for elderly people with multiple chronic disease in a situation of rapidly increasing healthcare costs [6] and assist in the task of prevention.

Commonly, fall detection systems are categorized into three different classes depending on the deployed sensor technology which includes wearable devices, ambient sensors, and vision-based sensors. The article by Noury et al. [7] from 2007 which contains description of systems, algorithms, and sensors for automatic fall detection can be considered as one of the first surveys in the field. Relatively recent status is described in publications by Mubashir et al. [8] and Igual et al. [9] providing valuable knowledge about principles, trends, issues, and challenges in fall detection area. As the number of contributions continued to expand some authors prefer to review a specific category within the field, that is, article by Bagalà et al. [10], specifically evaluating worn sensors-based fall detection methods. In publication

by Otanasap and Boonbrahm [11], the focus is made on computer vision exploiting various processing techniques to analyze critical phase and postfall phase. However, a recent trend is characterized by combination of different data sources, which are processed by a single multisensor fusion algorithm [12]. This novel approach can potentially provide a significant improvement in reliability and specificity of fall detection system but has never been reviewed before.

In this paper we present a systematic survey of fall detection research with focus on using multisensor fusion as a main method. Our aim is to provide a general insight into this novel approach and show its benefits compared to other methods in this emerging area. Unlike techniques with a single source channel, a multifusion approach exploits a combination of unrelated devices which are later fused on a data processing level. An explicit search was conducted deploying major databases like Google Scholar, IEEE, PubMed, and Mendeley with keywords including multisensor fusion, sensor combination, context-aware fall detection, and wearable fall detection. In total 299 related publications were found; 68 of them were sorted out based on relevance and representation and included in the final version of the paper. All the reviewed studies are categorized depending on sensors used for monitoring: combination of wearable/ambient devices, only wearable or only ambient. Cases when monitoring is based on sensors both from the same category and of the same type (i.e., multiple cameras) are not considered. We also give an assessment to this novel approach and discuss its perspective in the nearest future.

The rest of the paper is organized as follows. In Section 2 we provide a general definition of the fall and describe its major characteristics. Section 3 gives a brief overview of the popular trends and approaches in modern fall detection together with major benefits and challenges. We proceed with detailed survey on publications deploying multisensor fusion which is followed by discussion of the presented approach and its future perspective in Section 4.

2. Fall Characteristics and Popular Approaches

In the following section we will demonstrate complexity of the falling process, define various types of falls, and discuss several main characteristics which constitute a fall. A fall is commonly defined as “unintentionally coming to rest on the ground, floor, or other lower level.” Losing the balance and subsequent falling with the help of an assistant are also considered as a fall [13]. Based on possible scenarios 4 main types of falls can be distinguished: (1) fall from sleeping, (2) fall from sitting, (3) fall from walking/standing, and (4) fall from standing on support tools such as ladder. Each type has its own unique characteristics, which can help developers to adapt fall detector platforms to a wider spectrum of user requirements. According to the recent studies falls are more likely to occur inside patients’ room and in the bathroom or toilet during activities such as moving/transferring and showering/toileting [13, 14]. Weight, size, and corpulence of the person have also a substantial impact while determining the cinematic of falling. The majority of patients in the risk group usually fall in the evening or at night. Therefore, falls

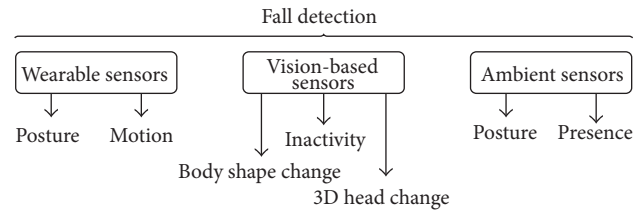


FIGURE 1: Fall detection classification.

databases are very limited due to the lack of records made in real-life testing [15].

Fall detecting techniques can be categorized into three different generations: first-generation systems that rely on the user to detect the fall, second-generation systems that are based on the first-generation systems but have an embedded level of intelligence, and third-generation systems that use data, often via ambient monitoring systems, to detect changes (e.g., changes in activity levels) which may increase the risk of falling (or risk factors for other negative events). The third-generation systems are more preemptive rather than reactive approach [16]. We will mostly focus on fall detectors from the second and third categories, which are discussed in terms of sensor fusion applicability in Section 3. Typically all the modern fall detection systems can be split into 3 main classes (see Figure 1) depending on the sensor technology deployed for monitoring: wearable sensors, ambient sensors, and vision-based sensors [17].

A vast majority of recently developed fall detection systems operate based on one general framework including (1) data acquisition, (2) data processing/feature extraction, (3) fall detection, and (4) caregiver notification. This framework can vary depending on number of devices involved in the monitoring, communication protocols for alarm delivery, and the end user, who is responsible for taking actions in case of emergency. In wearable sensor based systems data acquisition is often performed by using an accelerometer (sensing changes in orientation of wearable device), a gyroscope (which detects angular momentum), and/or other types of sensors like barometers, magnetometers, or microphones. An ambient sensor approach often includes infrared sensors, vibration, or acoustic sensors. The first type can locate and track thermal target within a sensor’s field of view [18]. Vibration sensors are able to differentiate vibration patterns acquired from Activity of Daily Living (ADL) and falls; meanwhile, acoustic sensors use loudness and height of the sound to recognize the fall. Unlike wearable sensor techniques, this approach is considered to be the least obtrusive as it implies minimum interaction with the patient [19]. The last fall detection method performs data acquisition via a set of video cameras embedded into monitoring environment [20]. Vision-based systems can carry out inactivity detection and analyze the body shape changes or 3D head motion. They provide an unobtrusive way to monitor the person of interest and rapidly decrease in price [21]. Several studies managed to achieve significant results in reducing positive false alarms while using single sensor technology representing each of the categories. However, performance of the comprehensive

TABLE 1: System improvement after deploying several sensor functionalities.

Subsystem	Efficiency	Reliability
3D vision	80.0%	97.3%
Accelerometer	88.4%	79.3%
Integrated system	94.3%	90.9%

approach indicates a significant raise in efficiency keeping reliability value over 90% (see Table 1). Therefore, a combination approach is among the latest trends in fall detection/posture recognition studies listed by Augustyniak et al. [22]:

- (i) building sensor networks instead of focusing on a sensor set for a particular disease,
- (ii) promoting multipurpose health prediction and prevention instead of monitoring patients with known medical records,
- (iii) designing monitoring process based on patients health conditions, habits, and life-style,
- (iv) unconstrained mobility of the monitored person,
- (v) real-time *fusion* and cooperation of ambient and wearable sensor networks.

Preliminary results [23] demonstrate significant improvement of fall detection system performance after deploying several sensor functionalities in one system. It can help to improve system performance and provide significant reduction of false positive alarm rate.

Assuming the overall complexity of the fall kinematics and diversity of fall characteristics, described in Section 2, we believe that a multisensor fusion approach is likely to become widely used in the fall detection area. Moreover, there is a strong demand in high standard of independent living for elderly people [30] and therefore particular focus should be on the unobtrusiveness of such systems. Single sensors-based systems are sometimes characterized by a low reliability rate or can only detect particular types of fall in specific environments or circumstances. In the following section we give a brief description of multisensor data fusion method, describe its adaption for fall detection area, and suggest possible classification of main approaches.

3. Sensor Fusion in Fall Detection

Multisensor data fusion is a technology to enable combining information from several sources in order to form a unified picture [31]. Systems based on data fusion are now successfully exploited in various areas including sensor networks [32], image processing, and healthcare [33], where they demonstrate enhanced performance in terms of accuracy and reliability compared to single source based systems [34]. Modern healthcare systems commonly deploy data fusion algorithm to avoid intrinsic ambiguities caused by exploitation of unrelated type of sensors. In study by Medjahed and Istrate [35] tele-monitoring system is proposed to integrate physiological and behavior data, the acoustic environment of the patient, and medical knowledge. In this

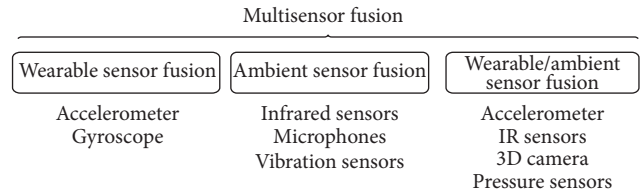


FIGURE 2: Fall detection classification.

case data fusion approach is based on fuzzy logic with a set of rules corresponding to medical recommendations and proved to increase the reliability of the whole system by detecting several distress situations. Another example of data fusion in healthcare is proposed in article by Yang and Huang [36], where Kinect and color cameras are combined together to perform human tracking and identification. Begum et al. [37] make an attempt to classify “stressed” and “relaxed” individuals fusing data from various physiological sensors, that is, Heart Rate, Finger Temperature, Respiration Rate, Carbon Dioxide, and Oxygen Saturation. In this case fusion algorithm performed on decision and data level is additionally combined with Case-Based Reasoning for further classification. The experimental results demonstrate an increased accuracy in comparison with an expert in the domain.

As it was previously mentioned in Section 2 fall detection systems based on single sensor technology are often lacking sufficient accuracy rates and require additional work to improve reliability. For instance, both ambient and video type of frameworks commonly have a constrained monitoring area and require installation, adjustment, and maintenance which can result in higher costs. At the same time, wearable sensors have issues including a certain level of unobtrusiveness if the users have to wear them under long period of time. Additionally, information collected during the monitoring process is communicated via wireless channels which are not completely reliable. Taking into account mentioned observations, we believe the main benefit of fusion approach is its flexibility in terms of changing environment and potential demands of the patient/user. Multisensor based systems can be easily adjusted to the current monitoring instance (indoor/outdoor scenario), provide a better insight into elderly falling problem (additional data sources), and initiate fall prevention analyses. In this case, continuous data collected from multiple sources can be analyzed for reoccurring patterns as suggested in our previous publication [38]. Multisensor fusion has proved its efficiency in various areas of the healthcare domain [37] and subsequently gained its popularity in fall detection domain. Moreover, with a recent development on ICT market more sensors are now available and can be combined to perform advanced level of activity tracking, which will increase number of publications.

In Section 2 fall detection methods were classified into three main categories based on different types of sensor technology: wearable, ambient, and vision-based (see Figure 2). According to the vast majority of recent publications within fall detection domain same types of sensors are involved in multisensor fusion process with 2 major exceptions:

TABLE 2: Context-aware sensors fusion.

Article	Year	Basis	Deployed sensors	Algorithm deployed	Evaluation	Performance
Brunin and Courtial [24]	2010	Fusion system architecture for fall detection	PIR, camera, thermopiles	Fuzzy logic + combination of location/posture duration	15 video sequences recorded in health smart home	Motion detection: 84%
Huang et al. [25]	2008	Intelligent cane fall detection based on sensor fusion	Laser range finder, CCD camera	Probability distribution function with relevant parameter, rule-based approach	Normal walking/fall detection experiments with cane robots	Effectiveness is confirmed through experiments
Zigel et al. [26]	2009	Fall detection based on detection of vibration and sound signals	Accelerometer, microphone	Feature extraction, Bayes decision rule classifier	Mimicking doll "Rescue Randy," 40 drops. Other objects: 80 drops	SE (sensitivity): 97.5% SP (specificity): 98.6%
Yazar et al. [27]	2014	Multisensor system for fall detection	Vibration sensor, PIR sensors	Winner-takes-all (WTA) decision fusion algorithm	Demo including falling person, human footstep, human motion, unusual inactivity detection	No data is provided
Toreyin et al. [28]	2008	Fall detection using multisensor signal processing	Infrared, sound sensors	Hidden Markov Models	2 minutes of walking falling and speech sounds generation	All falls are detected correctly
Ariani et al. [29]	2012	Unobtrusive falls detection with multiple persons	PIR and motion detector, pressure mats	Decision tree algorithm	3 ADL scenarios 12 types of falls	SE: 100% SP: 77.14% Accuracy: 89.33%
Li et al. [21]	2013	Improvement of acoustic fall detection using Kinect depth sensing	FADE (acoustic) Kinect	Segmentation, thresholding	Recorded video data	Error reduction by 80%

(1) ambient and vision-based sensors are both integrated into environment and can be considered as a unified context-aware category and (2) wearable devices can be combined together with context-aware sensors comprising additional category. Assuming these corrections we propose an alternative approach to classify all fusion systems operating in the fall detection domain. Unlike single based methods, the choice of category does not depend on utilized sensor technology but corresponds to a sensor type which is being fused: context-aware sensors, wearable sensors, and combination between context and wearable. In the rest of the paper we review each category, present the most significant studies in multifusion fall detection domain, and discuss its possible challenges and limitations.

3.1. Context-Aware Sensors Fusion. According to the recent review on fall detection methods, most of the systems which use a multimodal approach are wearable sensor oriented and exploit 3-axial accelerometers as a part of the process [39]. However, there is a number of works providing solutions that are excluding wearable sensors from the monitoring and fall detection in particular. These types of systems are effective when unobtrusiveness is the main requirement and patient rejects to wear any external devices on his/her body. They can detect persons movements and collect information

regarding the usage of furniture or household items and answer questions regarding the patients activity: that is, "is the patient eating/exercising regularly?" [40]. At the same time their operation capabilities are highly limited by the area of distribution.

Typically sensors involved in the context-aware monitoring are represented by cameras [24], vibration sensors [27], sound detector [26], pressure mats [29], and floor or infrared sensors [28]. Table 2 gives an overview of the most significant studies in this area. All the works are compared based on publication year, sensors involved in the monitoring process, multifusion algorithm, experimental part, and evaluation results depending on their availability.

Unlike single sensor-based approach, where feature extraction is followed by data classification, multisensor systems perform independent data analyses for each sensor technology with fusion method as a final step in fall detection [41]. Variation of the multisensor fusion techniques in each category including context-aware systems is highly dependent on sensors deployed in each study. In the early study from 2008 Huang et al. [25] propose a new human fall detection method based on fusing sensory information from a vision system and a laser range finder (LRF). In order to obtain data fusion from two sensors, unrelated types of measurements are integrated into the image coordinate

with a focus on the distance between the head and the center of two legs. Finally, the actual fall detection is based on probability distribution function (PDF) and simple rule approach. Another interesting solution is suggested by Zigel et al. [26] where microphone used to track the sound is combined with accelerometer, which is capturing floor vibrations after patient falls. In this case feature extraction and Bayes decision rule classifier provide information fusion. Camera systems are used in several studies and accompanied either by acoustic sensors [21] or by PIR sensors together with thermopiles [24]. Thresholding approach after preliminary segmentation and fuzzy logic combined with location/posture direction are used as fusion techniques, respectively. Ariani et al. [29] are using wireless ambient sensors (motion detectors and pressure mats) to track the movement of multiple persons and later apply decision tree algorithm to unobtrusively detect falls when they occur. Another fall detection system consisting of vibration sensor and two PIR sensors is primarily based on winner-take-all (WTA) decision fusion algorithm [27], which is activated after preliminary processing of measurements collected from both sources. Finally Hidden Markov Model (HMM) is deployed in [28] to combine infrared and sound sensors. The most popular sensor deployed by context-aware systems is PIR type mentioned in 3 different publications. At the same time, no preference was given to any specific algorithm applied for fusion analyses.

Initial sensor setup and preliminary processing play an essential role in subsequent evaluation of the system. Brulin and Courtial [24] deployed a Health Smart Phone and recorded 15 video sequences illustrating situations of everyday life or an emergency performed by two subjects. In another example experimental part is split into two related steps. First, the possibility distribution of “normal walking” is investigated and finally the validation of the fall detection method is performed. Other examples include dropping of “Rescue Randy” doll, falling and speech sound generation, ADL, and falls simulations. At this point, variability of trial approaches indicates an absence of common strategy for evaluation of the context-aware multisensor fusion systems. Due to the high variability of devices deployed for multisensor it becomes complicated to analyze and unify all the methods involved in the process or determine the most reliable one. Further investigation and experimental work are required.

Moreover, it is important to mention that none of the analyzed research works managed to perform experiments with elderly people, a group which is potentially in high risk of falling. This can be explained by patients privacy, which is still a sensitive issue in terms of ambient and especially vision-based fall detection systems. For historic reference, one of the first projects in the area was forced to shift from image processing to body placed sensors due to privacy concerns [42]. We believe this problem can be partly solved by alternate deployment of camera-based and ambient sensors depending on location, change in environment, or current emergency situation. In this way monitoring that violates patients privacy is only performed when the calculated risk of falling is significantly higher.

3.2. Wearable Sensors Fusion. With the recent development on ICT market, wearable devices start to play an essential role in modern healthcare systems. Most of them have already been utilized for automatic fall detection and showed its efficiency compared to other methods [57–59]. Unlike context-aware sensor technology, wearables attached to a patient’s body do not affect their privacy and can therefore perform monitoring on extended periods of time. In most of the cases fall detection systems based on fusing wearable sensors include accelerometer device as a main source of data. They are often complemented by other types of wearables, that is, gyroscopes and magnetometer [42], location tags [45], or barometric pressure sensors [44, 47, 48] (see Table 3). Moreover, physiological devices combined with accelerometers can be considered as a separate subgroup due to specific synchronization requirements and processing of collected measurements. For example, Yi et al. [46] deploy temperature sensor and ECG together with accelerometer and perform individual data processing for each device later fused into a unified alert message for medical staff.

Similar to the previous category described in Section 3.1, multisensor fusion algorithms applied for wearables can vary depending on specific device or authors choice. Three different techniques were deployed to combine body-worn inertial sensors and air pressure sensors including heuristically trained decision tree classifier, feature extraction/thresholding, and SVM. According to evaluation results, decision tree and feature extraction/thresholding are more efficient with 96.9% and 94.12% of accuracy. However, unlike studies in [44, 47], Greene et al. [48] perform experimental part with older adults which significantly affect the final result (see Table 3). In study by Felisberto et al. [42] a mash-up of various methods including fuzzy logic, extended Kalman filter (EKF), direct cosine matrix (DCM), and control algorithm is applied in order to fuse accelerometer, gyroscope, and magnetometer. Fall detection based on movement and sound data is performed by Doukas et al. [43, 56], where accelerometer is deployed together with microphones and collected data is fused by Support Vector Machine technique. An accuracy increase by 40% was demonstrated in [45] after accelerometer sensor was combined with location tag by rule-based reasoning. However, for a final discussion regarding the positive results, experimental conditions should be taken into account.

In the vast majority of fall related studies evaluation process is mainly performed by healthy volunteers or based on simulation [38, 60, 61]. This fact makes it almost impossible to give an accurate assessment for operational capabilities of developed system or reliability of deployed algorithm. More experimental data received from elderly population should be analyzed in order to improve sufficiency of developed fall detection system. In study from 2012 Greene et al. [48] estimate the risk of falling through multisensor assessment of standing balance. Pressure sensitive platform and body-worn inertial sensor are utilized during evaluation, which is based on monitoring 120 community dwelling older adults. It is one of few research studies where trials with elderly population are included as evaluation criteria. As a result the overall performance of the system was significantly

TABLE 3: Wearable sensors fusion.

Article	Year	Basis	Deployed sensors	Deployed algorithm	Evaluation	Performance
Felisberto et al. [42]	2014	Movement monitoring, accident detection based on sensor fusion	Accelerometer, gyroscope, magnetometer	Fuzzy logic + extended Kalman filter, direct cosine matrix (DCM), control algorithm	Movement state, Orientation state experiment with precollected data	Passing average: 84%
Doukas and Maglogiannis [43]	2008	Fall detection based on movement/sound data	Accelerometer, microphones	Support Vector Machine (SVM)	2 volunteers: (a) Simple walk (b) Walk and fall (c) Walk and run	All fall events successfully detected Run events: 96.72%
Bianchi et al. [44]	2010	Falls event detection with barometric pressure and triaxial accelerometer	Accelerometer, air pressure sensor	Heuristically trained decision tree classifier	20 healthy volunteers: falls/ADL simulation	Accuracy: 96.9% Sensitivity: 97.5% Specificity: 96.5%
Lustrek et al. [45]	2011	Fall detection with accelerometer and location sensor	Accelerometer, location tags	Rule-based reasoning	10 healthy volunteers, specific scenario	Methods utilized both context/accelerometer. Accuracy increase: 40%
Yi et al. [46]	2014	Wearable sensor data fusion for fall detection	Temperature, accelerometer ECG sensor	Data is processed individually and combined into alert message	No evaluation provided	Human postures successfully recognized. Full evaluation is not performed
Tolkiehn et al. [47]	2011	Fall detection with accelerometer and barometric pressure sensor	Accelerometer, barometric pressure sensor	Feature extraction, thresholding combination	12 healthy volunteers ADL/fall simulation, 297 data sequences	Fall identification accuracy: 94.12%
Greene et al. [48]	2012	Falls risk estimation through multisensor assessment of standing balance	Pressure sensor (platform), body-worn inertial sensor	SVM	120 community dwelling older adults	Classification accuracy: 71.52%

affected demonstrating only 71.52% of classification accuracy; meanwhile, the rest of the methods can reach 95%–97% for specificity, sensitivity, and accuracy. Fall detection systems based on wearable devices is still a novel method, therefore lacking a unified approach to effectively combine sensors due to different formats of collected data.

At the same time, additional number of digital devices attached to patient's body are inconvenient for the users and can potentially lead to a low acceptance rate of this method. This issue can be solved if different types of wearable sensors are incorporated in a single device performing collection of unrelated types of data simultaneously. This will help reduce data loss, improve processing time, and at the same time maintain patients independent life-style without affecting their privacy. Modern mobile phones are already equipped with advanced sensor functionality and can be suggested as a tool for synchronization and processing of collected measurements. However, modern smartphones and gadgets are still poorly distributed among elderly people [62], which complicates deployment and further progress of the proposed methodology.

3.3. Wearable/Ambient Sensor Fusion. The last category is characterized by combination of previously presented approaches and can potentially help to detect a wider spectrum of possible emergency situations connected with falls. Context-aware fall systems can provide long-term trend analysis describing patients behavior and recognizing abnormal patterns but are often limited by the area in which they can be used and distribution. Wearable fall detection is becoming increasingly available due to cheap embedded sensors included in smartphones and demonstrates relatively high performance but still produces significant number of fall alarms [63, 64] and has been mainly tested in laboratory environments. As a result, research studies which make an attempt to merge major benefits of both approaches into a self-complementing system are surpassing other methods by a number of publications (see Tables 2 and 3). In Table 4 we review the most significant studies to demonstrate the latest trends in multisensor fusion for context-aware and wearable sensors.

This approach is considered relatively new and therefore requires thorough investigation and experimental work. As

TABLE 4: Wearable/ambient sensor fusion.

Article	Year	Basis	Deployed sensors	Deployed algorithm	Evaluation	Performance
Aguilar et al. [49]	2014	Sensor fusion via evidential network for fall detection	RFPAT [49], GARDIEN [49]	Evidential network Dempster-Shafer Theory formalism	Data recorded at Telecom SudParis	SE: 94%
Cavalcante et al. [50]	2012	Evidential network for medical data fusion in remote monitoring	Wearable sensor, infrared sensors, sound analyzer	Dempster-Shafer Theory	Data recorded at Telecom SudParis	SE: 93.94%
Della Toffola et al. [51]	2011	Combine sensor networks and home robot to improve fall detection	Body-worn sensors, ambient sensors, home robot	Future work, flooding time synchronization protocol for nodes	Packet transmission delays power consumption	Built system suitable for fall detection
McIlwraith et al. [52]	2010	Wearable and ambient sensor fusion for human motion detection	Accelerometer (e-AR), video sensors, gyroscope	Spatial/temporal HMM	5 activities performed by volunteers in a constrained manner	Accuracy increase: Over vision system: 6.4% Over gyroscope: 17.2%
Kepski et al. [53]	2012	Fall detection using Kinect and accelerometer	Kinect, accelerometer, gyroscope	Fuzzy inference system	Intentional falls and ADLs performed by 3 volunteers	Fused sensors proved sufficiency to implement reliable fall detection system
Leone and Diraco [41]	2008	Multisensor approach for fall detection in home environment	3D camera, wearable acc-ter, microphone	Multithreading approach with fuzzy logic technique under development	13 volunteers perform 450 events including 210 falls	3D vision alarm: 81.3% Acc-ter alarm: 98% Audio alarm: 83%
Alemdar et al. [54]	2010	Multimodal fall detection within WeCare framework	Accelerometer, embedded cameras, RFID tags	Decision fusion mechanism	Volunteer performing ADL	Falls are successfully distinguished from ADL
Cagnoni et al. [55]	2009	Fall detection for assisted technologies applications	Accelerometer, video camera	PSO for visual data HTM for acceleration fusion algorithms multiple classifier sets fuzzy logic decision trees	Accelerometer: continuous flow of real-life events simulation Video sensor: limited set of image sequences	Joint system is guaranteed to provide a good level of fault-tolerance
Doukas and Maglogiannis [56]	2011	Fall detection utilizing motion, sound, and visual perceptual components	Tracking camera, accelerometer, microphones	Semantic rules based on semantic web rule language (SWRL)	2 male volunteers performing experimental protocol	Utilization of rules-based evaluation minimizes false positives to zero

a result, the choice of sensors can vary significantly from one study to another. Most of the systems deploy accelerometers as a main device which are additionally combined with either ambient sensors or 3D cameras [65, 66]. Other wearable devices can be represented by gyroscopes, microphones, physiological sensors, sound analyzer, infrared sensors, or RFID tags. Della Toffola et al. [51] in their study from 2011 pick up a different approach and complement a set of ambient and body-worn sensors with a home robot in order to improve fall detection. Slightly different concept is presented by McIlwraith et al. [52] and Kepski et al. [53] where accelerometer and gyroscope are accompanied by vision-based sensors. In the first publication surrounding vision sensors are deployed for accurate characterization of motion, and in the second case authors used commercially available

microsoft Kinect camera instead and performed reliable fall detection. In some cases gyroscope can be replaced by microphones [43] or alternatively by RFID tags [63], with embedded tracking camera and accelerometer still being part of the framework.

Due to high diversity in sensor technology deployed for fall detection, the choice of algorithms performing fusion function is still unique in each research work. The most common approach to combine wearable and context-aware systems includes individual low-complexity algorithms for every sensor technology, which are then followed by more advanced fusion algorithm. None of the reviewed studies deployed thresholding technique on individual or fusion level and the only example of rule-based approach was complicated by semantic web rule language. The most popular

algorithm is fuzzy logic utilized as fuzzy inference system [53] or fuzzy logic decision tree [55]. Other methods include evidential networks, Dempster-Shafer theory, or Hidden Markov Models. Similar to the previous categories, there is no possibility to determine a common approach or justify the choice of fusion methods since there is not enough experimental evidence to operate with.

Similar to previous categories, variation in sensors and methods deployed for multimodal fusion has a significant effect on experimental part of research. The evaluation process can be characterized by two different scenarios: (1) online testing with volunteers subsequently performing ADL or falls and (2) offline evaluation utilizing previously collected measurements. In both cases, combination of wearable and context-aware approaches had a positive impact and resulted in increased specificity, sensitivity, and accuracy. Doukas and Maglogiannis [56] in their attempt to merge tracking camera, accelerometer, and microphones managed to minimize the amount of fall positive alarms to zero. Evaluation based on elderly patients in real home-like environments is still a sensitive issue, assuming complexity of the sensor setup in this case.

In our previous studies we proposed a multisensor fusion system based on Dynamic Bayesian Networks and combined wearable device with context-aware sensor framework [67]. All the accelerometer measurements were obtained from the android based smartphone and analyzed for possible falls. Context-aware information was obtained from environmental sensors network consisting of PIR motion, door contact, pressure mats, and power usage detectors embedded into a smart home and deploying a special context recognition algorithm to deliver user activities. Physiological data was later interfered with ambient measurements and processed in Dynamic Bayesian Network performing fall detection. Evaluation process contains both simulation (MATLAB tools) and demonstration part (healthy volunteer). With the proposed technique we managed to compliment 2 different fall detection approaches and improve the reliability of the fall detection system. However, it is still far from deployment of developed or similar systems in everyday geriatric practice or explicit examples of commercially successful applications. Moreover, the vast majority of similar systems obtain high experimental results in unrealistic or restricted conditions with a pure reference to real-life environments, which is among the issues of this approach. Other challenges and limitations of multisensor fusion method in fall detection are discussed in Section 4 of the review.

4. Discussion

4.1. Challenges. Most of the challenges specific for modern single-based fall detection systems are still valid in case of multimodal approach. Igual et al. [9] provide a number of typical problems which can affect final results including (1) lack of performance under real-life conditions, (2) limited usability (which mostly applies to wearable and smartphone-based fall detectors), and (3) lack of publications regarding practicality and acceptability of modern fall detection technologies. Other suggested issues are connected with privacy

concerns, lack of human contact, and limited experimental conditions.

After including additional sensor functionality a single-based fall detector becomes a multimodal system inheriting challenges typical to other frameworks with data fusion requirement. Khaleghi et al. [31] introduced these issues in their study starting with imperfection of the collected data and diversity or low reliability of sensor technologies. Based on reviewed material we can complement the list of challenges in data fusion for fall detection with the issues listed below. All these items should be analyzed and taken into consideration before developing the fall detection framework.

4.1.1. Cost Efficiency. As previously mentioned in Section 3.3 multisensor fusion helps to improve reliability of fall detection system. At the same time additional medical devices can significantly increase the final cost of the monitoring framework. In this case cost efficiency assessment becomes an essential part of evaluation process. Our recommendation is to create a flexible structure which will allow us to adjust the number of components depending on individual contribution to the overall performance of the system.

4.1.2. Conflicting Output. During the monitoring process similar activities can be interpreted in a different way by unrelated sensor platforms. The amount of false alarms among modern fall detections is still relatively high. Therefore, it is essential to give a priority to the technology which is more reliable and can minimize unclassified falls or ADLs.

4.1.3. Data Correlation. Measurements collected during the monitoring process in case of multisensor fall detection are typically coming from different backgrounds and are unrelated to each other. These data should not only be merged together in a most efficient way, but also be analyzed for possible common trends and similarities.

4.1.4. Processing Framework. Firstly, majority of the systems analyze data for each component independently and deploy fusion algorithm as a final step to combine acquired results [33]. However, in some cases raw data collected from each sensor unit can be delivered to the common framework without preliminary processing. Alternatively, in case of wearable and context-aware fusion, particular categories can be processed in conjunction (i.e., various types of ambient sensors) and later fused with sensors from unrelated category. As a result, it leads to unnecessary complication of the fusion algorithm and subsequent increase in computational time.

4.1.5. Computational Power. Multiple monitoring items result in additional amount of data collected by the system and will subsequently increase computational costs. This issue can be avoided by separating data analyses into several stages including preprocessing, data filtering, and feature extraction. Each particular type of processing can be performed by a separate component with a processing center, where the final decision is made.

Another drawback, which is particularly specific for modern multisensor fusion systems, is a lack of simplified evaluation procedure. In a vast majority of articles evaluation method is often based on simulations or this information is not available at all. It is partly caused by complexity of the monitoring setup in real environment. Sensor functionality should be embedded into the regular apartment or specially designed test environment. Moreover, similarly to regular fall detection systems fusion based methods are evaluated on simulated falls performed by healthy volunteers, which is far from the real-life scenario. Testing with real patients who suffer from falling can help to improve the process; however, it requires ethical content and additional complications and is commonly not available in fall detection studies. Additional complexity is caused by distinctive technological background of the sensor technology involved in the monitoring process. This issue is specific to any fusion based system and becomes essential when developing the multisensor fall detection mechanism.

4.2. Future Trends. Based on the majority of reviewed papers the main trend in multisensor fall detection can be characterized by merging sensor technologies from different categories and unrelated platforms. Systems developed with this approach are fully interchangeable and can maintain monitoring even when one of the components is inactive.

4.2.1. Physiological Sensors. Most of the elderly patients suffer from various health problems including heart problem or Alzheimer which increases probability of falling in their daily life. Therefore, it is important to track patients activity in conjunction with significant physiological parameters. Physiological sensors combined with fall detectors can help to understand correlation between patients activity and health conditions and make monitoring process more detailed.

4.2.2. Long-Term Analyses. Monitoring people with high risk of falling on a regular basis during the long period of time will improve data analyses and help to detect interesting patterns. In perspective we will be able to develop an algorithm which can prevent the fall in case dangerous measurement sequence is repeating itself in time.

4.2.3. Integration into Smart Home Environments. Long-term analysis is almost impossible without an appropriate sensor setup. In many cases sensors are already integrated into everyday routine in form of smart home environments collecting valuable information regarding user's presence in the house. They can be further adopted for patient medical tracking and reliable fall detection without additional installation costs.

4.2.4. Patient-Oriented Systems. Assuming the individual approach in patient treatment most of the multimodal healthcare systems should be more patient-oriented. The choice of sensors and processing techniques should correspond to the actual patient demands and major health problems they are suffering from. Otherwise, developed platforms should cover a wide spectrum of healthcare problems or be as much universal as possible.

Due to complexity of falls and variation in falling circumstances the most effective approach implies fusing information from sensors related to different categories. As a step towards a full-scale remote monitoring framework, fall detection components can be deployed in conjunction with other healthcare systems to check patients well-being on a long-term basis. Following the recent trend, we suggest building a special environment with wearable, ambient, and vision sensors, where fusion techniques can be effectively evaluated. At the same time, it is recommended to complement these types of smart environments with additional sensor technology only based on current patients' demand or particular monitoring case in order to avoid data overload and unnecessary privacy violations.

5. Conclusion

Fall detection systems play an essential role in modern healthcare. Latest sensor technologies are deployed in order to distinguish between falls and regular ADLs with a recent trend to combine unrelated data sources. In the presented study we conducted a search among the latest works based on multisensor fall detection systems and made an attempt to classify all systems into various categories. Analyzed materials allowed us to start a useful discussion regarding major challenges faced by multifusion approach, its issues, and limitations. Based on this discussion we can suggest core topics that should be considered in fusion methodology in the future. Among other things we would like to make a special focus on (1) developing a multifunctional monitoring platform, where each component/sensor can be easily adjusted or removed depending on user demand or monitoring circumstances and (2) organizing continuous monitoring/experimental sessions involving elderly population in order to improve acceptability of fall detection systems. Both suggestions will introduce a certain level of structure to this novel but rapidly evolving approach and help to unify the choice of algorithm in each particular monitoring case.

Conflict of Interests

The authors declare that there is no conflict of interests regarding the publication of this paper.

References

- [1] Department of Economic Population Division and United Nations Social Affairs, *World Population Ageing*, 2009.
- [2] J. Dai, X. Bai, Z. Yang, Z. Shen, and D. Xuan, "Mobile phone-based pervasive fall detection," *Personal and Ubiquitous Computing*, vol. 14, no. 7, pp. 633–643, 2010.
- [3] S. Sadigh, A. Reimers, R. Andersson, and L. Laflamme, "Falls and fall-related injuries among the elderly: a survey of residential-care facilities in a Swedish municipality," *Journal of Community Health*, vol. 29, no. 2, pp. 129–140, 2004.
- [4] B. J. Vellas, S. J. Wayne, L. J. Romero, R. N. Baumgartner, and P. J. Garry, "Fear of falling and restriction of mobility in elderly fallers," *Age and Ageing*, vol. 26, no. 3, pp. 189–193, 1997.
- [5] M. Memon, S. R. Wagner, C. F. Pedersen, F. H. Aysha Beevi, and F. O. Hansen, "Ambient Assisted Living healthcare frameworks,

- platforms, standards, and quality attributes,” *Sensors*, vol. 14, no. 3, pp. 4312–4341, 2014.
- [6] P. Rashidi and A. Mihailidis, “A survey on ambient-assisted living tools for older adults,” *IEEE Journal of Biomedical and Health Informatics*, vol. 17, no. 3, pp. 579–590, 2013.
 - [7] N. Noury, A. Fleury, P. Rumeau et al., “Fall detection—principles and methods,” in *Proceedings of the 29th Annual International Conference of IEEE-EMBS Engineering in Medicine and Biology Society (EMBS '07)*, pp. 1663–1666, August 2007.
 - [8] M. Mubashir, L. Shao, and L. Seed, “A survey on fall detection: principles and approaches,” *Neurocomputing*, vol. 100, pp. 144–152, 2013.
 - [9] R. Igual, C. Medrano, and I. Plaza, “Challenges, issues and trends in fall detection systems,” *BioMedical Engineering Online*, vol. 12, no. 1, article 66, 2013.
 - [10] F. Bagalà, C. Becker, A. Cappello et al., “Evaluation of accelerometer-based fall detection algorithms on real-world falls,” *PLoS ONE*, vol. 7, no. 5, Article ID e37062, 2012.
 - [11] N. Otanasap and P. Boonbrahm, “Fall prevention using head velocity extracted from visual based VDO sequences,” in *Proceedings of the 5th Augmented Human International Conference*, 2012.
 - [12] I. Iliev, S. Tabakov, and V. Spasova, “Multipoint video control and fall detection system applicable in assistance of the elderly and people with disabilities,” *International Journal of Reasoning-based Intelligent Systems*, vol. 6, no. 1-2, pp. 34–39, 2014.
 - [13] X.-L. Chen, Y.-H. Liu, D. K. Y. Chan, Q. Shen, and H. van Nguyen, “Characteristics associated with falls among the elderly within aged care wards in a tertiary hospital: a retrospective case-control study,” *Chinese Medical Journal*, vol. 123, no. 13, pp. 1668–1672, 2010.
 - [14] B. Ni, C. D. Nguyen, and P. Moulin, “RGBD-camera based get-up event detection for hospital fall prevention,” in *Proceedings of the IEEE International Conference on Acoustics, Speech, and Signal Processing (ICASSP '12)*, pp. 1405–1408, March 2012.
 - [15] H. J. B. Dan Istrate, J. M. B. Dorizzi, M. Cesar, T. M. J. L. Baldinger, A. G. I. B. Paulo, and A. Cavalcante, “Evidential network-based multimodal fusion for fall detection,” in *Proceedings of the 8th International Conference on Wearable Micro and Nano Technologies for Personalised Health*, 2012.
 - [16] G. Ward, N. Holliday, S. Fielden, and S. Williams, “Fall detectors: a review of the literature,” *Journal of Assistive Technologies*, vol. 6, no. 3, pp. 202–215, 2012.
 - [17] X. Yu, “Approaches and principles of fall detection for elderly and patient,” in *Proceedings of the 10th International Conference on e-Health Networking, Applications and Services (HealthCom '08)*, pp. 42–47, July 2008.
 - [18] F. Hijaz, N. Afzal, T. Ahmad, and O. Hasan, “Survey of fall detection and daily activity monitoring techniques,” in *Proceedings of the 2nd International Conference on Information and Emerging Technologies (ICIET '10)*, pp. 1–6, June 2010.
 - [19] M. A. Habib, M. S. Mohktar, S. B. Kamaruzzaman, K. S. Lim, T. M. Pin, and F. Ibrahim, “Smartphone-based solutions for fall detection and prevention: challenges and open issues,” *Sensors*, vol. 14, no. 4, pp. 7181–7208, 2014.
 - [20] S. K. Tasoulis, C. N. Doukas, V. P. Plagianakos, and I. Maglogiannis, “Statistical data mining of streaming motion data for activity and fall recognition in assistive environments,” *Neurocomputing*, vol. 107, pp. 87–96, 2013.
 - [21] Y. Li, T. Banerjee, M. Popescu, and M. Skubic, “Improvement of acoustic fall detection using Kinect depth sensing,” in *Proceedings of the 35th Annual International Conference of the IEEE Engineering in Medicine and Biology Society (EMBC '13)*, pp. 6736–6739, IEEE, Osaka, Japan, July 2013.
 - [22] P. Augustyniak, M. Smoleń, Z. Mikrut, and E. Kańtoch, “Seamless tracing of human behavior using complementary wearable and house-embedded sensors,” *Sensors*, vol. 14, no. 5, pp. 7831–7856, 2014.
 - [23] M. Grassi, A. Lombardi, G. Rescio et al., “A hardware-software framework for high-reliability people fall detection,” in *Proceedings of the IEEE Sensors (SENSORS '08)*, pp. 1328–1331, October 2009.
 - [24] D. Brulin and E. Courtial, “Multi-sensors data fusion system for fall detection,” in *Proceedings of the 10th International Conference on Information Technology and Applications in Biomedicine (ITAB '10)*, pp. 1–4, IEEE, Corfu, Greece, November 2010.
 - [25] J. Huang, P. Di, K. Wakita, T. Fukuda, and K. Sekiyama, “Study of fall detection using intelligent cane based on sensor fusion,” in *Proceedings of the International Symposium on Micro-NanoMechatronics and Human Science (MHS '08)*, pp. 495–500, 2008.
 - [26] Y. Zigel, D. Litvak, and I. Gannot, “A method for automatic fall detection of elderly people using floor vibrations and sound Proof of concept on human mimicking doll falls,” *IEEE Transactions on Biomedical Engineering*, vol. 56, no. 12, pp. 2858–2867, 2009.
 - [27] A. Yazar, F. Erden, and A. E. Cetin, “Multi-sensor ambient assisted living system for fall detection,” in *Proceedings of the IEEE International Conference on Acoustics, Speech, and Signal Processing (ICASSP '14)*, pp. 1–3, 2014.
 - [28] B. U. Toreyin, E. B. Soyer, I. Onaran, and E. E. Cetin, “Falling person detection using multisensor signal processing,” *EURASIP Journal on Advances in Signal Processing*, vol. 2008, Article ID 149304, 2008.
 - [29] A. Ariani, S. J. Redmond, D. Chang, and N. H. Lovell, “Simulated unobtrusive falls detection with multiple persons,” *IEEE Transactions on Biomedical Engineering*, vol. 59, no. 12, pp. 3185–3196, 2012.
 - [30] R. Bragg, P. Catlin, J. Carlier, S. Brownsell, and D. A. Bradley, “Do users want telecare and can it be cost-effective,” in *Proceedings of the 1st Joint BMES/EMBS Conference Serving Humanity*, p. 714, October 1999.
 - [31] B. Khaleghi, A. Khamis, F. O. Karray, and S. N. Razavi, “Multi-sensor data fusion: a review of the state-of-the-art,” *Information Fusion*, vol. 14, no. 1, pp. 28–44, 2013.
 - [32] D. L. Hall and J. Llinas, “An introduction to multisensor data fusion,” *Proceedings of the IEEE*, vol. 85, no. 1, pp. 6–23, 1997.
 - [33] K. Park and B. Lee, “Issues in data fusion for healthcare monitoring,” in *Categories and Subject Descriptors*, ACM, 2008.
 - [34] G. Villarrubia, J. F. De Paz, J. Bajo, and J. M. Corchado, “Ambient agents: embedded agents for remote control and monitoring using the PANGEA platform,” *Sensors*, vol. 14, no. 8, pp. 13955–13979, 2014.
 - [35] H. Medjahed and D. Istrate, “Human activities of daily living recognition using fuzzy logic for elderly home monitoring,” in *Proceedings of the IEEE International Conference on Fuzzy Systems*, vol. 33, pp. 1466–1473, 2009.
 - [36] M.-T. Yang and S.-Y. Huang, “Appearance-based multimodal human tracking and identification for healthcare in the digital home,” *Sensors*, vol. 14, no. 8, pp. 14253–14277, 2014.
 - [37] S. Begum, S. Barua, and M. U. Ahmed, “Physiological sensor signals classification for healthcare using sensor data fusion and

- case-based reasoning,” *Sensors*, vol. 14, no. 7, pp. 11770–11785, 2014.
- [38] G. A. Koshmak, M. Linden, and A. Loutfi, “Evaluation of the android-based fall detection system with physiological data monitoring,” in *Proceedings of the 35th Annual International Conference of the IEEE Engineering in Medicine and Biology Society*, pp. 1164–1168, Osaka, Japan, July 2013.
- [39] J. T. Perry, S. Kellog, S. M. Vaidya, J.-H. Youn, H. Ali, and H. Sharif, “Survey and evaluation of real-time fall detection approaches,” in *Proceedings of the 6th International Symposium on High Capacity Optical Networks and Enabling Technologies (HONET '09)*, pp. 158–164, December 2009.
- [40] F. Pecora, M. Cirillo, F. Dell’Osa, J. Ullberg, and A. Saffiotti, “A constraint-based approach for proactive, context-aware human support,” *Journal of Ambient Intelligence and Smart Environments*, vol. 4, no. 4, pp. 347–367, 2012.
- [41] A. Leone and G. Diraco, “A multi-sensor approach for people fall detection in home environment,” in *Proceedings of the Workshop on Multi-Camera and Multi-Modal Sensor Fusion Algorithms and Applications*, pp. 1–12, 2008.
- [42] F. Felisberto, F. Fdez-Riverola, and A. Pereira, “A ubiquitous and low-cost solution for movement monitoring and accident detection based on sensor fusion,” *Sensors*, vol. 14, no. 5, pp. 8961–8983, 2014.
- [43] C. Doukas and I. Maglogiannis, “Advanced patient or elder fall detection based on movement and sound data,” in *Proceedings of the 2nd International Conference on Pervasive Computing Technologies for Healthcare*, pp. 103–107, IEEE, Tampere, Finland, February 2008.
- [44] F. Bianchi, S. J. Redmond, M. R. Narayanan, S. Cerutti, and N. H. Lovell, “Barometric pressure and triaxial accelerometry-based falls event detection,” *IEEE Transactions on Neural Systems and Rehabilitation Engineering*, vol. 18, no. 6, pp. 619–627, 2010.
- [45] M. Lustrek, H. Gjoreski, S. Kozina, B. Cvetković, V. Mirchevska, and M. Gams, “Detecting falls with location sensors and accelerometers,” in *Proceedings of the 23rd Innovative Applications of Artificial Intelligence Conference*, pp. 1662–1667, August 2011.
- [46] W.-J. Yi, O. Sarkar, S. Mathavan, and J. Saniie, “Wearable sensor data fusion for remote health assessment and fall detection,” in *Proceedings of the IEEE International Conference on Electro/Information Technology (EIT '14)*, pp. 303–307, June 2014.
- [47] M. Tolkiehn, L. Atallah, B. Lo, and G.-Z. Yang, “Direction sensitive fall detection using a triaxial accelerometer and a barometric pressure sensor,” in *Proceedings of the Annual International Conference of the IEEE Engineering in Medicine and Biology Society*, pp. 369–372, Boston, Mass, USA, August 2011.
- [48] B. R. Greene, D. McGrath, L. Walsh et al., “Quantitative falls risk estimation through multi-sensor assessment of standing balance,” *Physiological Measurement*, vol. 33, no. 12, pp. 2049–2063, 2012.
- [49] P. A. C. Aguilar, J. Boudy, D. Istrate, B. Dorizzi, and J. C. M. Mota, “A dynamic evidential network for fall detection,” *IEEE Journal of Biomedical and Health Informatics*, vol. 18, no. 4, pp. 1103–1113, 2014.
- [50] P. A. Cavalcante, M. A. Sehili, M. Herbin et al., “First steps in adaptation of an evidential network for data fusion in the framework of medical remote monitoring,” in *Proceedings of the 34th Annual International Conference of the IEEE Engineering in Medicine and Biology Society (EMBS '12)*, pp. 2044–2047, San Diego, Calif, USA, September 2012.
- [51] L. Della Toffola, S. Patel, B.-R. Chen, Y. M. Ozsecen, A. Puiatti, and P. Bonato, “Development of a platform to combine sensor networks and home robots to improve fall detection in the home environment,” in *Proceedings of the 33rd Annual International Conference of the IEEE Engineering in Medicine and Biology Society (EMBS '11)*, pp. 5331–5334, September 2011.
- [52] D. McIlwraith, J. Pansiot, and G.-Z. Yang, “Wearable and ambient sensor fusion for the characterisation of human motion,” in *Proceedings of the 23rd IEEE/RSJ International Conference on Intelligent Robots and Systems (IROS '10)*, pp. 5505–5510, IEEE, Taipei, Taiwan, October 2010.
- [53] M. Kepski, B. Kwolek, and I. Austvoll, “Fuzzy inference-based reliable fall detection using kinect and accelerometer,” in *Artificial Intelligence and Soft Computing*, vol. 7267 of *Lecture Notes in Computer Science*, pp. 266–273, Springer, Berlin, Germany, 2012.
- [54] H. Ö. Alemdar, G. R. Yavuz, M. O. Özen et al., “Multi-modal fall detection within the wecare framework,” in *Proceedings of the 9th ACM/IEEE International Conference on Information Processing in Sensor Networks (IPSN '10)*, pp. 436–437, April 2010.
- [55] S. Cagnoni, G. Matrella, M. Mordonini, F. Sassi, and L. Ascari, “Sensor fusion-oriented fall detection for assistive technologies applications,” in *Proceedings of the 9th International Conference on Intelligent Systems Design and Applications*, pp. 673–678, December 2009.
- [56] C. N. Doukas and I. Maglogiannis, “Emergency fall incidents detection in assisted living environments utilizing motion, sound, and visual perceptual components,” *IEEE Transactions on Information Technology in Biomedicine*, vol. 15, no. 2, pp. 277–289, 2011.
- [57] J. W. Zheng, Z. B. Zhang, T. H. Wu, and Y. Zhang, “A wearable mobihealth care system supporting real-time diagnosis and alarm,” *Medical and Biological Engineering and Computing*, vol. 45, no. 9, pp. 877–885, 2007.
- [58] K. Arai, “Wearable physical and psychological health monitoring system,” in *Proceedings of the Science and Information Conference (SAI '13)*, pp. 133–138, October 2013.
- [59] A. Lombardi, M. Ferri, G. Rescio, M. Grassi, and P. Malcovati, “Wearable wireless accelerometer with embedded fall-detection logic for multi-sensor ambient assisted living applications,” in *Proceedings of the IEEE Sensors*, pp. 1967–1970, October 2009.
- [60] D. Naranjo-Hernández, L. M. Roa, J. Reina-Tosina, and M. A. Estudillo-Valderrama, “Personalization and adaptation to the medium and context in a fall detection system,” *IEEE Transactions on Information Technology in Biomedicine*, vol. 16, no. 2, pp. 264–271, 2012.
- [61] L. Schwickert, C. Becker, U. Lindemann et al., “Fall detection with body-worn sensors,” *Zeitschrift für Gerontologie und Geriatrie*, vol. 46, no. 8, pp. 706–719, 2013.
- [62] S. K. Goel, N. Haryani, P. Tiwari, A. Jain, and P. Kuvalekar, “Smart phone for elderly populace,” *International Journal of Research in Engineering and Technology*, vol. 2, no. 10, pp. 33–37, 2013.
- [63] R. Luque, E. Casilari, M.-J. Morón, and G. Redondo, “Comparison and characterization of android-based fall detection systems,” *Sensors*, vol. 14, no. 10, pp. 18543–18574, 2014.
- [64] A. K. Bourke, P. van de Ven, M. Gamble et al., “Evaluation of waist-mounted tri-axial accelerometer based fall-detection algorithms during scripted and continuous unscripted activities,” *Journal of Biomechanics*, vol. 43, no. 15, pp. 3051–3057, 2010.

- [65] S. Wang, Z. Xu, Y. Yang, X. Li, C. Pang, and A. G. Hauptmann, "Fall detection in multi-camera surveillance videos: experimentations and observations," in *Proceedings of the 1st ACM International Workshop on Multimedia Indexing and Information Retrieval for Healthcare (MIIRH '13)*, pp. 33–38, ACM, October 2013.
- [66] M. Grassi, A. Lombardi, G. Rescio et al., "An integrated system for people fall-detection with data fusion capabilities based on 3D ToF camera and wireless accelerometer," in *Proceedings of the 9th IEEE Sensors Conference (SENSORS '10)*, pp. 1016–1019, November 2010.
- [67] G. Koshmak, M. Linden, and A. Loutfi, "Dynamic Bayesian networks for context-aware fall risk assessment," *Sensors*, vol. 14, no. 5, pp. 9330–9348, 2014.

Research Article

Interrupt-Based Step-Counting to Extend Battery Life in an Activity Monitor

Seung Young Kim and Gu-In Kwon

School of Computer and Information Engineering, Inha University, Incheon 402-751, Republic of Korea

Correspondence should be addressed to Gu-In Kwon; gikwon@inha.ac.kr

Received 11 May 2015; Revised 16 June 2015; Accepted 23 June 2015

Academic Editor: Toshiyo Tamura

Copyright © 2016 S. Y. Kim and G.-I. Kwon. This is an open access article distributed under the Creative Commons Attribution License, which permits unrestricted use, distribution, and reproduction in any medium, provided the original work is properly cited.

Most activity monitors use an accelerometer and gyroscope sensors to characterize the wearer's physical activity. The monitor measures the motion by polling an accelerometer or gyroscope sensor or both every 20–30 ms and frequent polling affects the battery life of a wearable device. One of the key features of a commercial daily-activity monitoring device is longer battery life so that the user can keep track of his or her activity for a week or so without recharging the battery of the monitoring device. Many low-power approaches for a step-counting system use either a polling-based algorithm or an interrupt-based algorithm. In this paper, we propose a novel approach that uses the tap interrupt of an accelerometer to count steps while consuming low power. We compared the accuracy of step counting and measured system-level power consumption to a periodic sensor-reading algorithm. Our tap interrupt approach shows a battery lifetime that is 175% longer than that of a 30 ms polling method without gyroscope. The battery lifetime can be extended up to 863% with a gyroscope by putting both the processor and the gyroscope into sleep state during the majority of operation time.

1. Introduction

The growing interest in health has motivated the development of smart accessories that monitor the wearers' physical activities, including walking, running, sitting down, and lying in bed. Recently there has been a lot of research on method of counting steps using a three-axis accelerometer in association with different algorithms, including these found in commercially produced pedometers [1].

An activity monitor or digital pedometer typically reads an accelerometer sensor periodically, at a frequency of 30–50 Hz to measure the number of steps taken in walking or running. In a polling algorithm of this sort, the monitoring processor wakes up from its sleep state every 20–30 ms, reads the sensor data, and then runs the step-counting algorithm. This approach is 99.5% accurate for walking speeds over 90 m/min, which is usually considered satisfactory. However, polling consumes more power than the alternative event-based interrupt approach [1], in which the system only wakes from its sleep state when the acceleration crosses some

threshold. Research shows the acceleration change in human walking is between 0.4 and 0.8 g along the vertical axis [2].

Because an activity monitor or pedometer is usually worn on the wrist, on ankle, or on a belt around the waist, the system needs to have a form factor similar to that of a watch. Nevertheless, users expect a battery life of a week at least. For example, the electrical specification of the Misfit Shine, which is a highly optimized commercial activity monitor, indicates that a 3 V CR2032 battery, with a capacity of approximately 200 mAh, lasts three months. To obtain this kind of battery life, a system needs to stay in its sleep state for as long as possible, and the all electrical components have to be low-power types. For instance, the MSP430 or STM32L MCUS only draws a few nA in sleep mode [3].

In this paper, we propose a low-power approach to step-counting which uses the tap interrupt which is provided by several accelerometer chips, including the most popular Analog Devices ADXL345 and Freescale MMA8451. This interrupt is triggered by an acceleration exceeding a preprogrammed value. To the best of our knowledge, a tap interrupt

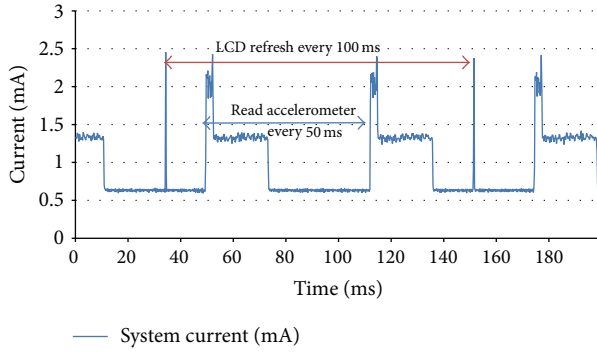


FIGURE 1: System current when polling at 20 Hz.

function has not previously been used for step-counting. We have compared the power consumption of a system running our algorithm and running a polling algorithm. We measured average power usage with and without gyroscope, which can draw a lot of power. The accuracy of our tap interrupt algorithm ranges between 83.5% and 90.25%, depending on the weight of the users, but the battery life is extended by factors ranging up to 8.6 when compared with polling. Comparing these figures with the performance of commercial pedometers suggests that our algorithm is suitable for devices in which battery life is paramount.

2. Methods

2.1. Step-Counting by Polling an Accelerometer. A polling algorithm uses a timer-based routine to wake the accelerometer sensor to read accelerations and then return it to sleep state to save power [4]. We experimented with a polling algorithm running on 20 Hz and measured the system power consumption. As shown in Figure 1, the system wakes at every 50 ms and reads the sensor which produces a peak in power consumption; then it processes the sensor data for about 20 ms which also uses significant power consumption. The number of steps is displayed on an LCD every 100 ms.

The power consumption in sleep state P_s is 1.91 mW (P_s); the power P_a used for reading accelerometer is 6.04 mW; and the processor running the polling algorithm uses a power P_p of 3.95 mW when it wakes up at a polling frequency of f . The power consumption of the system P_{system} can be expressed as follows:

$$P_{\text{system}} = f \times V \times \left\{ (P_a \times T_a) + (P_p \times T_p) + \left(P_s \times \left(\frac{1}{f} - (T_a + T_p) \right) \right) \right\}, \quad (1)$$

where P_a is power consumption during reading of the accelerometer, P_p is power consumption running the step-counting algorithm, P_s is power consumption in sleep state, T_a is processing time required to read the reading accelerometer, T_p is processing time required by the polling algorithm, f is frequency of polling, and V is supply voltage.

TABLE 1: Averages value of power consumption and processing times.

P_a	P_p	P_s	T_a	T_p
6.04 mW	3.95 mW	1.91 mW	8.97 mW	62.19 mW

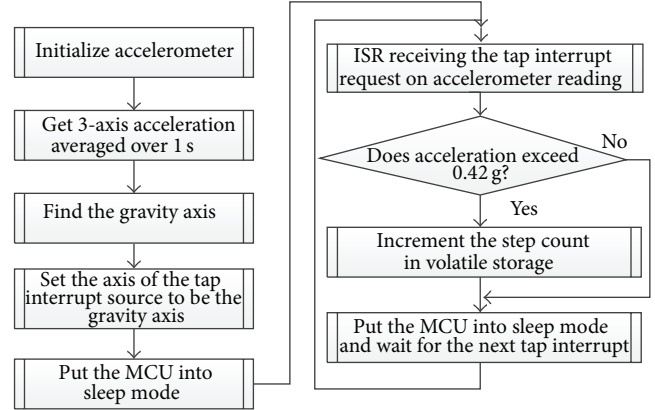


FIGURE 2: Algorithm for counting steps using the tap interrupt facility of the ADXL345 accelerometer.

Table 1 shows the average power consumption of system for 1 second.

It is clear from (1) that actually energy can be saved by running the frequency at which the step-counting algorithm is waken up. But accuracy declined at frequency below 20 Hz [5], even though a human cannot walk or run at over 5 Hz. This motivates the development of an interrupt-based algorithm.

2.2. Step-Counting Using a Tap Interrupt. The tap interrupt provided by the ADXL345 accelerometer chip can reduce the processing time required for counting steps, hence saving power.

Figure 2 shows our step-counting algorithm which uses this interrupt. An interrupt is triggered by acceleration along one of the accelerometer three fixed axes which exceed a specific threshold. To avoid unexpected interrupt, our algorithm finds the gravity axis among three axes by averaging the acceleration along each axis over 1 second and selects the axis whose average is around -1.0 g for interrupt source axis to trigger the tap interrupt. The interrupt service routine (ISR) handling the tap interrupt checks both the tap interrupt flag and the data-available flag before it decides to count a step. And this interrupt can be triggered by accelerometer even in its sleep mode and we can put processor also in its sleep to save system power.

Figure 3 shows the power consumption of the system over 1 second using the tap interrupt technique: one step is taken and one power peak occurs. During the resulting wake-up period the system consumes 5.92 mW for 12.6 ms and most of the time the system stays in sleep state to save the power. We will present results showing that the tap interrupt algorithm does save system-level power and assess its accuracy in Section 3.

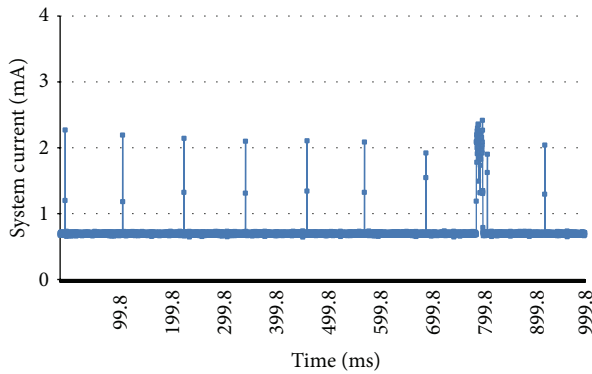


FIGURE 3: Current consumption of the system running the tap interrupt algorithm for 1 second.

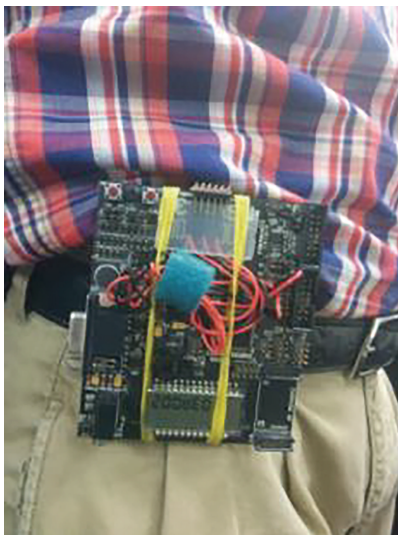


FIGURE 4: Experimental pedometer and battery worn on a belt.

2.3. System Implementation. We implemented our step-counting algorithm in a pedometer, shown in Figure 4, constructed from a Texas Instruments MSP430F4618 experimenter's board, populated with an ADXL345 and a ITG3200 gyroscope. Both sensors are connected to the I2C bus on MSP430F4618, and this I2C bus was configured to run at 100 kHz to save power. All unnecessary components were removed from the board to avoid spurious power consumption.

The ADXL345 was configured to run at a sampling rate of 200 Hz, at which frequency it drew $145 \mu\text{A}$ [6]. The ITG3200 was put into its sleep state immediately after initialization, where it draws just $6 \mu\text{A}$; when operating normally it draws 6.5 mA [7], and this power consumption is too great for a 200 mAh battery-powered system. The ADXL345 needs to be operating normally so that it can wake the MCU up by means of an interrupt. The MCU is put into LPM4 mode, in which it typically draws $0.3 \mu\text{A}$, against $400 \mu\text{A}$ in active mode at room temperature [8]. To compare the power consumed by a polling algorithm and our tap interrupt algorithm, both algorithms were implemented in the single source code

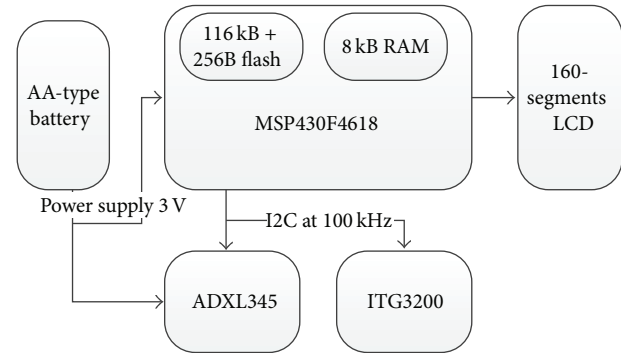


FIGURE 5: Block diagram of an experimental pedometer implemented on an MSP430F4618 experimenter's board, with an accelerometer and a gyroscope.

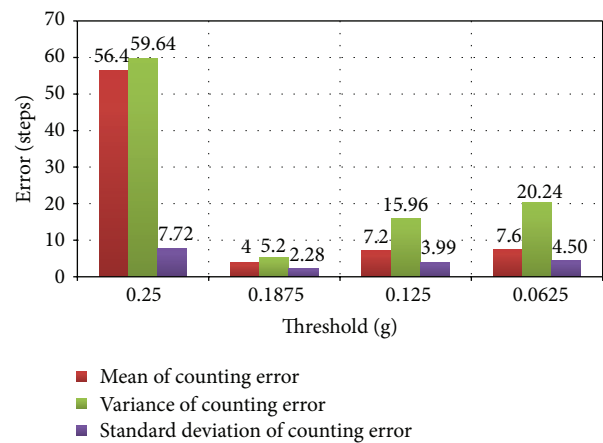


FIGURE 6: Mean and standard deviation of the errors in step count for different acceleration thresholds for the tap interrupt.

file, and one algorithm was selected at compilation time. The step count is displayed by an LCD driven by the LCD controller built into the MSP430F4618. Figure 5 shows the block diagram of this system.

3. Experimental Results

3.1. Step-Counting Accuracy. The threshold value of acceleration that triggers a tap interrupt needs to be carefully selected to balance accuracy against the powers saved by the MCU in its sleep state. We searched for an optimal acceleration threshold by measuring the error in step-counting using thresholds between 0.0625 g and 0.25 g (Figure 6).

The procedure involved 10 trials of 40 steps by 65 kg adult. The smallest error corresponds to an acceleration threshold of 0.187 g, and this threshold uses further experiments. All experiments were approved by the Inha University Ethics Committee.

The accuracy of our algorithm was compared with that of an Omron HJ303 pedometer (which uses triaxis technology), the Runtastic (the most downloaded Android pedometer app), and Pedometer (implemented by Levente Bagi based on a public step-counting algorithm). These tests were

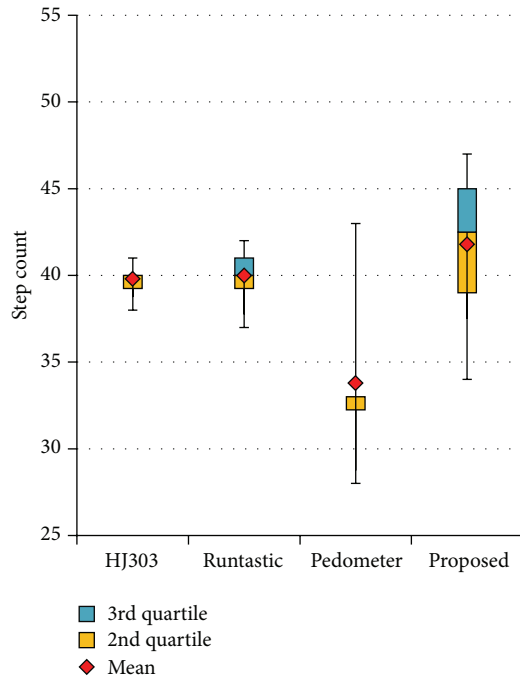


FIGURE 7: “Box and whiskers” plot showing the mean, standard deviation, and quartile of results from four pedometers.

conducted at walking speed of 80 m/min, because many commercial pedometers are accurate at this speed [9]. Each test involved 10 trials of 40 steps by each of two adults, weighing 65 kg and 72 kg. Because accuracy can be affected by the position in which a pedometer is worn, all the devices were attached to the wear’s belt above their right hip.

The result for the 65 kg walks is shown as a “box and whiskers” plot in Figure 7 of the 10 time trials.

The mean step counts (and standard deviations) for our device, the HJ303, the Runtastic, and the Android pedometer app were 41.8 (4.46), 39.8 (0.92), 40.0 (1.63), and 33.8 (3.90), respectively. Our pedometer is less accurate than the commercial pedometers but performs considerably better than the Android app.

We conducted a further experiment on our devices, involving walkers with a wider range of weights, again involving 10 trials of 40 steps. The accuracy of the results varied between 83.5% and 90.25% as shown in Table 2. Schneider et al. [10] suggested an error of up to 10% is acceptable when a pedometer is used to measure the wearer’s activity over long periods. This is exactly the sort of application in which a long battery life is essential.

3.2. Energy Consumption. To measure the system power consumption, we connected our pedometer to a Monson Solutions Power Monitor, connected in turn to a PC running Power Tool 4.0.4. The output voltage of the monitor was set to 3.0 V, and the current across a 0.56 Ω resistor was measured every 200 μ s [11]. We performed tests with the tap interrupt algorithm and the polling algorithm, with the frequency of polling set to 20, 32, and 100 Hz.

TABLE 2: Accuracy of our pedometers with walkers of different weights.

Weight (kg)	35	44	63	65	65	72	94
Accuracy (%)	87.5	83.5	90.25	90.5	90.0	83.75	88.0

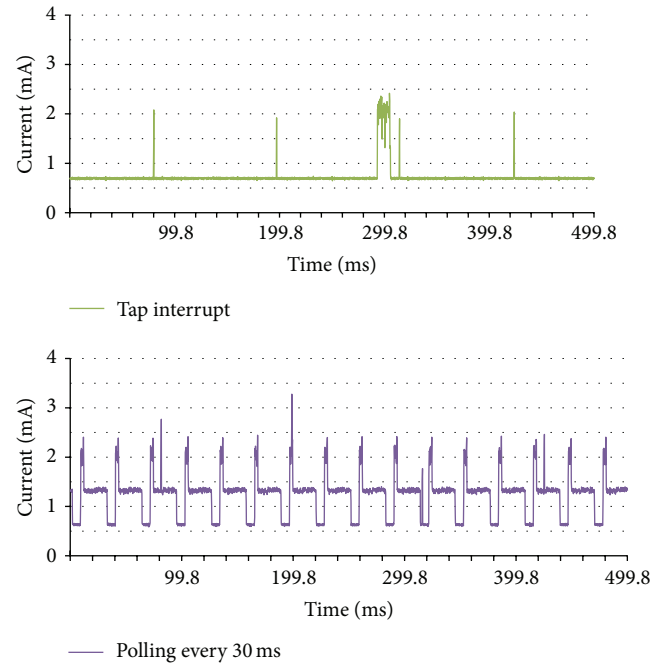


FIGURE 8: Power drawn by the system over 500 ms, running tap interrupt and polling algorithms. The results at 100 ms intervals correspond to LCD refresh, and the wide peak in the upper chart is the tap interrupt service routine.

Figure 8 shows the patterns of current consumption over 500 ms for the tap interrupt algorithm and the polling algorithm running at 32 Hz. The tap interrupt produces peak of 1.98 mA while the polling algorithm has 16 reads of 1.732 mA.

3.3. Gyroscope Power Consumption. The accelerometer alone is sufficient to count steps, but the monitoring of other activities requires a gyroscope to be used in addition. Brajdic and Harle evaluated several more algorithms for waking detection and step-counting using accelerometer, gyroscope, and both [12]. This increases power consumption by a factor of about 5 times. Figure 9 shows the pattern of current consumption when running the tap interrupt algorithm with and without the gyroscope. The gyroscope is only waken from sleep state when an interrupt is received from the accelerometer. The ETHOS system [3] draws 7.4 mA where the gyroscope is enabled, and the estimated battery life of the 4.2 V 200 mAh Li-ion battery is 27 hours. Table 3 compares the battery life for the polling and the interrupt algorithm with and without gyroscope. Our tap interrupt algorithm extends battery life by 175%, compared with polling without

TABLE 3: Power consumptions and expected battery life using the polling and tap interrupt algorithms.

Supply voltage	Measure time (ms)	Consumed energy (uAh)	Average current (mA)	Battery life (minutes)
2.99 V				
Polling at 30 ms	60936	20.95	1.24	9690.6
Polling at 50 ms	60519	15.75	0.94	12808.8
Tap interrupt	60012	11.92	0.72	16775.4
Polling at 30 ms with gyroscope	60885	18.99	6.35	1890.6
Tap interrupt with gyroscope	61083	12.47	0.74	16324.8

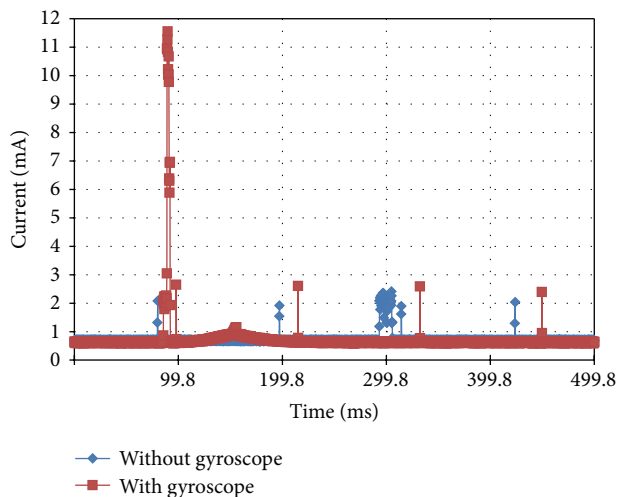


FIGURE 9: Current drain over 500 ms for the tap interrupt algorithm, with and without a gyroscope. The ITG3200 gyroscope draws approximately 6.5 mA in active mode, which results in a large difference in power consumption between the polling and interrupt algorithms.

a gyroscope. With the gyroscope, the battery life can be extended by up to 863% by putting both the processor and gyroscope into sleep state for most of the time.

4. Discussion

This paper proposes a new approach for a low-power step-counting algorithm by using a tap interrupt algorithm and we conducted power profiling to analyze power consumption of popular polling algorithm.

By reducing wake-up frequency from the sleep state and shortening process time at every wake-up, we can reduce the average power consumption. By using the threshold interrupt of the accelerometer, the tap interrupt algorithm can contribute to a longer battery life for activity monitoring devices. A minimum of 30 minutes of daily physical activity, such as walking, is now considered necessary to maintain fitness

[13]. Patients with conditions such as obstructive pulmonary disease may require long-term activity monitoring, but this does not need to be very accurate. In future work, we plan to investigate whether the tap interrupt can be used to detect unexpected fall for elders or to recognize posture in humans and animals in long-term application in which frequent battery recharging is inconvenient [14].

Conflict of Interests

The authors declare that there is no conflict of interests regarding the publication of this paper.

Acknowledgments

This work was supported by the National Research Foundation of Korea (NRF) grant funded by the Korea government (MSIP) (no. 2015R1A2A2A01003501). This work was supported by Inha University.

References

- [1] C. G. Ryan, P. M. Grant, W. W. Tigbe, and M. H. Granat, "The validity and reliability of a novel activity monitor as a measure of walking," *British Journal of Sports Medicine*, vol. 40, no. 9, pp. 779–784, 2006.
- [2] R. Cross, "Standing, walking, running, and jumping on a force plate," *American Journal of Physics*, vol. 67, no. 4, pp. 304–309, 1999.
- [3] H. Harms, O. Amft, R. Winkler, J. Schumm, M. Kusserow, and G. Troester, "ETHOS: miniature orientation sensor for wearable human motion analysis," in *Proceedings of the 9th IEEE Sensors Conference (SENSORS '10)*, pp. 1037–1042, IEEE, Kona, Hawaii, USA, November 2010.
- [4] A. Krause, M. Ihmig, E. Rankin et al., "Trading off prediction accuracy and power consumption for context-aware wearable computing," in *Proceedings of the IEEE International Symposium on Wearable Computers (ISWC '05)*, pp. 20–26, October 2005.
- [5] H. Junker, P. Lukowicz, and G. Tröster, "Sampling frequency, signal resolution and the accuracy of wearable context recognition systems," in *Proceedings of the 8th International Symposium on Wearable Computers (ISWC '04)*, pp. 176–177, November 2004.
- [6] N. Zhao, "Full-featured pedometer design realized with 3-axis digital accelerometer," *Analog Dialogue*, p. 44–06, 2010.
- [7] K. Leuenberger and R. Gassert, "Low-power sensor module for long-term activity monitoring," in *Proceedings of the 33rd Annual International Conference of the IEEE Engineering in Medicine and Biology Society (EMBS '11)*, pp. 2237–2241, September 2011.
- [8] T. Hornos, *Wireless ECG/EEG with the MSP430 microcontroller [M.S. thesis]*, University of Glasgow, Glasgow, UK, 2009.
- [9] S. E. Crouter, P. L. Schneider, M. Karabulut, and D. R. Bassett Jr., "Validity of 10 electronic pedometers for measuring steps, distance, and energy cost," *Medicine & Science in Sports & Exercise*, vol. 35, no. 8, pp. 1455–1460, 2003.
- [10] P. L. Schneider, S. E. Crouter, and D. R. Bassett Jr., "Pedometer measures of free-living physical activity: comparison of 13 models," *Medicine and Science in Sports and Exercise*, vol. 36, no. 2, pp. 331–335, 2004.

- [11] L. Zhang, B. Tiwana, R. P. Dick et al., "Accurate online power estimation and automatic battery behavior based power model generation for smartphones," in *Proceedings of the 8th IEEE/ACM International Conference on Hardware/Software-Co-Design and System Synthesis (CODES+ISSS '10)*, pp. 105–114, October 2010.
- [12] A. Brajdic and R. Harle, "Walk detection and step counting on unconstrained smartphones," in *Proceedings of the ACM International Joint Conference on Pervasive and Ubiquitous Computing (UbiComp '13)*, pp. 225–234, September 2013.
- [13] R. R. Pate, M. Pratt, S. N. Blair et al., "Physical activity and public health. A recommendation from the Centers for Disease Control and Prevention and the American College of Sports Medicine," *The Journal of the American Medical Association*, vol. 273, no. 5, pp. 402–407, 1995.
- [14] Q. Li, J. A. Stankovic, M. A. Hanson, A. T. Barth, J. Lach, and G. Zhou, "Accurate, fast fall detection using gyroscopes and accelerometer-derived posture information," in *Proceedings of the 6th International Workshop on Wearable and Implantable Body Sensor Networks (BSN '09)*, pp. 138–143, IEEE, Berkeley, Calif, USA, June 2009.

Research Article

Miniaturized Human Insertable Cardiac Monitoring System with Wireless Power Transmission Technique

Jong-Ha Lee

Department of Biomedical Engineering, School of Medicine, Keimyung University, Daegu 704-701, Republic of Korea

Correspondence should be addressed to Jong-Ha Lee; segeberg@gmail.com

Received 28 January 2015; Revised 26 April 2015; Accepted 12 May 2015

Academic Editor: Toshiyo Tamura

Copyright © 2016 Jong-Ha Lee. This is an open access article distributed under the Creative Commons Attribution License, which permits unrestricted use, distribution, and reproduction in any medium, provided the original work is properly cited.

Prolonged monitoring is more likely to diagnose atrial fibrillation accurately than intermittent or short-term monitoring. In this study, an implantable electrocardiograph (ECG) sensor to monitor atrial fibrillation patients in real time was developed. The implantable sensor is composed of a micro controller unit, an analog-to-digital converter, a signal transmitter, an antenna, and two electrodes. The sensor detects ECG signals from the two electrodes and transmits these to an external receiver carried by the patient. Because the sensor continuously transmits signals, its battery consumption rate is extremely high; therefore, the sensor includes a wireless power transmission module that allows it to charge wirelessly from an external power source. The integrated sensor has the approximate dimensions $3\text{ mm} \times 4\text{ mm} \times 14\text{ mm}$, which is small enough to be inserted into a patient without the need for major surgery. The signal and power transmission data sampling rate and frequency of the unit are 300 samples/s and 430 Hz, respectively. To validate the developed sensor, experiments were conducted on small animals.

1. Introduction

There are numerous medical problems whose treatment requires the constant monitoring of vital signs from several body organs. Although patients are typically hospitalized and kept under observation using wired equipment to measure vital signs, remote patients must stay at home along with expensive monitoring equipment and dedicated medical staff, which increases medical expenditure and reduces human resources available at the hospital. Several studies have therefore been conducted recently in researching and developing wearable and implantable biomedical devices, and progress in this field has provided benefits in terms of lower costs, freer patient movement, and uninterrupted diagnostic data streams for medical monitoring. Wireless biomedical devices can provide enhanced mobility and efficiency with minimum disruption of monitored data [1], and networks based on biomedical sensors can create effective solutions for distributing patient information along multiple platforms.

Diabetes and cardiovascular diseases are two health conditions that require effective, round-the-clock monitoring. Twenty-four percent of the population of developed countries has diabetes and related complications such as cardiovascular

diseases, making this a widespread health issue that can only be addressed through active monitoring of blood glucose levels (BGL) [2].

The vital signs that are most often monitored in health diagnostics are:

- (i) blood glucose level;
- (ii) blood pressure and pulse rate;
- (iii) electrocardiograph (ECG);
- (iv) respiration efficacy.

Advancements in the use of wireless technologies in biomedical implant design have opened avenues for marked improvement in medical care and diagnostic systems as wired equipment is replaced with implanted on-body sensors. Biomedical implant-based monitoring systems can wirelessly transmit data consisting of critical information related to patient health. Implant-based vital-sign monitoring allows for round-the-clock monitoring and health management, with updates provided on handheld devices using wireless protocols. A range of medical diagnoses can be performed using implants through the monitoring of parameters such

as blood pressure, glucose level, and cardiac response. However, efficient invasive monitoring using wireless biomedical implants comes with numerous challenges that must be addressed beforehand.

Recently there are several noninvasive ECG monitoring in the market such as ZioPatch. The patch fuses power-efficient electronics and standardized communication. The ECG patch records up to 3 lead ECG signals and tissue-contact impedance and includes a 3D accelerometer for physical activity monitoring. The data are processed and analyzed locally, and relevant events and information are transmitted through BLE wireless link. However, the patch-type noninvasive sensor is not suitable for users to hold 24 hours. The advantage of implantable sensor is more suitable to continuously monitor the human for 24 hours 7 days. Research on implants has progressed significantly in the last decade and is being actively pursued owing to the viability of implants in a broad range of applications including medicine, health, and sports. On-time diagnostics have become a major benefit for patients with chronic diseases as the continuous monitoring of health indicators can significantly assist in curtailing emergency events. The design of wireless biomedical implants is a difficult task, however, as there are many challenges that must be addressed for operational systems. Some important key issues are as follows.

- (i) *Power Requirements.* Biomedical implants vary in power requirements based on their operational issues. To improve implant lifetime and range of communication, and because excessive power dissipation by a medical implant can seriously increase the chances of tissue damage [3], low power consumption is generally sought. Implants can be powered using batteries or wireless power transfer; however, batteries are bulky and hazardous and require recurrent replacement, while wireless power allows for continuous power transfer, making it more suitable for 24-hour monitoring systems.
- (ii) *Sensors and Communication.* Accurately reading and monitoring signals from a human body require sensitive transducers and amplification units. Algorithms for the interpretation of signals must also be carefully designed to cater to any signal pattern anomalies in a timely manner. Wireless system must also be carefully designed to comply with power requirements and transmission ranges [4].
- (iii) *Implant Size.* Implant size has serious impacts on overall design [5]. Power requirements, carrier frequency, and transducer design are all primarily governed by the size of the implant, which in turn is governed by where in the body the implant is placed. Smaller implants also allow for minimally invasive surgical procedures.
- (iv) *Reliability.* The reliability and efficacy of an implantable medical device are paramount for enabling active monitoring and timely warning under emergency situations. In cardiac cases in particular, emergencies can be avoided through the use of implants

that can produce reliable measurements. Good reliability will also reduce the need for periodic surgery in order to install replacements. To sustain future requirements ensuring the viability of biomedical implant technology, prolonged reliability is essential.

The above concerns must be kept in mind when designing an implant as they represent the major limiting factors for advances in implant technology. In this study, an implantable ECG sensor using wireless communication and power transmission was developed. With the increased pace of living in contemporary society and the related reliance on tobacco, alcohol, and caffeine, the number of patients with heart conditions such as arrhythmia is increasing. Arrhythmia (also known as cardiac dysrhythmia) is caused by an abnormal ejection fraction and presents as an irregular heartbeat that is either faster (tachycardia) or slower (bradycardia) than the usual heart rate. It can occur unexpectedly anytime and anywhere and can lead to shortness of breath, dizziness, and fainting; in serious cases, it can cause sudden cardiac arrest owing to noncontraction of the ventricles, resulting in a life-threatening myocardial infarction (heart attack). An electrocardiography (or electrocardiograph) (ECG) can be used to detect cardiac abnormalities and thus predict arrhythmia. The ECG produces a graph on which changes in electrical potential associated with the pattern of the heartbeat are recorded. Measurements using an ECG can be performed with either patch- or insertion-type ECG sensors. The most widely used ECG sensor is the standard patch-type 12-lead ECG, in which electrodes are attached to the four limbs and to the anterior chest near the heart in order to measure and record ECG signals using standard limb, unipolar limb, and chest leads. However, in the case of arrhythmia a short-term ECG measurement is of little help because of the short duration of symptoms; it is therefore necessary to use an ECG device that can be carried by the patient and has electrodes attached to the body's surface. The heart rhythm can be recorded using either a Holter monitor or an implantable loop recorder (ILR) surgically inserted under the skin. Unfortunately, the Holter monitor is inconvenient as it disrupts daily activities because it must be worn constantly. Although the insertion-type ILR is more comfortable as it is implanted into the body and does not need to be carried, its use requires surgical intervention for implantation, which raises safety and confidence issues. In addition, a similar surgical procedure is necessary at the end of battery life to either replace or remove it, which again raises safety and cost issues.

The drawbacks of ILR can be overcome through the use of a quasipermanent battery that is recharged via wireless power transmission. While this is technically possible, further investigation of effects on the human body must be conducted before such systems can be considered safe and reliable. Therefore, in this study an insertion-type wireless ECG sensor was developed and its performance within a human body phantom was tested using a thermal imaging camera. Further tests of the implanted sensor were then conducted on an animal model. Based on the results of these tests, it was

possible to identify any potential problems that could occur in the use of a wireless ECG sensor.

2. System Design Concepts

In this section, the design concept of the implantable ECG sensor is presented. Numerical simulations were performed to verify the principle behind sensor and tactile images of phantom tissue inclusions were obtained.

2.1. Cardiac ECG Measurement and Electrodes. Cardiac activity is normally monitored by recording electrocardiograph (ECG) signals in a clinical setting, which requires the physical presence of the patient at the facility. The ECG signal is composed of multiple electrical activities that begin from the sinus at the top of the right atrium. The signal is generated from the sinus node and propagates through the atrioventricular (AV) node. One cardiac cycle consists of a P wave, a T wave, and a QRS complex, all of which were identified by Willem Einthoven. When a sinus node releases an electrical impulse, it creates the basis for an atrial depolarization leading to atrial contraction, which is sensed as a P wave. The signal then passes through the AV node, where the QRS complex signal is induced by ventricular depolarization and is followed by generation of a T wave from the repolarization of the ventricular node.

Monitoring heart activity through ECG signals is carried out using at least three electrodes placed on specific points on the skin in order to sense electrical signals generated by heart constituents. The Holter monitor is one such diagnostic device and is commonly employed for active monitoring of heart activity after major heart procedures [6]. Holter monitors have proven technologically capable but are large, must be connected to electrodes using wires that limit free movement of the patient, and require continuous placement of electrodes for long-term monitoring. Standard Holter monitors are therefore incapable of providing smooth and seamless unobtrusive continuous monitoring, and although Holter devices have evolved over the past few years into complete wire-free miniaturized modules, they still require further improvements to ensure totally unobtrusive monitoring architecture.

In this study, Ag/AgCl electrodes were used. An ECG traces the electrical potential differences between electrodes placed on the body's surface; however, the action potential that gives rise to the contraction and relaxation of the cardiac muscle is only about 1 mV, which is extremely difficult to measure. It is therefore necessary to amplify electrocardiographic data to make it easily perceivable to the human eye; this is done through the use of an operational amplifier (op-amp), which amplifies an input electrical potential in order to produce an output potential augmented to the level desired by the user. In this study, an instrumentation amplifier using op-amps was fabricated and configured to amplify the microfine ECG by a factor of about 100 using a band-pass filter (BPS). The current consumption of the proposed ECG sensor is about 11 mA and its noise generation is inversely proportional to the length of the wireless communication

antenna inside the sensor. Traditionally, the ECG sensor needs three electrodes as positive, negative, and ground. In the proposed system, however, the ground electrode is emitted and only two electrodes were used. On the main sensor body, in the left and right sides of the body, two electrodes were attached.

2.2. Telemetry Methods. Currently used systems for health monitoring employ a variety of methods to relay information between the sensors and the data display module. Data are normally shared between these two units using wires, which increases the redundancy of the system and limits movement of the patient. Although wire-based equipment provides a robust means for communication in health monitoring systems and is low-cost, it reduces the ability for normal movement of a patient in her everyday routines.

Another problem arising in wired systems is the improper connection of wires for various reasons, which can seriously interrupt the system and pose serious consequences for the patient. Continuous improvisation and research are being carried out to develop smart health monitoring systems and many alternative communication techniques have emerged, with wireless communication being the most suitable communication method for curtailing the need for wired connections between sensors and equipment. Wireless technologies enable intrabody communication to complement systems for continual health monitoring without the need for admitting patients and attaching wires. Wireless communication allows for real-time monitoring of vital signs on an unwired display device in proximity to the patient as well as for remote observation by a doctor via the internet. Wireless connectivity can also help patients to track their own health indicators using smart-phones or PDAs connected to implants or wearable sensors in real-time. This can result in better health management and prompt alerts in the case of health related emergencies.

Biomedical implanting is a vibrant technology that has shown promise in improving real-time medical diagnostics. Research has shown that implants can be used to provide a feedback control; for example, an implant variant was used to record neural signals in brain-machine interfaces in order to control prostheses or paralyzed limbs [6, 7]. Implants that use wireless communication have been shown to significantly reduce drawbacks attributed to wire connections, as has been reported with wired deep brain systems, implantable cardioverter-defibrillators, and pacemakers [8].

In this study, the Medical Implant Communication Service (MICS) was used as a communications protocol. MICS operates in the frequency range of 402–405 MHz and is normally used for communication between body-worn monitoring systems and implants. Implantable antennas in this frequency range have been developed to transmit data from pacemakers and cardiac sensors; however, regulatory restrictions in hospitals have limited their full utilization in wireless body area networks (WBANs).

2.3. Wireless Power for Biomedical Implants. Supplying adequate power to biomedical implants is currently the main

challenge limiting functionality and performance in such devices. Power consumption affects many characteristics of an implant, including size, processing power, transmission range, and life span.

Batteries can power implants for long periods of time by exploiting design techniques that require extremely low power consumption. The average power consumption for a battery used in a pacemaker is about $8 \mu\text{W}$ and the typical battery comprises 90% of the total size of the implant and requires periodic replacement through costly invasive surgery every few years [9, 10]. Power-hungry implants such as mechanical pump-based cardiac and orthopedic implants require significant amounts of power to function, making batteries an ineffective power source option for such implants [11, 12]. Thus, the prospects for and applicability of biomedical implant technology are currently severely limited by the unavailability of adequate power sources, a problem that can be successfully addressed by using wireless power transfer techniques capable of delivering uninterrupted power to ensure continuous monitoring and communication by implants.

In this study, a near-field wireless power transmission system was used. It is assumed that the radiated fields produced by inductive coupling are not rapidly changing; as the displacement current at low frequencies does not affect the generated fields, it can be ignored. This is generally called the quasistatic approximation. Using this approximation, the magnetic field was found to be concentrated in the vicinity of the source. Problems such as these can be analytically solved using the Biot-Savart law or by finding a solution using the diffusion equation.

Many techniques for implementing coupled power links have been reported in the literature. In one study [13], the authors used coupled self-resonant coils to power a 60 W bulb over a distance of 2 m with an efficiency of 40%. This was accomplished by nonradiating magnetic induction using resonant loops: employing two identical helical coils as coupling elements, a standard Colpitts oscillator with a single copper wire loop inductive element was used to generate frequencies in the MHz range. The copper loop coupled inductive power to the source coil for further transmission and a light-bulb served as the load of the power transfer system. Experimental results showed that power transfer using nonradiative magnetic coupling could be achieved over a range of 8~9 times the radius of the coils. The authors also presented a quantitative model with an accuracy of around 5% for explaining the power transfer.

2.4. Circuit Design. An ECG traces the electrical potential differences between electrodes placed on the surface of a body. However, the action potential that gives rise to the contraction and relaxation of the cardiac muscle is about 1 mV and thus extremely difficult to measure; in this design, operational amplifiers (op-amps) are used to amplify the electrocardiographic data. An op-amp amplifies an input electrical potential to the level desired by the user and produces an output potential augmented to this intended level. For this study an instrumentation amplifier was fabricated

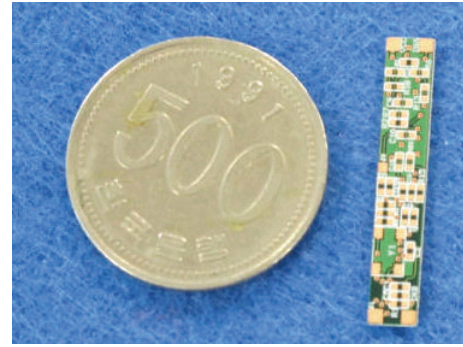


FIGURE 1: Circuit design of implantable ECG sensor.

using op-amps and configured to amplify microfine ECG signals by a factor of about 100 using a band-pass filter (BPF). The proposed ECG sensor has a current consumption of about 11 mA and a noise generation inversely proportional to the length of the wireless communication antenna inside the sensor. Figure 1 shows the circuit design of the implantable ECG sensor.

2.5. Packaging. The packaging materials selected must be biocompatible to avoid causing inflammation or necrosis of human tissues. Additionally, they need to satisfy the strength standards of the insertion location and should not absorb electric waves passing through them. It is also necessary to take packaging design into account in order to avoid any risk of damage to tissues caused by sensor insertion and postinsertion movements. Foreign-body sensation needs to be minimized by reducing the size of the object. As feedthrough needs to meet several requirements, conductivity should be ensured between the internal circuit and electrodes, noise should be minimized, and air-tightness should be maintained. In this study, the elasticity of polymer films was exploited to develop electrode sealing methods.

ECG sensor electrodes must have an electrode-to-electrode distance of ≥ 40 mm and an electrode width of ≥ 5 mm. In order to satisfy the requirements for electrodes, they were fabricated using titanium. The rigid packaging materials need to be coated to protect tissues and must be hermetically joined using a proper joining technique to completely block any interaction between the interior of the human body and the sensor environment; to accomplish this, either adhesives or a laser can be used. In this study, adhesives were used to produce a packaging prototype. Polydimethylsiloxane (PDMS) and medical epoxy are suitable adhesives, while PDMS, parylene, polyethylene, glycol, and silicone can be used as coating materials as their biocompatibilities have been verified in numerous studies. Figure 2 shows the packaged implantable ECG sensor.

The full diagram of the proposed system is shown in Figure 3.

3. Experimental Results

3.1. Self-Sealing Air-Tightness Testing. Testing for self-sealing air-tightness was performed in two steps. In the first step,

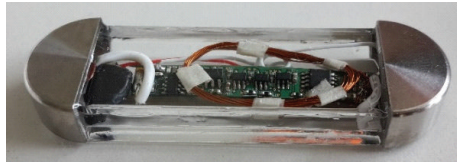


FIGURE 2: Packaged implantable ECG sensor.

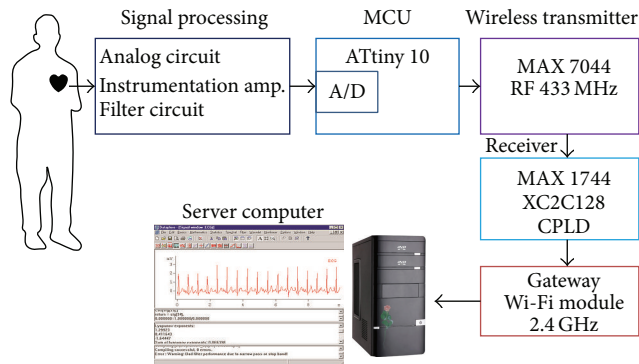


FIGURE 3: Implantable sensor and workstation diagram.

the packaging was submersed in deionized (DI) water for one hour with no sensor included, and in the second test the packaging containing the sensor was submersed in DI water for five hours. Results of tests show that the materials joined with adhesives are air-tight. Figure 3 shows the self-sealing test using the packaged sensor.

3.2. Thermal Testing. Coil charging was prepared in relation to the wireless power transmission to the ECG sensor. To establish a wireless network-driven environment for transmitting and receiving ECG data for measurement, a device was prepared that emitted an electric current identical to that of a real ECG and connected to the ECG sensor. An infrared temperature camera was then used to measure the temperature changes of the sensor itself; temperature changes were measured prior to the initiation of power transmission and then continued for one hour after transmission began with the aim of determining the average temperature change. Figure 4 shows the thermal testing experimental setup.

From the experiments, we found that the baseline average temperature was 23.5°C. The temperature then sharply rose by about 3.0°C after about 10 minutes and continued to rise to reach 27.2°C after one hour. As this temperature is far below 36.9°C—the average temperature of the interior of the human body—it can be assumed that the packaged sensor will not undergo considerable temperature change once inserted into the human body. Figure 5 shows the thermal testing experimental setup and Figure 6 shows the insertion experiment using animal model.

3.3. Insertion Experiment Using Animal Model. Before using the sensor within a human body, it was necessary to test the in vivo safety of the instrument to ensure both the efficient operation of the insertion-type ECG measurement system in

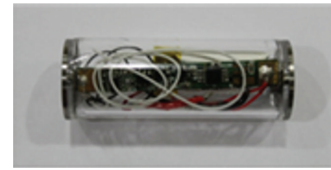


FIGURE 4: Self-sealing test using the packaged sensor.

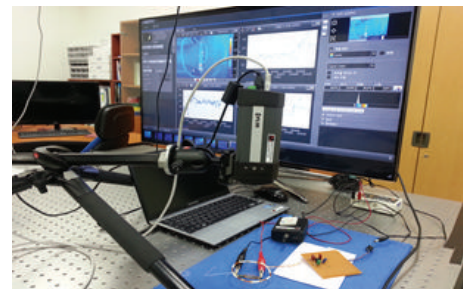


FIGURE 5: Thermal testing experimental setup.

measuring physiological functions and its efficacy in receiving external signals. A pig was therefore used as a sensor-implanted animal model because the animal's physiological characteristics are similar to those of humans. The species selected was a Hanford mini pig because its heart size is very similar to that of a human. A female pig of specific pathogen free (SPF) quality with no history of pregnancy, 46–60 kg, and 50–57-week old, was purchased from Optipharm Medipig (Chungbuk, South Korea).

The insertion surgery was performed in the Daegu High-Tech Medical Complex as follows. Anesthesia was induced using Zoletil (Tiletamine/Zolazepam) (2.5 mg/kg, IM) and Xylazine (2.3 mg/kg, IM) and maintained with Isoflurane (1–3%). Lactated ringer's solution (5 mL/kg/h, IV) was administered intraoperatively. After the anesthesia, the left anterior corselet was depilated and disinfected with alcohol and povidone. An incision was made between the left 5th and 7th ribs and separated using blunt dissection to a depth of 4 mm under the skin. The sensor was placed at the site, and the skin was sutured. On completion of the wireless ECG sensor implantation, the pig's ECG data were received by wireless network, as shown in Figure 7. In this data, two leads were continuously corrected. In the current experiments, we tried a short-term animal experiment. In the future work, the long-term experiment will be conducted to guaranty the proposed sensor safety issue.

4. Discussions

The current power consumption is relatively high due to the real-time communication between implanted sensor and



FIGURE 6: Insertion experiment using animal model.

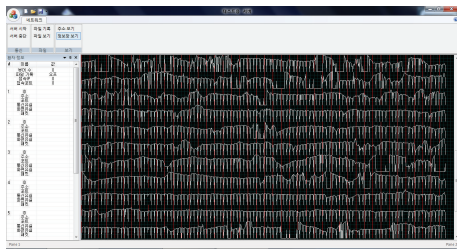


FIGURE 7: ECG monitoring results using animal model.

outside workstation with 300/sec sampling rate. To decrease the power consumption, the lower sampling rate or the discrete communication method can be considered in the future work. In the current animal experiments, two pigs were studied. The pig with similar human weights was considered with the IRB (institutional review board) guideline. In this paper, we suggested the real-time data transmission device. The reason is that the raw data should be corrected to determine the abnormality of ECG from doctors without computer aided diagnosis system.

5. Conclusion

This study demonstrated that the use of a quasipermanent ECG employing a double loop coil-shaped magnetic resonance-type wireless power transmission system sensor eliminates the need for surgical replacement. An ultrasmall antenna (20 mm in width, 10 mm in length) with a spiral-shape metal pattern was developed and used to minimize sensor size while securing a sufficient electric length. A human body phantom that had similar electrical properties to those of human skin within the MICS band, with a 10% error range of measurement values (specific permittivity = 43.2, conductivity = 0701 S/m), was developed and used to verify the communication performance of the antenna. The hermetic joining of packaging using adhesives and biocompatibility were also experimentally verified. Finally, sensor insertion surgery was performed on a laboratory pig and successful ECG data were obtained via a wireless network.

Conflict of Interests

The author declares that there is no conflict of interests regarding the publication of this paper.

Acknowledgments

This work was supported by a Grant (R0101-15-0147) from the Technology Innovation Program funded by the Ministry of Knowledge Economy (MKE, Republic of Korea) and supported by the R&D Program of the Ministry of Trade, Industry and Energy of Korea (Program of Advanced Technology Development for Future Industry, 10044353), and supported by Basic Science Research Program through the National Research Foundation of Korea (NRF) funded by the Ministry of Education (2014R1A1A2056420).

References

- [1] Y. Hao and R. Foster, "Wireless body sensor networks for health-monitoring applications," *Physiological Measurement*, vol. 29, no. 11, pp. R27–R56, 2008.
- [2] J. D. Newman and A. P. F. Turner, "Home blood glucose biosensors: a commercial perspective," *Biosensors and Bioelectronics*, vol. 20, no. 12, pp. 2435–2453, 2005.
- [3] IEEE Standard 1528/D1.2, "Recommended Practice for determining the spatial-peak specific absorption rate (SAR) in the human body due to wireless communications devices: measurement techniques," 2003.
- [4] A. Pantelopoulos and N. G. Bourbakis, "A survey on wearable sensor-based systems for health monitoring and prognosis," *IEEE Transactions on Systems, Man and Cybernetics, Part C: Applications and Reviews*, vol. 40, no. 1, pp. 1–12, 2010.
- [5] J. Malmivuo and R. Plonsey, *Bioelectromagnetism*, Oxford University Press, New York, NY, USA, 1995.
- [6] P. J. Zimetbaum and M. E. Josephson, "The evolving role of ambulatory arrhythmia monitoring in general clinical practice," *Annals of Internal Medicine*, vol. 130, no. 10, pp. 848–856, 1999.
- [7] G. E. Bergey, R. D. Squires, and W. C. Sipple, "Electrocardiogram recording with pasteless electrodes," *IEEE Transactions on Biomedical Engineering*, vol. BME-18, no. 3, pp. 206–211, 1971.
- [8] A. Searle and L. Kirkup, "A direct comparison of wet, dry and insulating bioelectric recording electrodes," *Physiological Measurement*, vol. 21, no. 2, pp. 271–283, 2000.
- [9] G. Cho, K. Jeong, M. J. Paik, Y. Kwun, and M. Sung, "Performance evaluation of textile-based electrodes and motion sensors for smart clothing," *IEEE Sensors Journal*, vol. 11, no. 12, pp. 3183–3193, 2011.
- [10] J. Mühlsteff and O. Such, "Dry electrodes for monitoring of vital signs in functional textiles," in *Proceedings of the 26th Annual International Conference of the IEEE Engineering in Medicine and Biology Society (EMBC '04)*, pp. 2212–2215, San Francisco, Calif, USA, September 2004.

- [11] R. Matthews, N. J. McDonald, I. Fridman, P. Hervieux, and T. Nielsen, "The invisible electrode zero prep time, ultra low capacitive sensing," in *Proceedings of the 11th International Conference on Human-Computer Interaction*, pp. 22–27, Las Vegas, Nev, USA, 2005.
- [12] Y. M. Chi and G. Cauwenberghs, "Wireless non-contact EEG/ECG electrodes for body sensor networks," in *Proceedings of the International Conference on Body Sensor Networks (BSN '10)*, pp. 297–301, IEEE, Singapore, June 2010.
- [13] A. D. Droitcour, O. Boric-Lubecke, V. M. Lubecke, J. Lin, and G. T. A. Kovacs, "Range correlation and I/Q performance benefits in single-chip silicon Doppler radars for noncontact cardiopulmonary monitoring," *IEEE Transactions on Microwave Theory and Techniques*, vol. 52, no. 3, pp. 838–848, 2004.